MECHANISM UNDERLYING ENHANCED PREDICTIONS OF ATLANTIC NIÑO IN THE EQUATORIAL ATLANTIC

By

GYUK, NEHEMIAH JOHN

B. Sc., M. Sc. (Kaduna)

MCS/20/7724

A Thesis of the Doctoral Research Programme of the West African Climate Systems, under the West African Science Service Centre on Climate Change and Adapted Land Use, in the Department of Meteorology and Climate Science submitted to the School of Postgraduate Studies in partial fulfillment of the requirements for the award of the Degree of Doctor of Philosophy in Meteorology and Climate Science of The Federal University of Technology, Akure, Nigeria.

AUGUST, 2025

DECLARATION

I hereby declare that this is my own work and that it has not been submitted previously as a dissertation or thesis at any other University for the award of a degree.

Candidate's Name: GYUK Nehemiah John

Signature……... **Date**……...……

CERTIFICATION OF ORIGINALITY

We certify that this thesis entitled "Mechanism Underlying Enhanced Predictions of Atlantic Niño in the Equatorial Atlantic" is the outcome of the research carried out by Gyuk Nehemiah John under the WASCAL DRP-WACS in the Department of Meteorology and Climate Science of The Federal University of Technology, Akure, Nigeria.

Supervisor's Name:

Major Supervisor: Dr. Adedeji A. Adelodun

Signature……... **Date**……...…….

Co-supervisor: Prof. Vincent O. Ajayi

Signature……... **Date**……...…….

Co-supervisor: Dr Hyacinth C. Nnamchi

Signature……... **Date**……...…….

Director of WASCAL DRP: Prof. Ife A. Balogun

Signature……... **Date**……...…….

Head of Department: Prof. Vincent O. Ajayi

Signature……... **Date**……...…….

ABSTRACT

The Atlantic Niño is the dominant mode of interannual sea surface temperature (SST) anomalies in the equatorial Atlantic, exerting a profound influence on modulating global and regional weather patterns, including West African rainfall and tropical Atlantic hurricane activity. The dynamics of the Atlantic Niño share similarities with the El Niño-Southern Oscillation (ENSO) in the tropical Pacific, both involving atmosphere-ocean coupled positive feedback processes referred to as the Bjerknes positive feedback. Despite similarities with ENSO-particularly in its coupled ocean-atmosphere interactions, the Atlantic Niño has historically shown lower predictability and weaker ocean-atmosphere positive feedback strength. This thesis investigates the underlying physical mechanisms, classification, and evolving predictability of Atlantic Niño events using a combination of observational datasets, reanalysis products, and state-of-the-art seasonal forecast and global climate model outputs. The first component of the present study is to revisit the classical Bjerknes positive feedback loop that governs the dynamics of equatorial Atlantic SST anomalies. Using regression analyses of SST, zonal winds, zonal wind stress, upper heat content, sea surface height, and precipitation, the presence of a complete coupled positive feedback loop in the equatorial Atlantic was investigated. The results indicate that the SST-wind, SST-thermocline, and SST-heat content couplings are all active, with explained variances ranging from 21% to 46%. Additionally, the seasonal migration of the intertropical convergence zone (ITCZ) and associated changes in deep atmospheric convection are found to modulate the strength and spatial structure of the feedback processes. These findings underscore the central role of atmospheric diabatic heating in initiating and sustaining Atlantic Niño events.

The second component of the present study examines the evolving nature of atmosphere-to-ocean coupling over the equatorial Atlantic in recent decades. By comparing the periods 1979-1999 and 2000-2021 using both observations and a multi-model ensemble from the CMIP6 Atmospheric

Model Intercomparison Project (AMIP), the significant post-2000 weakening in key subprocesses of the Bjerknes feedback was identified and investigated. Specifically, the study observes a diminished sensitivity of deep convection to zonal SST gradients and a weaker relationship between precipitation and sea level pressure gradients. While the wind stress response to pressure gradients remains essentially unchanged, the overall weakening is most pronounced in the western and central equatorial Atlantic regions associated with peak convection and SST variability. These findings suggest a decline in the efficiency of coupled ocean-atmosphere feedback, with implications for the intensity, evolution, and forecast skill of Atlantic Niño events in a changing climate.

The third component of this research is to investigate the prediction skill of the Atlantic Niño events by distinguishing between canonical and non-canonical Atlantic Niño event types. Canonical Atlantic Niño events exhibit strong coupled dynamics analogous to Pacific ENSO events and are often preceded by La Niña-like SST variability in the tropical Pacific. These events can be predicted up to six months in advance using a 51-member ensemble operational seasonal forecast system from the European Centre for Medium-Range Weather Forecasts (ECMWF). In contrast, the non-canonical Atlantic Niño events lack strong atmosphere-ocean coupling and are scarcely predictable, but they lead to the emergence of a Pacific La Niña-like variability. This classification provides a new framework to disentangle the two-way connection between the equatorial Atlantic and the Pacific Oceans and improve seasonal climate prediction across the tropics.

The study results provide new insights into the coupled dynamics, classification, and evolving predictability of Atlantic Niño events.

DEDICATION

This thesis is dedicated to God Almighty and my parents, Mr. and Mrs. Gyuk John Musa, for their love and support.

ACKNOWLEDGMENTS

I thank God Almighty for his guidance and protection during this PhD journey and throughout my life. Many thanks to the Federal Ministry of Education and Research (BMBF), Germany, for sponsoring the WASCAL programme at the Federal University of Technology, Akure (FUTA DRP-WACS).

My appreciation goes to my supervisors, Dr. Adedeji A. Adelodun, Prof. Vincent O. Ajayi, and Dr Hyacinth C. Nnamchi for their supervision, assistance, guidance, support, and patience amidst their tight schedules. May God reward them and their families abundantly. I am greatly indebted to you all. I also thank the Director and staff of WASCAL Head Office, Accra, Ghana, and the Director, Prof. I. A. Balogun and staff of WASCAL DRP-WACS, FUTA, Nigeria, for their support during this study.

I also acknowledge the contributions of the management and staff of GEOM AR Helmholtz Zentrum für Ozeanforschung, Kiel, Germany, for hosting, mentoring, and providing resources during and after my research stay in Germany.

To my parents, Mr. and Mrs. Gyuk John Musa, and my siblings, Mrs. Abba Manasseh, Mrs. John Ukaeru, Joshua, Obed, and Benjamin, words cannot express my appreciation, because all I have achieved is a result of your support, love, and constant prayers. Thank you.

My appreciation goes to Dr. Henry Eke and Mrs. Esther Henry Eke for their assistance and contributions to ensure the completion of this programme.

Finally, to my colleagues in research at FUTA DRP-WACS and beyond, thank you all for your help. Thank you for the bond we share. God bless you all.

TABLE OF CONTENTS

LIST OF TABLES

LIST OF FIGURES

LIST OF ACRONYMS

Acronym	Meaning
AEWs	African Easterly Waves
ACC	Anomaly Correlation Coefficient
AGCM	Atmospheric General Circulation Model
AMIP	Atmospheric Model Intercomparison Project
AMM	Atlantic Meridional Mode
AMO	Atlantic Multidecadal Oscillation
Atl3	Atlantic Niño Index Region (3°S–3°N, 0°–20°W)
CFS	Climate Forecast System
C3S	Copernicus Climate Change Service
CMIP6	Coupled Model Intercomparison Project Phase 6
DJF	December-January-February
EAO	Equatorial Atlantic Oscillation
ECT	Equatorial Cold Tongue
ECMWF	European Centre for Medium-Range Weather Forecasts
ENSO	El Niño–Southern Oscillation
ERA5	ECMWF Reanalysis 5
EUC	Equatorial Undercurrent
GCM	General Circulation Model
GPCC	Global Precipitation Climatology Centre
GODAS	Global Ocean Data Assimilation System
HadISST	Hadley Centre Sea Ice and Sea Surface Temperature dataset
ITCZ	Intertropical Convergence Zone

JJA	June-July-August
MAM	March-April-May
MME	Multi-Model Ensemble
NCEP	National Centers for Environmental Prediction
NEC	North Equatorial Current
NECC	North Equatorial Countercurrent
ND	November-December
NOAA	National Oceanic and Atmospheric Administration
NorCPM	Norwegian Climate Prediction Model (NorCPM)
NMME	North American Multi-Model Ensemble
ORAS5	Ocean Reanalysis System 5
RMSE	Root Mean Square Error
SEC	South Equatorial Current
SST	Sea Surface Temperature
SSTA	Sea Surface Temperature Anomaly
SSH	Sea Surface Height
SLP	Sea Level Pressure
TAV	Tropical Atlantic Variability
WEA	Western Equatorial Atlantic index region (3°S-3°N, 40°-20°W)
WES	Wind-Evaporation-SST feedback
WMO	World Meteorological Organization

CHAPTER ONE

INTRODUCTION

1.1 BACKGROUND OF THE STUDY

Atmosphere-ocean interactions play a fundamental role in the climate system. The atmosphere and ocean interact with each other through exchange of energy, momentum, and moisture across the ocean-atmosphere interface, regulating key climate processes on timescales ranging from days to decades (Trenberth et al., 1998; Kirtman et al., 2009). The ocean stores and redistributes vast amounts of heat, while the atmosphere responds to and reinforces oceanic variabilities through changes in wind, precipitation, and pressure. These interactions form a complex, coupled feedback mechanism that regulates climate variability and influences climate changes at the global and regional scales (Wang et al., 2004; McPhaden et al., 2006).

Among these interactions, sea surface temperature (SST) variability is a key driver of the atmosphere-ocean coupling. SST anomalies interact with the atmosphere to modify atmospheric convection, alter wind patterns, and trigger feedback mechanisms such as the Bjerknes positive feedback (Bjerknes, 1969; Neelin et al., 1998). These coupled interactions are especially pronounced in tropical ocean basins, where strong coupling leads to recurring climate phenomena like the El Niño-Southern Oscillation (ENSO) in the Pacific (Xie & Carton, 2004).

The tropical Pacific Ocean is home to the most prominent and extensively studied coupled climate phenomenon: El Niño Southern Oscillation (ENSO). It arises from complex interactions between SST anomalies, trade wind variability, and changes in thermocline depth along the equatorial Pacific. During El Niño events, weakened easterly winds reduce upwelling in the eastern Pacific, deepen the thermocline, and allow warm waters to accumulate at the surface, enhancing warming through the Bjerknes positive feedback (Bjerknes, 1969). In contrast, the La Niña phase of ENSO is associated

with increased upwelling and stronger easterly winds, which amplify cold anomalies. ENSO has a significant influence on the global climate, affecting precipitation, droughts, floods, and tropical cyclones (Cai et al., 2021).

Given its pronounced global influence and relatively high predictability, ENSO is widely regarded as a benchmark for investigating tropical climate variability. Its extensive basin size, strong ocean–atmosphere coupling, and systematic alignment with the seasonal cycle underpin forecast skill that, in some cases, extends to lead times of approximately 12 months (Luo et al., 2008; Capotondi et al., 2015). Other tropical basins also exhibit interannual variability involving coupled atmosphere-ocean dynamics, such as the Indian Ocean Dipole and basin-wide modes (Wu & Tang, 2019; Zhao et al., 2020; Liu et al., 2021), as well as several modes in the Atlantic Ocean, including the Atlantic Meridional Mode (AMM) and the Atlantic Niño (Cai et al., 2019; Li et al., 2020; Wang et al., 2021; Richter et al., 2017).

Two dominant modes characterize tropical Atlantic SST variability: the AMM and the Atlantic Zonal Mode, often referred to as the Atlantic Niño. The AMM exhibits a meridional gradient of SST anomalies between the Northern and Southern Hemispheres and is governed by positive wind-evaporation-SST (WES) feedback. This feedback typically peaks in the boreal spring (March to May, MAM) and influences the seasonal migration of the Intertropical Convergence Zone (ITCZ) (Xie & Philander, 1994; Chang et al., 1997). For instance, anomalously warm SST in one hemisphere reduces surface pressure, enhances cross-equatorial winds, and amplifies SST gradients. The AMM modulates the precipitation patterns, the position of the ITCZ, and hurricane activity in the Atlantic. Its interactions with other climate modes, such as the Atlantic Zonal Mode and ENSO, add further complexity to tropical Atlantic variability (Ruiz-Barradas et al., 2000; Knight et al., 2006; Richter et al., 2014). Also known as the interhemispheric gradient mode or dipole mode, the AMM's structure extends across the subtropical North and South Atlantic (Hastenrath & Heller, 1977).

In contrast, the Atlantic Niño is a zonal mode centered along the equator, involving warm SST anomalies in the cold tongue region and associated atmospheric responses. It resembles ENSO in dynamics and exhibits zonal structures in wind stress, thermocline, and SST variability that are primarily governed by dynamics similar to ENSO, but with weaker amplitude, distinct seasonal phase locking, and lower predictability (Xie & Carton, 2004; Lübbecke et al., 2018; Nnamchi et al., 2021).

The Atlantic Niño typically develops in the boreal spring (March-May, MAM), peaks in the summer (June-August, JJA), and then dissipates in the fall, with anomalies concentrated in the eastern equatorial Atlantic cold tongue (Xie et al., 2004; Richter et al., 2017; Vallès-Casanova et al., 2020).

The ocean-atmospheric coupled processes during Atlantic Niño events are marked by weakened trade winds, a deepened thermocline, and enhanced convection, impacting rainfall over West Africa, Brazil, and parts of Europe, and modulating Atlantic hurricane activity (Okumura & Xie, 2006; Giannini et al., 2003; Rodríguez-Fonseca et al., 2011).

Beyond this canonical feedback, several other mechanisms influence Atlantic Niño variability. Equatorial wave dynamics, particularly Kelvin and Rossby waves, modulate thermocline depth and surface warming (Philander & Pacanowski, 1986; Foltz & McPhaden, 2010). Deep equatorial jets can propagate upward and modify subsurface heat, potentially surfacing later as SST anomalies (Brandt et al., 2011).

Remote influences also play a role. Anomalously warm SSTs in the northern tropical Atlantic during spring can induce cross-equatorial wind anomalies and drive warm water advection into the cold tongue region, preconditioning the basin for event development (Richter et al., 2012). In addition, stochastic atmospheric perturbations, such as synoptic wind bursts, can drive thermodynamic SST anomalies even without strong oceanic feedback (Chang et al., 2006; Nnamchi et al., 2015). These

processes contribute to the diversity and intermittency of Atlantic Niño events, making them challenging to characterize with a single mechanism.

Predicting Atlantic Niño events remains challenging. Predictive skill is typically limited to a 2-3 month lead time and declines rapidly after boreal spring due to weaker ocean-atmosphere coupling, sensitivity of model initialization, and perturbations from atmospheric noise (Ding et al., 2010). Systematic model biases, particularly cold-induced SST biases in the cold tongue and errors in the representation of the trade winds, further limit prediction skill (Richter et al., 2014; Grodsky et al., 2012).

Despite ongoing efforts, major gaps persist in understanding the physical mechanisms, event diversity, and drivers of the recent weakening associated with the prediction skill of Atlantic Niño events. The phenomenon's lower predictability compared to ENSO has been attributed to a mix of unresolved dynamics (Davey et al., 2002), model biases (Richter & Xie, 2008; Ding et al., 2012; Lübbecke et al., 2018), and strong stochastic forcing (Tang et al., 2018; Hu & Huang, 2007).

Moreover, recent studies indicate a weakening trend in Atlantic Niño variability over the past two decades (Tokinaga et al., 2011; Prigent et al., 2020; Silva et al., 2021). This shift has been linked to a declining Bjerknes feedback efficiency (Prigent et al., 2020) and potential influences from anthropogenic climate change (Yang et al., 2022). These emerging complexities contribute to the low predictive skill of the Atlantic Niño and underscore the urgent need for a refined understanding of the Atlantic Niño's dynamics for better representation in forecast systems.

This study aims to provide a clearer understanding of the dynamic atmosphere-ocean mechanisms driving Atlantic Niño events in the equatorial Atlantic, to improve their prediction skill. The approach emphasizes two key components: (i) atmospheric deep convection-ocean coupling linked to the meridional migration of the Intertropical Convergence Zone (ITCZ), and (ii) the zonal thermocline feedback, which together regulate the seasonality of the Atlantic Niño as explained here:

An initial SST anomaly in the eastern equatorial Atlantic alters the zonal SST gradient, which in turn modifies the vertical profile of atmospheric diabatic heating through changes in convection, water vapor, cloud cover, and precipitation (Houze, 1982; Hartmann et al., 1984) over the equatorial Atlantic. The net effect is an increase in the vertical gradient of diabatic heating. The increased diabatic heating slows the tropospheric zonal circulation at the equator (Houze, 1982; Chiang et al., 2001), known as the Walker circulation. As a result, a westerly zonal wind stress anomaly develops (Nnamchi et al., 2021).

In response to the wind stress anomaly, the zonal slope of the equatorial thermocline decreases, resulting in an increase in upper ocean heat content in the east and a decrease in the west. As heat content increases, sea surface height also increases (Keenlyside and Latif, 2007; Dippe et al., 2018). Therefore, sea surface height can be used as an indicator of upper ocean heat content (Rebert et al., 1985). Finally, the so-called thermocline feedback amplifies the initially positive SST anomaly in the east. The change in diabatic heating drives the atmospheric circulation and is thus intensely involved in the positive ocean-atmosphere feedback, summarized in the Bjerknes feedback loop (Figure 1.1).

Recent studies indicate a weakening trend in the variability of the Atlantic Niño over the past two decades (Tokinaga et al., 2011; Prigent et al., 2020; Silva et al., 2021). Prigent et al. (2020) reported that the changes in SST variability in the eastern equatorial Atlantic are due to the combined effect of the weakening of the positive Bjerknes feedback since 2000. Yang et al. (2022), on the other hand, discussed the possible roles of global warming in the weakening of the Atlantic Niño/Niña. This weakening may have important implications for the frequency, intensity, and predictability of Atlantic Niño events, although the extent of these impacts remains uncertain.

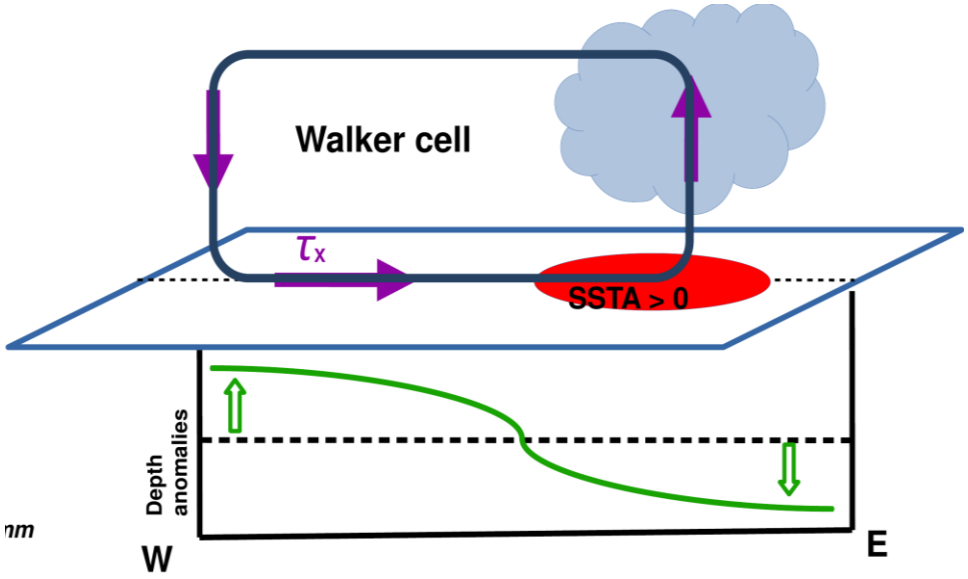

Figure 1.1: Graphical representation of atmospheric deep convection-ocean coupling and thermocline feedback (Nnamchi et al., 2021).

1.2 STATEMENT OF PROBLEM

The Intergovernmental Panel on Climate Change (IPCC, 2021) highlights that variability of tropical sea surface temperatures (SSTs), particularly in the equatorial oceans, is crucial in modulating regional and global climate extremes. In the equatorial Atlantic, the Atlantic Niño is the dominant mode of interannual SST variability and exerts a significant influence on climate-sensitive regions.

In West Africa, positive SST anomalies in the cold tongue region enhance deep atmospheric convection and promote increased moisture transport to the Sahel and the Gulf of Guinea, strengthening the West African monsoon and leading to wetter-than-normal conditions (Folland et al., 1986; Mohino et al., 2011). Conversely, cold-phase events suppress convection and are associated with precipitation deficits and drought.

In South America, particularly in the Amazon Basin and northeastern Brazil, Atlantic Niño events disrupt the regional Hadley circulation and delay the onset of the rainy season. This results in reduced precipitation and increased vulnerability to agriculture (Giannini et al., 2003; Nobre & Shukla, 1996; Rodrigues et al., 2020).

Atlantic Niño conditions also influence hurricane activity in the Atlantic, often suppressing storm formation by enhancing vertical wind shear and stabilizing the lower troposphere over the main development region (Okumura & Xie, 2006; Murakami et al., 2018; Vallès-Casanova et al., 2020). These far-reaching and diverse impacts underscore the need for a better understanding and prediction of the variability of the Atlantic Niño, as its dynamics directly affect water resources, food production, disaster risk reduction, and socioeconomic resilience in several vulnerable regions.

Although the Atlantic Niño shares similar dynamical characteristics with ENSO in the Pacific-particularly the positive atmosphere-ocean interaction (thermocline feedback), its predictive skill remains significantly lower (Timmermann et al., 2018; Hu & Huang, 2007; Ding et al., 2012). This

limited predictability is partly due to the incomplete understanding of the coupled ocean-atmosphere processes that determine SST variability in the equatorial Atlantic, as well as the recently reported weakening of the positive atmosphere-ocean feedback in recent decades (Prigent et al., 2020; Yang et al., 2022).

Other important factors include persistent mean state biases in coupled climate and ocean models, particularly in the simulation of the Atlantic cold tongue, trade wind strength, and thermocline slope. These biases limit the models' ability to reproduce the spatial and temporal structure of Atlantic Niño events (Richter & Xie, 2008; Xu et al., 2014; Dippe et al., 2019). As a result, seasonal forecasting systems struggle to capture the signals of Atlantic Niño events accurately, in contrast to the relatively good predictions for ENSO (Luo et al., 2008; Counillon et al., 2021).

Furthermore, teleconnections, particularly those associated with ENSO, exert an additional influence on the evolution and dynamics of the Atlantic Niño through atmospheric bridging and wave responses (Lübbecke & McPhaden, 2012; Exarchou et al., 2021). These external influences interact nonlinearly with the local dynamics, complicating event attribution and biasing model-based predictions (Keenlyside & Latif, 2007; Mohino et al., 2011; Bellenger et al., 2014).

Despite significant progress in observing and modeling tropical Atlantic variability, the predictive skill of the Atlantic Niño event remains persistently low. This understanding underscores the need to comprehend its underlying mechanisms better and to develop forecast frameworks tailored explicitly to the equatorial Atlantic (Nnamchi & Latif, 2025).

1.3 RESEARCH QUESTIONS

This research study is guided by the following research questions, which aim to deepen our understanding of the dynamics, evolution, and predictability of Atlantic Niño events in the equatorial Atlantic.

The research questions are:

i. How does the coupling between deep atmospheric convection and thermocline feedback influence SST variability in the equatorial Atlantic?

ii. What are the causes of the observed weakening of coupled atmosphere-ocean feedback processes in the equatorial Atlantic since 2000?

iii. What role does atmospheric preconditioning associated with the northward migration of the Intertropical Convergence Zone (ITCZ) play in the initiation and development of Atlantic Niño events?

iv. How predictable are Atlantic Niño events in the seasonal forecast systems of the European Centre for Medium-Range Weather Forecasts (ECMWF)?

1.4 AIM AND OBJECTIVES

This study aims to investigate the underlying mechanisms that enhance the seasonal predictability of Atlantic Niño events in the equatorial Atlantic.

The specific objectives of the research are to:

i. evaluate the ocean-atmosphere coupled processes influencing Atlantic Niño variability in the equatorial Atlantic;

ii. investigate key mechanisms potentially driving the weakened atmosphere-to-ocean Bjerknes positive feedback processes using CMIP6 AMIP models;

iii. characterize and analyze the evolution of extreme Atlantic Niño events; and

iv. assess the forecast skill of Atlantic Niño events using seasonal forecast systems.

1.5 JUSTIFICATION

Interannual and seasonal variability in sea surface temperature (SST) over the equatorial Atlantic is a characteristic feature of the tropical Atlantic climate system, with far-reaching implications for regional hydrology, atmospheric circulation, and marine ecosystem (Richter et al., 2018; Doi et al., 2019; Worou et al., 2022).

One of the most prominent variabilities is the Atlantic Niño, characterized by warm SST anomalies in the eastern equatorial Atlantic. This mode typically peaks during the boreal summer (June-August), with some events also exhibiting a second peak during the boreal winter (November-December), often referred to as Atlantic Niño II (Lübbecke & McPhaden, 2017). Although the Atlantic Niño shares dynamical similarities with the Pacific ENSO, including coupled ocean-atmosphere feedback, it generally exhibits weaker amplitude, shorter persistence, and lower predictability (Lübbecke & McPhaden, 2013; Bellenger et al., 2014; Richter et al., 2017).

In recent decades, the amplitude and frequency of Atlantic Niño events have decreased, leading to recent interest in the scientific community due to their implications for seasonal forecasting and regional precipitation variability, particularly in West Africa and northeastern South America (Prigent et al., 2020; Silva et al., 2021; Rodrigues et al., 2020). These changes are associated with a reduction in the strength of the atmosphere-ocean feedback, enhanced damping by turbulent heat fluxes, and increased background SST warming. All of these factors have contributed to altered SST dynamics

in the eastern equatorial Atlantic (Tokinaga & Xie, 2011; Yang et al., 2022). These physical changes challenge the assumption of stationarity in Atlantic Niño dynamics and raise concerns about the reliability of existing forecast skill in a warmer climate.

Studies have shown that modern seasonal forecast systems continue to have limited predictive skills for Atlantic Niño events, especially beyond short lead times (Richter et al., 2018; Exarchou et al., 2021). This knowledge gap is attributed to several factors, including the incomplete representation of key atmosphere-ocean feedback processes, systematic biases in the simulation of the Atlantic cold tongue and trade winds, and inadequate initialization of ocean subsurface conditions (Dippe et al., 2019; Bayr et al., 2020).

Given these challenges, there is a need to revisit and refine the underlying physical mechanisms governing Atlantic Niño dynamics, with a focus on diagnosing the dynamics of ocean-atmosphere coupling. Investigating the role of ENSO-like dynamics, the influence of the atmospheric convection-ocean coupling associated with the Intertropical Convergence Zone (ITCZ), and the dynamics of thermocline feedback is crucial for enhancing seasonal forecasts.

Furthermore, the Atlantic Niño's teleconnections with other climate modes, particularly ENSO, remain underrepresented in operational forecast systems, despite their potential to modulate the evolution of Atlantic SSTs and associated precipitation anomalies (Exarchou et al., 2021; Doi et al., 2019). A deeper understanding of these cross-basin interactions is essential not only for gaining theoretical knowledge but also for improving operational seasonal forecasts in climate-sensitive regions, such as the West African region, the Sahel, the Amazon Basin, and the Atlantic tropical hurricane belt. Such improvements have direct implications for disaster risk reduction, agricultural planning, and water resource management.

1.6 STRUCTURE OF THE THESIS

This thesis is divided into five chapters. Chapter one introduces the study and explains its background, the underlying problem, and the associated research questions. It also outlines the study's aim and objectives and its justification. Chapter Two focuses on reviewing literature relevant to this study. Chapter Three provides a detailed discussion of the methodological approaches adopted, including the data used to address each objective. Chapter Four presents and discusses the research findings. Lastly, Chapter Five concludes the thesis by discussing the conclusion and recommendations.

CHAPTER TWO

2.0 LITERATURE REVIEW

2.1 Tropical Atlantic Variability

Tropical Atlantic variability (TAV) refers to the fluctuations in sea surface temperature (SST), atmospheric circulation, and coupled air-sea interactions that occur over the equatorial and tropical Atlantic. These fluctuations occur on interannual, seasonal, and decadal timescales and are driven by a range of dynamic and thermodynamic processes, including feedback loops involving the exchange of heat, momentum, and moisture. TAV is spatially and temporally heterogeneous, significantly influencing regional and global climate patterns, particularly precipitation variability over West Africa, South America, and the Atlantic tropical hurricane belt.

In recent decades, significant progress has been made in understanding its mechanisms, modes, impacts, and predictability in the tropical Atlantic. This progress is supported by improved observations (e.g., the PIRATA buoy array; Bourlès et al., 2008), several satellite-based remote sensing measurements, and improved coupled climate modeling efforts, such as those of the Coupled Model Intercomparison Project (CMIP). Despite the challenges in simulating the mean state and variability of the tropical/equatorial Atlantic, these instruments have advanced knowledge of TAV dynamics and improved forecasting skill (Richter et al., 2014).

These advances have not only deepened our understanding of TAV but have also improved forecasting capabilities and provided essential tools for addressing the socioeconomic impacts of climate variability in the tropical/equatorial Atlantic region.

Historical research on TAV began in the 1960s and 1970s. Initial studies examined recurring patterns of tropical sea surface temperature (SST) variability and trade wind anomalies and their impacts on regional precipitation patterns (Folland et al., 1986). The Sahel drought of the 1970s highlighted the

climatic importance of the tropical Atlantic, particularly its role in modulating the position of the Intertropical Convergence Zone (ITCZ) and associated precipitation variability over West Africa (Lamb, 1978). These early findings led to increased research into the mechanisms linking SST anomalies, atmospheric convection, and precipitation.

TAVs also modulate regional climate dynamics, influencing precipitation patterns, hurricane activity, and the annual climate variability of surrounding continents. For example, SST variability in the tropical Atlantic can modulate the latitude of the ITCZ, thereby influencing precipitation patterns over West Africa and northeastern South America (Zebiak, 1993). SST anomalies affect not only regional precipitation but also the frequency and intensity of tropical cyclones in the Atlantic hurricane basin, thus affecting the livelihoods and economies of coastal communities in the Caribbean and the Americas (Goldenberg et al., 2001).

The TAV is also linked to global climate variability through cross-basin teleconnections. Fluctuations in SST anomalies in the tropical Atlantic can influence and be influenced by climate anomalies in the Pacific, such as the El Niño-Southern Oscillation (ENSO) and the Indian Ocean. These cross-basin interactions affect monsoon systems, atmospheric circulation, seasonal precipitation patterns, and global climate forecasting. Such interactions underline the importance of understanding the TAV for improving monthly, seasonal, and decadal climate forecasts.

2.1.1 Characteristics and Drivers of Variability in the Tropical Atlantic

The dynamics in the tropical Atlantic are determined by a combination of atmosphere-ocean interactions that regulate the exchange of heat, moisture, and momentum between the ocean and atmosphere via coupled positive-negative feedback mechanisms. Several distinct modes of variability have been identified:

Atlantic Zonal Mode (Atlantic Niño): This mode, characterized by interannual SST anomalies along the eastern equatorial Atlantic (3°S-3°N, 0°-20°W), which typically peaks during the boreal summer,

is one of the dominant modes of the annual TAV characteristics (Foltz and McPhaden 2010; Wang, 2019; Martín-Rey et al., 2019; Richter and Tokinaga, 2020). The Atlantic Niño typically develops in the boreal spring, peaks in summer, and dissipates in autumn (Xie et al., 2004; Richter et al., 2017; Lübbecke et al., 2018; Vallès-Casanova et al., 2020; Nnamchi et al., 2021). The Atlantic Niño is characterized by anomalously warm SST anomalies in the eastern part of the equatorial Atlantic (Carton and Huang, 1994; Lübbecke et al., 2018) and large-scale air-sea interactions, which particularly influence deep atmospheric convection over the ocean and surrounding continents (Ruiz Barradas et al., 2000; Giannini, 2003). The Atlantic Niño is associated with rainfall in West Africa and northeastern Brazil (Nobre and Shukla, 1996; Giannini et al., 2003; Vallès-Casanova et al., 2020), the development of tropical hurricanes in the Atlantic (Kim et al., 2023), and the European climate (Chen et al., 2024).

The Atlantic Niño shares some similarities with the El Niño-Southern Oscillation (ENSO). Like ENSO, the Atlantic Niño is primarily driven by the Bjerknes feedback (Bjerknes, 1969; Planton et al., 2018; Prodhomme et al., 2019). This is the coupling between atmospheric and oceanic variability, which leads to characteristic Niño-like SST variability (Zebiak, 1993; Keenlyside and Latif, 2007; Dippe et al., 2018). However, compared to ENSO, the Atlantic Niño is scarcely predictable, and the reasons for this are not yet fully understood (Davey et al., 2002; Kushnir et al., 2006; Hu and Huang, 2007; Luo et al., 2008; Tang et al., 2018; Brierley and Wainer, 2018). In addition to the Bjerknes positive feedback, other mechanisms have been proposed for the Atlantic Niño. These include vertical energy propagation by deep equatorial jets (Brandt et al., 2011), advection of warm waters from the northern tropical Atlantic (Richter et al., 2013), reflection of the equatorial Rossby wave into an equatorially trapped Kelvin wave (Foltz and McPhaden, 2010), and thermodynamic feedback, as represented in simplified models without active ocean circulation (Nnamchi et al., 2015).

Atlantic Meridional Mode (AMM): The Atlantic Meridional Mode refers to the meridional dipole of SST anomalies with opposing SST anomalies in the Northern and Southern Hemispheres. It is often

active in boreal spring and is related to equatorial winds, ITCZ shift, and interhemispheric energy exchange (Servain et al., 2000; Foltz and McPhaden, 2010).

Several critical dynamical and thermodynamic processes additionally modulate the variability of the tropical Atlantic:

Bjerknes positive feedback: This positive feedback involves interactions between SST gradients, weakened trade winds, and reduced upwelling and deepening of the thermocline in the eastern equatorial Atlantic, which further amplifies SST anomalies (Bjerknes, 1969; Zebiak, 1993; Keenlyside and Latif, 2007).

Wind-evaporation-SST feedback (WES): This mechanism is a surface process that describes how surface winds modulate evaporation rates and SSTs, thus creating a positive feedback loop. For example, stronger trade wind anomalies increase evaporation and cool the ocean surface, which amplifies initial SST anomalies and influences atmospheric circulation patterns (Xie and Carton, 2004).

Ocean wave dynamics: Equatorial Kelvin and Rossby waves, generated by changes in zonal wind stress, influence the depth of the thermocline and redistribute heat. They thereby influence the evolution of surface temperatures (SST) and the heat content of the upper ocean layers in the tropical Atlantic (Philander and Pacanowski, 1986).

ITCZ migration: The seasonal and interannual dynamics of the Intertropical Convergence Zone (ITCZ) modulate solar heating and vertical convection, which in turn influences ocean stratification and SST gradients (Mitchell and Wallace, 1992; Xie and Carton, 2004).

In his study of tropical ocean-atmosphere interactions, Bjerknes (1969) identified a positive feedback mechanism in which anomalously warm SST in the equatorial Pacific leads to weakened trade winds, which further deepen the thermocline and reduce buoyancy, thereby amplifying SST anomalies. This concept, known as the Bjerknes positive feedback, has since been applied to the tropical Atlantic and

underpins much of the understanding of the Atlantic Niño mode of variability, which also involves ocean-atmosphere coupling.

Zebiak (1993) examined ocean-atmosphere interactions over the equatorial Atlantic and proposed that while the Atlantic Niño shares similarities with the Pacific ENSO, it differs in that it has a weaker coupling strength and more erratic behavior. He showed that thermocline variations, zonal wind stress anomalies, and oceanic wave dynamics influence SST variability in the equatorial Atlantic. He emphasized the role of equatorial Kelvin and Rossby waves in shaping interannual variability in the region.

Servain et al. (2000) analyzed long-term data on SST, wind, and sea level. They were among the first to empirically establish the Atlantic zonal mode and the AMM as dominant interannual modes in the tropical Atlantic. Their study showed that interhemispheric SST gradients and the seasonal pattern of wind stress anomalies contribute significantly to variability in the tropical Atlantic. They concluded that both local feedback and large-scale atmospheric circulation patterns contribute to the development of SST anomalies in the region.

Xie and Carton (2004) provided a comprehensive review of tropical Atlantic variability (TAV), emphasizing the presence of three dominant modes: the Atlantic zonal mode, the Atlantic meridional mode, and a seasonal SST mode. They stressed the importance of the positive Bjerknes feedback and the wind-evaporation-SST feedback in maintaining SST variability. They highlighted the role of continental monsoon systems in modulating atmosphere-ocean interactions over the Atlantic. Their work established a fundamental understanding of the local and remote drivers of TAV. Okumura and Xie (2006) shed light on previously overlooked aspects of the tropical Atlantic climate and introduced a new Niño-like mode in the central equatorial Atlantic, which exhibits unique seasonality and spatial structure. They showed that long-range wind forcing and asymmetric SST distribution play a more critical role in the development of the cold tongue than local processes. Their study

challenged the notion of a purely Pacific-Atlantic Niño and advocated a more nuanced view that considers ITCZ migration and extra-equatorial influences.

Richter and Xie (2008) investigated the causes of equatorial Atlantic SST biases in coupled general circulation models and found that systematic errors, including a cold tongue bias, a mislocated ITCZ, and inaccurate trade winds, significantly affect the simulation of Atlantic variability. Their results linked these mean errors to model deficiencies in the representation of zonal wind stress and thermocline slope, highlighting the need for better parameterizations to improve Atlantic Niño simulations.

Polo et al. (2008) focused on the role of equatorial wave dynamics in interannual SST variability. They demonstrated that Kelvin and Rossby waves, generated by changes in zonal wind stress, play a central role in modulating thermocline depth and, consequently, in shaping SST evolution during Atlantic Niño events. Their study provided necessary observational and modeling evidence for the influence of wave propagation timescales on the timing and intensity of Atlantic Niño events.

Foltz and McPhaden (2010) investigated the interaction between the Atlantic Meridional Mode (AMM) and the Atlantic Niño Mode. They found that the AMM causes equatorial wind anomalies, which in turn influence thermocline depth and the evolution of SST variability in the eastern equatorial Atlantic. Their work suggests that off-equatorial variability, particularly during boreal spring, plays a significant role in the development of Atlantic Niño events.

Lübbecke et al. (2018) summarized research on equatorial Atlantic variability and identified three major SST modes: the Atlantic Niño, the Atlantic meridional mode, and a spring SST mode. They demonstrated how thermocline depth anomalies, wind stress variability, and seasonal phase coupling determine the amplitude and timing of Atlantic Niño events. The authors also emphasized the importance of global teleconnections, particularly those related to ENSO and the Indian Ocean Dipole, in modulating variability in the equatorial Atlantic. Martín-Rey et al. (2019) investigated the

role of ocean dynamics in shaping Atlantic equatorial modes. They found that variability in zonal currents, wind forcing, and thermocline structure critically influences the spatial distribution and seasonal timing of equatorial SST anomalies. Their work demonstrated that the interplay between oceanic internal dynamics and atmospheric forcing is crucial in explaining the diversity and irregularity of Atlantic Niño events. It suggests that changes in oceanic memory and background conditions contribute to event-to-event variability.

Despite these advances, key gaps remain in our understanding of tropical Atlantic variability. First, the relative importance of different drivers such as local air–sea interactions versus remote ENSO and Indian Ocean influences remains debated. Second, observations indicate a weakening of Atlantic Niño variability since 2000; however, the causes, whether anthropogenic warming, natural decadal variability, or changes in coupling strength, remain unclear. Third, the role of subsurface processes (e.g., thermocline feedback, Kelvin wave propagation) in shaping SST variability compared to surface forcing requires further clarification. Fourth, the predictability of Atlantic Niño events is significantly lower than that of ENSO, and the mechanisms limiting prediction skill are not well established. Finally, many climate and forecast models exhibit persistent biases in the equatorial Atlantic cold tongue, raising questions about the reliability of simulated variability and its predictability.

2.1.2 Seasonal Cycle and Coupled Feedback

The seasonal cycle is a fundamental component of Tropical Atlantic Variability (TAV), driven primarily by the annual solar radiation cycle and the resulting migration of the Intertropical Convergence Zone (ITCZ). Seasonal SST variations in the equatorial Atlantic are closely linked to changes in wind intensity, thermocline depth, upwelling strength, and atmospheric convection, all of which interact through coupled ocean-atmosphere feedback.

As the year progresses, the seasonal cycle of sea surface temperature (SST) anomalies in the eastern equatorial Atlantic is closely linked to variations in trade wind intensity and the position of the Intertropical Convergence Zone (ITCZ). In this narrow band, the northeast and southeast trade wind systems converge. During boreal spring (March-May), weakening of the southeasterly trade winds leads to reduced upwelling and enhanced surface heating in the eastern equatorial Atlantic. These conditions give rise to a warming of SST anomalies that peaks between June and August, known as the seasonal Atlantic warming. This warming coincides with the northward shift of the ITCZ, which transports moisture and energy into the northern tropics and supports the West African monsoon (Mitchell and Wallace, 1992). By July, intensified zonal trade winds reestablish the east-west zonal pressure gradient, driving upwelling and leading to seasonal cooling and the formation of a prominent equatorial cold tongue, centered slightly south of the equator, reflecting the interplay of dynamic and thermodynamic processes. This cooling is particularly strong along the eastern boundary due to coastal upwelling and is further enhanced by equatorial divergence and thermocline shoaling (Houghton, 1983; Philander and Pacanowski, 1986).

Despite the nearly symmetric distribution of solar radiation across the equator, the climatological ITCZ and associated rainfall band are persistently displaced 5°-10° north of the equator (Xie and Carton, 2004). This asymmetry arises from the SST structure and cross-equatorial winds that maintain a strong meridional gradient. The ITCZ reaches its northernmost extent in boreal summer (July-September), when rainfall over land is intensified, while the oceanic ITCZ lags due to the ocean's higher heat capacity (Grodsky and Carton, 2003). The ITCZ is also associated with the latitude of minimum seasonal variance of SST and the latitude of maximum vertical displacement of the thermocline (Houghton, 1983).

The Intertropical Convergence Zone (ITCZ) and its associated band of continental convection exhibit significant seasonal shifts over the Atlantic. Over land, the position of the rain band generally tracks

the seasonal movement of the sun, reaching its northernmost extent during July–September and its southernmost position in December-February (Fu et al., 2001; Biasutti et al., 2004). However, the observed delay between the sun's position and the meridional migration of the continental rain band suggests the influence of additional heat sources, including oceanic influences and heat stored in soil moisture. Key contributors to this delay include soil moisture dynamics and the thermal impact of adjacent oceans.

Over the ocean, sea surface temperature (SST) variability and the position of the ITCZ are closely linked, with major rainfall concentrated within a band of high SSTs exceeding 27°C. During March-April, the ITCZ aligns nearly with the equator, where trade winds from both hemispheres converge. During this period, SSTs in the equatorial region (10°S-5°N) are uniformly warm, making the Atlantic ITCZ particularly sensitive to even minor variations in the interhemispheric SST gradient. As the equatorial cold tongue forms in June and persists through September, the ITCZ remains north of the equator, following the seasonal migration of the high-SST band. Simultaneously, a secondary, smaller convective zone develops south of the equator, west of 30°W (Grodsky and Carton, 2003). The oceanic ITCZ reaches its northernmost position in September, lagging behind its continental counterpart due to the higher heat capacity of the ocean's mixed layer. Notably, precipitation over the ocean is strongest during July-August, despite a 1°C decrease in underlying SSTs compared to March-April. The strengthening of ITCZ convection during this period may be attributed to the prevalence of strong westward-propagating easterly wave disturbances, which play a critical role in triggering convection over the ocean. These disturbances originate from the African rain band (Thorncroft et al., 2003) and intensify as they traverse the tropical Atlantic, with some developing into tropical storms and hurricanes that significantly impact the Caribbean and southern United States (Gray and Landsea, 1992). In addition to the 3-9-day African easterly waves, the tropics also exhibit a quasi-stationary summer pattern of winds and precipitation with a periodicity of approximately two

weeks. This longer-period variability appears to result from complex land-atmosphere interactions (Janicot and Sultan, 2001; Grodsky and Carton, 2001).

Along the equator, SST exhibits a pronounced annual cycle despite the predominantly semiannual nature of solar heating, a pattern also observed in the eastern Pacific. On average, at 10°W along the equator, SST peaks at 28°C during March-April but drops sharply to below 23°C by July-August. This seasonal warming and cooling are highly asymmetric, with the cooling phase occurring over just three months, compared to the seven months required for warming. From an oceanic perspective, this rapid cooling is driven by the abrupt onset of the West African monsoon and the rapid intensification of southerly winds in the Gulf of Guinea during May-June. These southerly winds induce upwelling slightly south of the equator and downwelling slightly north, with the upwelling cooling the equatorial ocean (Philander and Pacanowski, 1981). The winds in the equatorial Atlantic exhibit pronounced convergence and divergence patterns, decelerating over the cold tongue and accelerating again over the warmer waters just north of the equator. These wind variations play a crucial role in shaping the annual SST cycle by driving upwelling through zonal and meridional divergence and tilting the thermocline depth along the equator. From April to August, the thermocline in the equatorial Gulf of Guinea shoals by over 60 meters, contributing significantly to the cooling of SST in this region (Houghton, 1983; Philander and Pacanowski, 1986).

Changes in zonal wind strength also influence wind-induced evaporation, further impacting the equatorial SST annual cycle. From a coupled perspective, Xie (1994) demonstrates that the northward displacement of the climatological ITCZ is the primary driver of the SST annual cycle in both the Pacific and Atlantic. This displacement sustains southerly cross-equatorial winds, which strengthen during boreal summer and fall and weaken in boreal spring (Giese and Carton, 1994). Observational analysis by Mitchell and Wallace (1992) suggests that in the equatorial Pacific, the SST annual cycle begins in the east due to seasonal monsoonal winds and propagates westward

through air-sea interactions. However, unlike the equatorial Pacific, where air-sea interaction dominates, the narrower tropical Atlantic and the influence of strong continental convective zones mean that continental monsoons play a more prominent role in shaping the SST annual cycle.

Atmospheric general circulation model (AGCM) experiments revealed that seasonal variations in cross-equatorial winds over the Gulf of Guinea are primarily driven by the continental monsoon (Li and Philander, 1997). The annual cycle of equatorial zonal wind, however, is influenced by both the continental monsoon and its interaction with equatorial SST-mechanisms that dominate in the eastern and western halves of the basin, respectively (Okumura and Xie, 2006). In experiments where the seasonal development of the equatorial cold tongue is suppressed, anomalous easterlies still emerge in May and June over the eastern equatorial Atlantic. These anomalies are attributed to increased cross-equatorial advection of zonal momentum and a redistribution of monsoonal rainfall, highlighting the critical role of atmospheric processes in shaping the region's seasonal dynamics.

Philander and Pacanowski (1981) provided earlier observational insights into the equatorial Atlantic's annual SST cycle, emphasizing the role of southerly wind surges during boreal spring and early summer in inducing upwelling-driven cooling. Their work highlighted the asymmetric timing of the seasonal SST cycle, with cooling occurring more rapidly than warming, influenced by the onset of the West African monsoon.

Houghton (1983) investigated the seasonal variation in SST and thermocline depth along the equator and showed that the strongest upwelling and cold tongue formation occur in the eastern equatorial Atlantic from June to August. His findings linked southeasterly wind intensification, ocean divergence, and thermocline shoaling to the rapid SST cooling phase observed during boreal summer. These dynamics help explain the strong asymmetry between the seasonal warming and cooling phases.

Philander and Pacanowski (1986) examined the role of equatorial ocean wave dynamics in the development of the Atlantic cold tongue and seasonal SST variability. They demonstrated that Kelvin and Rossby waves, generated by seasonal changes in wind forcing, control the shoaling and deepening of the thermocline, which in turn modulates SST variability in the equatorial Atlantic. Their study showed that upwelling and thermocline adjustments peak during boreal summer, giving rise to a prominent cold tongue in the eastern equatorial Atlantic basin.

Elsewhere, Mitchell and Wallace (1992) examined seasonal variations in SST and surface winds in both the Pacific and Atlantic Oceans. They concluded that the annual cycle in SST originates in the eastern basin due to continental monsoon-driven wind anomalies, which then propagate westward through coupled ocean-atmosphere interactions. Their findings suggested that continental heating and wind convergence play a more significant role in the Atlantic than in the Pacific, where atmosphere-ocean interactions dominate.

Giese and Carton (1994) focused on the seasonality of cross-equatorial winds, showing that these are closely tied to SST gradients and the latitudinal displacement of the ITCZ. They demonstrated that southerly wind strengthening during boreal summer enhances upwelling and SST cooling, reinforcing the meridional SST gradient that sustains the ITCZ's northward migration.

Xie (1994) conducted coupled model simulations and demonstrated that ITCZ displacement and the associated cross-equatorial winds are central to explaining the annual SST cycle in both the Pacific and Atlantic. His study emphasized that the interhemispheric SST gradient modulates wind stress patterns, evaporation rates, and ocean mixing, thereby sustaining the observed seasonal asymmetry in SST evolution.

Li and Philander (1997), using atmospheric general circulation model (AGCM) experiments, showed that the seasonal cycle of zonal winds in the equatorial Atlantic is driven by both monsoonal heating over adjacent continents and feedback from local SST anomalies. Their results confirmed that

continental influences are particularly strong in the eastern basin, where monsoonal forcing plays a larger role than in the Pacific counterpart.

Janicot and Sultan (2001) explored the role of land-atmosphere interactions in modulating tropical Atlantic convection and the seasonal migration of the ITCZ. Their study suggested that soil moisture dynamics and continental heat storage contribute to the lagged response of rainfall and convection relative to solar forcing, adding complexity to the seasonal SST-rainfall relationship over both land and ocean.

Grodsky and Carton (2003) utilized observational data to examine the seasonal migration of the ITCZ and its connection to SST variability in the tropical Atlantic. They found that the ITCZ lags behind solar forcing due to the ocean's high heat capacity and responds more directly to SST gradients. They also identified a secondary convective zone south of the equator during boreal summer, coinciding with the peak of the equatorial cold tongue. Their results underscore the asymmetric and phase-locked relationship between SST patterns and atmospheric convection.

Thorncroft et al. (2003) studied African Easterly Waves (AEWs) and their connection to convective activity over the tropical Atlantic. They found that AEWs originating from the continental ITCZ can initiate convection over oceanic regions, especially during boreal summer. Their study linked the peak of oceanic rainfall and storm genesis to wave activity modulated by the seasonal migration of the ITCZ, emphasizing the role of intra-seasonal variability in shaping the seasonal SST variability and convection pattern.

Xie (2004) analyzed the dynamics of SST gradients and their relationship with the Intertropical Convergence Zone (ITCZ). He demonstrated that the northward displacement of the ITCZ, maintained by asymmetric SST gradients across the equator, plays a key role in sustaining cross-equatorial winds. These winds, in turn, affect evaporation, surface fluxes, and upwelling, thereby

reinforcing the SST asymmetry through wind-evaporation-SST (WES) feedback. His findings highlighted the coupled nature of seasonal SST variability and atmospheric circulation.

Okumura and Xie (2004) extended this work by showing that even when cold tongue development is suppressed in models, anomalous easterlies still emerge in May–June, driven by increased momentum advection and redistribution of monsoon rainfall. Their findings supported the view that atmospheric processes, particularly linked to monsoon systems, can initiate seasonal SST changes independent of local SST feedback.

Chang et al. (2006) investigated how the seasonal cycle interacts with interannual variability in the Atlantic, particularly the Atlantic Niño. They found that seasonal phase-locking and asymmetric wind responses contribute to the irregular occurrence and evolution of warm events. Their results emphasized the importance of understanding how seasonal and interannual processes interact in modulating the amplitude and predictability of SST anomalies.

Richter et al. (2017) explored the seasonal phase-locking of equatorial Atlantic SST anomalies and showed that this is linked to the seasonal migration of the ITCZ. Their analysis suggested that coupling strength between the ocean and atmosphere varies seasonally and spatially, explaining why Atlantic Niño events tend to peak during boreal summer. This phase-locking behavior provides insight into why predictive skill is higher during certain times of the year.

Nnamchi et al. (2021) provided observational evidence that diabatic heating associated with the northward migration of the ITCZ governs the seasonality of the Atlantic Niño. They argued that the thermodynamic influence of the atmosphere plays a more dominant role than ocean dynamics in determining the timing and intensity of SST variability. Their study challenged the classical Bjerknes-centric view by highlighting the importance of atmospheric control in shaping seasonal SST variability.

2.1.3 Improved Representation of Key Atmospheric and Oceanic Processes

Beyond advancements in modeling, a deeper understanding of the underlying atmospheric and oceanic processes is crucial for enhancing Atlantic Niño predictions. The role of large-scale atmospheric circulation patterns, particularly the St. Helena high, appears to be strongly linked to prediction skill in the equatorial Atlantic (Prodhomme et al., 2019). Models that accurately represent these patterns demonstrate improved predictive capability (Prodhomme et al., 2019). Conversely, the skill in predicting the Atlantic Niño is weakly related to local SST drift in the first month of the forecast, but not to the SST bias during the peak (Prodhomme et al., 2019). This finding suggests that the focus should shift towards improving the representation of large-scale atmospheric dynamics rather than solely addressing local SST biases.

The seasonal migration of the Intertropical Convergence Zone (ITCZ) and its associated diabatic heating are also key factors influencing the seasonality of the Atlantic Niño (Nnamch et al., 2021). The ITCZ's influence on precipitation patterns correlates with the Atlantic Niño's behavior, challenging the classical Bjerknes feedback mechanism by suggesting a more minor oceanic impact on the atmosphere than previously thought (Nnamchi et al., 2021). It highlights the critical role of atmospheric processes in governing the Atlantic Niño's seasonal dynamics and underscores the need for improved representation of atmospheric forcing mechanisms in prediction models. Furthermore, the South Atlantic Anticyclone (SAA) plays a dominant role in driving Atlantic Niño variability, accounting for approximately 50% of the observed variability (Lübbecke et al., 2018). The impact of the SAA is most pronounced during boreal spring and autumn, highlighting the significance of extra-tropical influences on equatorial Atlantic variability (Lübbecke et al., 2018). Accurate simulation of the SAA's role and its thermodynamic ocean-atmosphere interactions is crucial for capturing observed Atlantic Niño variability (Lübbecke et al., 2018).

Richter and Xie (2008) diagnosed the cold tongue bias and found that it results from weak vertical mixing, insufficient thermocline tilt, and mislocated ITCZ convection in CGCMs. These errors reduce upwelling and weaken the Bjerknes feedback loop. Their study linked mean-state errors directly to reduced interannual variability, providing a foundation for bias correction efforts in seasonal forecasting.

Ding et al. (2010) explored upper ocean heat content variability and showed that models that better capture ocean preconditioning (e.g., in February-April) simulate more realistic Atlantic Niño events. Their findings supported the idea that improved vertical temperature structure and subsurface assimilation are key to accurate predictions.

Richter et al. (2012) compared atmospheric model simulations and satellite observations, finding that low-level stratiform clouds, which modulate shortwave radiation and latent heat fluxes, are poorly represented in models. This bias leads to excessive surface heating and weakening of vertical thermal structure. Their findings pushed for better cloud parameterizations as a prerequisite for improving SST variability and feedback.

Xu et al. (2014) evaluated the impact of ocean reanalyses and surface forcing quality on the simulation of the equatorial Atlantic. They found that improved reanalyses incorporating satellite wind and SST observations significantly enhanced the representation of seasonal thermocline variability, allowing for better initialization of Atlantic Niño forecasts.

Jouanno et al. (2017) used a high-resolution ocean model to demonstrate that improving vertical resolution and mixed-layer turbulence schemes yields more realistic simulations of the cold tongue and Atlantic Niño. Their work highlighted the importance of resolving equatorial wave propagation, eastern boundary reflection, and vertical heat fluxes, particularly in the top 100 m.

Prodhomme et al. (2019) analyzed model skill in MMEs like NMME and C3S and found that models with a better representation of zonal advection, thermocline depth, and air-sea feedback show higher

anomaly correlation coefficients (up to 0.8) for boreal summer events. However, models that overestimate surface fluxes or misplace ITCZ convection tend to overpredict warming, highlighting the role of bias-aware model development.

2.1.4 Inter-Basin Teleconnections and Global Climate Linkages

The influence of the Atlantic Niño extends beyond the tropical Atlantic, affecting other ocean basins and shaping global climate patterns. The interaction between the equatorial Atlantic SST anomalies and ENSO is weaker than previously thought (Jansen et al., 2009), yet feedback from the Atlantic SST anomalies to ENSO exists, slightly improving retrospective forecasting skill (Jansen et al., 2009). Furthermore, knowledge of equatorial Atlantic SST anomalies significantly improves predictions of major El Niño events in boreal spring (Keenlyside et al., 2013). Equatorial Atlantic SST modulates El Niño variability rather than triggering events (Keenlyside et al., 2013), highlighting the importance of accurately representing this interaction in climate models. This modulation of El Niño variability by Atlantic SST anomalies highlights the interconnectedness of tropical ocean basins and the potential for improved ENSO forecasting by incorporating information on Atlantic SST anomalies. The Indian Ocean Dipole (IOD) also impacts the predictability of the Atlantic Niño (Zhang and Han, 2021). SST anomalies in the tropical Indian Ocean, particularly those related to the IOD, can trigger the Atlantic Niño through atmospheric teleconnections (Zhang and Han, 2021). Models that detect a stronger connection between the autumnal IOD and the winteral Atlantic Niño exhibit higher forecast skill (Zhang and Han, 2021), suggesting a significant in-phase relationship. Mean state biases of SST variability in the tropical Indian Ocean influence the strength of the IOD-Atlantic Niño connection and forecast skill (Zhang and Han, 2021). This idea highlights the need for an accurate representation of inter-basin teleconnections in climate models to improve Atlantic Niño forecasting.

Furthermore, the influence of the Atlantic Niño on ENSO has increased since the mid-1970s (Park et al., 2024). Global warming has altered the mean state of the tropical Atlantic SST and enhanced the influence of the Atlantic Niño on local precipitation and atmospheric circulation (Park et al., 2024). A warmer tropical Atlantic SST enhances divergence and near-surface easterlies in the Pacific, leading to a more substantial impact of the Atlantic Niño on the Pacific climate (Park et al., 2024). Even weak warming in the Atlantic Niño can promote La Niña conditions through cross-basin interactions and Kelvin wave responses (Park et al., 2024). This highlights the complex interplay between global warming, cross-basin connections, and the influence of the Atlantic Niño on broader climate patterns.

The Benguela Niño, a near-coastal SST variability off Angola, also exhibits a precursor relationship to the Atlantic Niño (Illig et al., 2020). Near-coastal SST variability tends to precede equatorial anomalies by about a month (Illig et al., 2020). This suggests that local forcing mechanisms may trigger the Benguela Niño before remotely driven equatorial waves influence the eastern equatorial SST (Illig et al., 2020). This connection underscores the importance of considering both local and remote forcing mechanisms to improve Atlantic Niño predictions. Both warming events are due to a decrease in the strength of the South Atlantic anticyclone (Illig et al., 2020). Still, local processes trigger coastal warming before remote equatorial waves affect the eastern equatorial SST (Illig et al., 2020). The connection between the two regions appears to be related to the thermodynamic interaction between the ocean and the atmosphere (Keenlyside et al., 2018).

Jansen et al. (2009) analyzed the feedback between the Atlantic and Pacific basins. They found that while the impact of equatorial Atlantic SST anomalies on ENSO is weaker than previously thought, there is evidence of a retrospective improvement in the prediction of El Niño events when Atlantic conditions are included. Their study suggests that while the Atlantic Niño does not directly trigger

ENSO events, it can modulate their development, particularly through atmospheric bridging and wind adjustments.

Keenlyside et al. (2012) investigated the role of Atlantic SST in modulating ENSO events. They showed that warming of the equatorial Atlantic SST anomalies during boreal spring increases the probability of El Niño occurrence later in the year. Their results showed that Atlantic-induced subsidence in the western Pacific weakens convection and can initiate the propagation of Kelvin waves, creating favorable conditions for El Niño. However, they emphasized that Atlantic SSTs modulate rather than trigger ENSO, suggesting a unidirectional, seasonally dependent influence.

Liu et al. (2023) investigated the impact of the Indian Ocean Dipole (IOD) on the predictability of the Atlantic Niño and found that positive IOD events in autumn can trigger wind anomalies over the Atlantic through atmospheric teleconnections, favoring the development of the Atlantic Niño in the subsequent boreal winter. Their study showed that models with a stronger IOD-Atlantic connection exhibited higher forecast performance, especially when correcting for mean state biases in the Indian Ocean. These results suggest that interbasin connections extend beyond the Pacific and that the Indian Ocean also plays a role in modulating Atlantic variability.

Park et al. (2024) investigated how global warming has enhanced the influence of the Atlantic Niño on ENSO. They found that under warmer background conditions, Atlantic Niño events generate more substantial divergence and low-level easterly winds in the Pacific, favoring the onset of La Niña conditions. Their analysis showed that even weak warming of the Atlantic Niño can now have significant teleconnections due to the altered Walker circulation and enhanced cross-basin coupling under climate change. The study highlights the nonstationary nature of cross-basin teleconnections and the increasing role of the Atlantic in shaping Pacific climate variability.

Exarchou et al. (2021) investigated how equatorial Atlantic variability affects ENSO forecast skill and found that incorporating Atlantic SST anomalies into coupled models improves the accuracy of

ENSO forecasts, particularly when the Atlantic Niño precedes ENSO events by a season. Their results confirmed that the Atlantic influence has predictive power, particularly during the boreal spring, when ENSO forecasts are typically less reliable. The study highlights the importance of multi-basin initialization in seasonal forecast systems. Lübbecke and McPhaden (2012) analyzed the relationship between Atlantic and Pacific Niños and found that this connection is highly inconsistent and changes over time. They attributed this variability to changes in the background state and seasonal differences in coupling strength. Their results challenge the theory of a fixed Atlantic-ENSO teleconnection and instead suggest that the connection is modulated by internal variability and external forcings, such as greenhouse gas-induced warming.

Wang et al. (2009) conducted a comprehensive study of the interactions between tropical ocean basins, documenting how anomalies in the Atlantic, Pacific, and Indian Oceans influence each other through global adjustments of the Walker circulation, subsidence patterns, and equatorial heat transport. They found that El Niño events can suppress Atlantic convection through downwelling motion, and vice versa. Their study laid the foundation for understanding multi-basin climate coherence and emphasized the need for a global perspective in climate diagnostics and modeling. Illig et al. (2020) investigated the precursor role of the Benguela Niño (a coastal SST anomaly off Angola) in the development of the Atlantic Niño. Their analysis showed that coastal warming in the southeastern Atlantic often follows equatorial warming.

2.2.1 Atlantic Niño mode: Structure, Seasonality, Mechanisms, and Evolution

2.2.1.1 Structure and seasonality

The Atlantic Niño or Atlantic Niña mode is characterized by anomalous warming or cooling in the eastern basin. Structurally, Atlantic Niño events typically manifest as positive SST anomalies between 10°W and 0°W along the equator, peaking in the boreal summer months of June to August

(Lübbecke et al., 2018; Zebiak, 1993). These anomalies are often confined to the upper ocean, with their spatial extent varying from east-anchored warming events to developments in the more central basin, depending on the dominant feedback processes and the timing of their onset (Lübbecke et al., 2013; Martin-Rey et al., 2019). In contrast to the ENSO in the Pacific, the Atlantic Niño exhibits a strong phase coupling to the seasonal cycle, with a well-documented preference for onset in boreal spring (April-May) and maturation in early to mid-summer (June-August) (Carton & Huang, 1994; Lübbecke et al., 2013). This seasonality is attributed to the seasonal migration of the Intertropical Convergence Zone (ITCZ), the enhanced wind-SST coupling in late spring, and the seasonally varying thermocline structure that modulates the strength of the Bjerknes feedback (Richter et al., 2017; Nnamchi et al., 2021). The shallow thermocline depth in the eastern equatorial Atlantic makes the region particularly sensitive to zonal wind anomalies during this seasonal window, promoting rapid SST responses (Philander & Pacanowski, 1986). The structure of Atlantic Niño events is closely related to the vertical inclination of the thermocline, zonal heat advection by equatorial currents, and the dynamics of Kelvin and Rossby waves, which influence the location and intensity of surface warming (Polo et al., 2008; Brandt et al., 2011). Most Atlantic Niño events are spatially confined to the eastern equatorial Atlantic. However, recent studies indicate an increasing importance of events in central basins or "Atlantic Modoki" types, which differ in structure and climate impacts (Tokinaga et al., 2011; Vallès-Casanova et al., 2020). This diversity is attributed to the interannual variability of the background state and the strength of the zonal SST gradient, as well as telecontrol from other tropical basins, particularly the Pacific (Lübbecke & McPhaden, 2012). The relatively short duration and smaller amplitude of Atlantic Niño events compared to their Pacific counterparts are due to stronger atmospheric attenuation, a narrower basin geometry, and the presence of continental boundaries that limit the growth of coupled feedback (Zebiak, 1993; Xie & Carton, 2004). Nevertheless, Atlantic Niño events exert a significant influence on regional precipitation patterns, particularly over coastal Guinea, northeastern Brazil, and parts of the Sahel. Therefore,

understanding their structure and seasonality is crucial for improving seasonal forecasting systems (Folland et al., 1986; Nobre & Shukla, 1996; Giannini et al., 2003).

Keenlyside and Latif (2007) investigated the dynamics of interannual variability in the equatorial Atlantic using a hybrid coupled model. They found that the Bjerknes feedback, which involves the interaction between zonal winds, SST anomalies, and thermocline depth, plays a crucial role in the development of the Atlantic Niño, similar to ENSO. However, they noted that the Atlantic has a weaker air-sea coupling, resulting in more irregular and shorter-lived events. Their study also showed that surface wind anomalies over the western basin—rather than the eastern basin—are most effective in triggering thermocline fluctuations and triggering warm periods. Lübbecke and McPhaden (2012) analyzed the inconsistencies in the Atlantic-Pacific Niño connection and showed that the relationship between ENSO and the Atlantic Niño is highly variable and episodic. They attributed this to changes in the mean background state, atmospheric noise, and seasonal differences in coupling strength. Their results suggest that while ENSO can sometimes influence the Atlantic Niño via atmospheric bridges, such as subsidence over the Atlantic during El Niño events, this connection is not robust or stationary and depends on the gradients and timing of sea surface temperatures between the basins.

Richter et al. (2017) investigated the seasonal phase coupling of equatorial Atlantic variability and showed that it is driven by the migration of the Intertropical Convergence Zone (ITCZ). Using observational data and models, they showed that the strength and timing of air-sea coupling vary seasonally, peaking during the boreal summer when the ITCZ is closest to the equator. This coupling leads to a systematic coupling of the Atlantic Niño events to the seasonal cycle, thus contributing to the explanation of their recurrent timing and limited duration.

Jouanno et al. (2017) used a high-resolution ocean model to investigate the dynamics of the equatorial Atlantic cold tongue and its relationship with Atlantic Niño events. They found that

vertical mixing, zonal advection, and equatorial wave reflection at the eastern boundary are crucial in shaping the thermocline and SST anomalies during the evolution of the cold tongue. Their analysis showed that intraseasonal wind variability can significantly modulate the cold tongue and prepare the ocean for Atlantic Niño events, highlighting the role of high-frequency forcing in event development.

Lübbecke et al. (2018) provided a comprehensive review of equatorial Atlantic variability, focusing on its modes, mechanisms, and global teleconnections. They identified the Atlantic Zonal Mode (Atlantic Niño), the Atlantic Meridional Mode (AMM), and spring SST variability as the primary modes in the region. Their results showed that Atlantic Niño events are seasonally phase-locked, reaching their maximum development in the boreal summer. Coupled ocean-atmosphere interactions, including zonal wind stress anomalies, thermocline fluctuations, and the propagation of Kelvin waves, drive this. They also emphasized the nonlinear evolution and diversity of events, the role of extra-equatorial influences, and the need to account for model biases to improve predictability.

Dippe et al. (2019) investigated the relative contributions of thermocline, zonal advection, and surface heat flux anomalies to the evolution of the Atlantic Niño. Their results, based on a decomposition of the mixed-layer heat budget, showed that the dominant processes vary between events. Still, that zonal advection and thermocline feedback are often the main drivers of SST anomalies in the eastern equatorial Atlantic. They also found that local surface heat fluxes, although secondary, play a role in modulating the amplitude and duration of events, highlighting the diverse and non-canonical nature of Atlantic Niño dynamics.

2.2.1.2 Mechanisms and Evolution

The development of Atlantic Niño events is determined by a complex interplay of dynamic and thermodynamic feedback within the tropical Atlantic climate system. Central to this development is

the Bjerknes feedback mechanism, which involves a positive coupling between eastern equatorial SST anomalies, zonal wind stress, and thermocline depth (Bjerknes, 1969; Zebiak, 1993; Keenlyside & Latif, 2007). When westerly wind anomalies weaken the mean easterlies in boreal spring, the equatorial thermocline deepens to the east, reducing upwelling and enhancing SST warming-a process that further amplifies the wind anomalies and reinforces the initial disturbance. The onset of Atlantic Niño events is often triggered by intraseasonal zonal wind anomalies in the western equatorial Atlantic during April and May. These initiate downward Kelvin waves that propagate eastward, deepening the thermocline and warming the sea surfaces in the eastern basin (Polo et al., 2008; Lübbecke et al., 2013; Jouanno et al., 2017). At the same time, extra-equatorial influences-particularly the Atlantic Meridional Mode (AMM)-can modulate the equatorial winds and the inclination of the thermocline, thus predisposing the equatorial ocean to event development (Foltz & McPhaden, 2010; Martin-Rey et al., 2012). This multiscale interplay helps explain the differences in event onset and intensity across years. During the growth phase, the wind-SST-thermocline coupling intensifies, as SST anomalies peak between June and August. This is supported by zonal advection of warm water, weakened upwelling, and reduced latent heat loss at the surface (Dippe et al., 2019; Brandt et al., 2011). However, unlike Pacific ENSO events, Atlantic Niño episodes tend to be short-lived and irregular, often decaying rapidly within one to two months of their peak. This brevity is attributed to the strong dampening effects of the overlying atmosphere, particularly the post-August drift of the ITCZ away from the equator, which reduces the coupling strength and restores climatological upwelling conditions (Richter et al., 2017; Nnamchi et al., 2021). The decay of Atlantic Niño events is associated with a combination of negative feedback processes. These include the resumption of easterly winds, the upwelling of cooler subsurface waters, and the arrival of reflected Rossby waves, which flatten the thermocline in the east (Philander & Pacanowski, 1986; Cane, 1992). Furthermore, the seasonal transition plays a crucial role, as the background state becomes less favorable for coupled instability after the boreal summer (Xie & Carton, 2004).

Recent studies have shown that Atlantic Niño events are neither monolithic in their structure nor in their evolution. Some are more thermodynamically driven, with surface heat fluxes (particularly net shortwave radiation and latent heat) dominating the SST anomaly balance, while others are dynamically driven, with strong contributions from subsurface anomalies and equatorial wave propagation (Nnamchi et al., 2015; Dippe et al., 2019; Prigent et al., 2020). This diversity has led to the classification of different Atlantic Niño "variants"-including eastern- and central-type events-that evolve differently and have distinct atmospheric impacts (Vallès-Casanova et al., 2020). Furthermore, the Atlantic Niño amplitude and feedback strength weakened in the post-2000 period, possibly due to altered mean-state conditions, such as shallower thermocline slopes, reduced wind stress variability, and increased stratification in the upper ocean (Lübbecke & McPhaden, 2012; Prigent et al., 2024; Crespo et al., 2022). These changes could shift the balance of controlling mechanisms, reduce predictability, and favor more thermodynamically dominated SST anomalies, posing challenges for both understanding and forecasting Atlantic Niño evolution in a warmer climate.

Carton and Huang (1994) documented several Atlantic warm periods based on observations and model simulations, finding that they tended to originate in the eastern basin and propagate westward. They emphasized that anomalous westerlies along the equator often precede warm events and lead to a deepening of the thermocline, similar to the onset of the El Niño event in the Pacific. Their study highlighted the zonal asymmetry and short-lived nature of Atlantic Niño episodes.

Brandt et al. (2011) investigated the role of deep equatorial ocean dynamics in shaping atmospheric variability over the equatorial Atlantic. Using observations and modeling at anchor points, they found that the annual variability of deep zonal jets and equatorial heat content has a measurable influence on the surface wind field and SST anomalies. Their results provided new evidence that oceanic processes below the thermocline, particularly the quasi-periodic deep jets, can feed back into the

atmospheric circulation, suggesting a deeper layer of ocean-atmosphere interaction relevant to the evolution and predictability of the Atlantic Niño.

Lübbecke et al. (2013) used observational datasets to show that Atlantic Niño events are strongly coupled to the seasonal cycle, typically peaking between June and August and often triggered by boreal spring wind anomalies. They identified two distinct modes: an early-onset mode caused by zonal wind bursts in April/May, and a late-onset mode related to feedback with the ITCZ and thermocline dynamics, which contribute to event diversity.

Martín-Rey et al. (2019) analyzed the structure and timing of Atlantic Niño events using ocean reanalysis and showed that the position of thermocline anomalies, zonal flow fluctuations, and Kelvin wave activity critically influence both the onset and amplitude of warm events. Their results indicated a strong dependence on the mean background state, including annual shifts in the ITCZ and surface wind fields.

Ruiz-Barradas et al. (2000) identified the interannual to decadal variability of equatorial Atlantic SSTs and showed that SST anomalies tend to occur in the eastern equatorial basin, with the strongest anomalies related to weakened southeasterly trade winds and positive subsurface heat anomalies. They also documented the reversal of zonal wind stress as a precursor to warm events.

Latif and Grötzner (2000) introduced the concept of the Equatorial Atlantic Oscillation (EAO) and demonstrated how this mode influences interannual SST anomalies through atmospheric and oceanic interactions. They emphasized that the EAO can be synchronized with the Atlantic Niño, thereby amplifying its amplitude and influencing the timing of wind and thermocline anomalies. Wang and Chang (2008) performed a linear stability analysis of coupled tropical Atlantic variability and showed that the Atlantic Niño is conditionally unstable, with its growth dependent on seasonal background winds and the slope of the thermocline. This explained the seasonal confinement of warm events.

Foltz and McPhaden (2010) investigated the interaction between the Atlantic Meridional Mode (AMM) and the Atlantic Niño using reanalyses and observational data. They demonstrated that the equatorial wind anomalies of the AMM, which are often active in boreal spring, can precondition the equatorial ocean by altering the thermocline slope and SST gradients, thereby triggering or amplifying Atlantic Niño events. Their work emphasized the importance of off-equatorial variability and meridional SST gradients for the dynamics of the zonal equatorial modes, suggesting a strong link between AMM activity and the onset of the Atlantic Niño.

Ding et al. (2010) investigated the role of upper ocean heat content in interannual variability in the equatorial Atlantic and found that ocean preconditioning in winter and early spring sets the stage for warm events. Their analysis suggested that forecasting of the Atlantic Niño could benefit from monitoring subsurface temperature anomalies months in advance. Richter et al. (2013) investigated the multiple drivers of interannual SST variability in the equatorial Atlantic. Their analysis showed that zonal wind stress anomalies, surface heat fluxes, vertical entrainment, and remote heating forcing from extra-equatorial regions contribute to SST development. In particular, they identified zonal advection of warm waters and the seasonally modulated Bjerknes feedback as key mechanisms for generating Atlantic Niño events. They also emphasized that the model representation of these processes remains inconsistent, which has implications for forecast quality and simulation accuracy.

Nnamchi et al. (2015) analyzed the thermodynamic controls of the Atlantic Niño using satellite observations and reanalysis data. They found that the net surface heat flux, rather than subsurface ocean dynamics alone, plays a dominant role in driving SST anomalies, particularly in the eastern equatorial Atlantic. Their results challenged the traditional Bjerknes feedback. They showed that shortwave surface radiation and latent heat fluxes are more critical than previously thought. This suggests that atmospheric thermodynamic influence is a key driver of Atlantic Niño variability. This perspective opened a new dimension for understanding non-dynamical contributions to warm events.

2.2.2 Eastern vs. Central Atlantic Niño Modes and Their Climate Impacts

Recent studies have shown that Atlantic Niño events exhibit considerable spatial and temporal diversity and are no longer exclusively confined to the eastern equatorial basin. This has led to the classification of distinct event types, commonly referred to as East Atlantic Niño (EA Niño), Central Atlantic Niño (CA Niño), or Atlantic Modoki events (Tokinaga et al., 2011; Vallès-Casanova et al., 2020; Wang et al., 2004). These variations differ in their SST anomalies, seasonality, and climate impacts, which have important implications for regional precipitation patterns and cross-basin teleconnections. Niño events in the eastern Atlantic typically peak in the east equatorial Atlantic between 10°W and 0°W and are characterized by a stronger thermocline feedback, sharper SST gradients, and robust coupling with zonal wind anomalies (Lübbecke et al., 2018; Polo et al., 2008; Wang et al., 2024). These events are more directly linked to the classical Bjerknes feedback and tend to exhibit stronger coherence with coastal upwelling signals and precipitation variability along the Guinean coast and the Gulf of Guinea (Prigent et al., 2020; Folland et al., 1986). In contrast, Central Atlantic Niño events exhibit SST anomalies centered further west (approximately 20°W to 40°W) and often develop outside the peak Bjerknes season. They exhibit weaker coupling to the thermocline and a stronger influence of surface fluxes and long-range currents (Tokinaga et al., 2011; Vallès-Casanova et al., 2020). These CA Niño events have become more important in the post-2000 period, possibly due to the climate-induced weakening of subsurface feedback and increased atmospheric stability, which reduces convective responses to SST anomalies in the eastern basin (Crespo et al., 2022; Prigent et al., 2024).

The climate impacts of these event types also differ. EA-Niño events are closely associated with increased rainfall over West Africa, particularly near the Guinean coast, and with anomalous subsidence in the tropical Pacific, which can modulate ENSO development (Lübbecke & McPhaden, 2012; Exarchou et al., 2021). In contrast, CA-Niño events have stronger impacts on northeastern

South America and are associated with the modulation of regional convection and interhemispheric pressure gradients (Giannini et al., 2003; Vallès-Casanova et al., 2020). Some evidence also suggests that CA-Niño events influence hurricane activity in the Atlantic, particularly through changes in vertical wind shear and atmospheric circulation over the main development area (Wang et al., 2024). Recent research also suggests that the two modes interact differently with distant climate drivers. EA Niño exhibits more consistent teleconnections with ENSO, while CA Niño appears more sensitive to stochastic atmospheric forcings such as the Madden-Julian Oscillation (MJO) or intraseasonal wind gusts (Chen et al., 2024; Gan et al., 2024). This has important implications for predictability, as CA events are typically less phase-locked to the seasonal cycle, develop more rapidly, and are more difficult to predict.

In summary, the distinction between the East and Central Atlantic Niño modes underscores the nonlinear and evolving nature of tropical Atlantic variability. It also highlights the need to go beyond basin-wide SST indices and develop spatially resolved diagnostic and forecasting tools that capture the diversity of Atlantic Niño expressions and their regionally distinct climate consequences. Understanding these differentiated impacts is crucial for improving seasonal climate forecasts in different regions. In their analysis of climate variability in the tropical Atlantic, Folland et al. (1986) showed that sea surface temperature (SST) anomalies in the tropical Atlantic strongly influence rainfall in West Africa, particularly during the boreal summer. They showed that positive SST anomalies in the northern tropical Atlantic are associated with a northward shift of the Intertropical Convergence Zone (ITCZ), thus enhancing rainfall over the Sahel. In contrast, cool anomalies in the south suppress rainfall. Their work was fundamental in establishing the link between Atlantic SST gradients and continental precipitation variability. It highlighted the role of ocean-atmosphere coupling and interhemispheric SST contrasts in modulating African climate.

Nobre and Shukla (1996) used observational analyses to investigate the influence of tropical SST and wind stress anomalies in the Atlantic on South American and African precipitation patterns. They found that anomalously warm SSTs in the tropical North Atlantic correlate with increased precipitation over the Sahel and northeastern South America, while warm anomalies in the southern tropical Atlantic are associated with decreased precipitation in these regions. Their results further supported the importance of SST-induced atmospheric circulation anomalies, particularly in modulating the latitudinal position of the ITCZ, and of the interhemispheric SST gradient as a critical driver of seasonal climate anomalies in adjacent land regions.

Giannini et al. (2003) investigated the role of oceanic influences in modulating Sahel precipitation over interannual to interdecadal timescales. They showed that Atlantic SST anomalies, particularly in the subtropical and tropical belts, precondition the atmosphere and modulate Sahel precipitation. Their findings emphasized the role of persistent SST patterns, such as those associated with the Atlantic Multidecadal Oscillation (AMO), in shaping long-term precipitation trends and drought events. They argued that tropical Atlantic variability plays a dominant role in influencing the Sahel climate through its control of atmospheric stability and moisture fluxes, particularly in the presence of weak or absent ENSO influence.

Vallès-Casanova et al. (2020) investigated the spatiotemporal diversity of Atlantic Niño events and the associated precipitation variability over West Africa and South America. They found that different Atlantic Niño types exhibit distinct telecontrol patterns. The eastern Niño type has a stronger connection to precipitation along the Guinea coast, and the central Niño type has a stronger connection to precipitation in South America. Their study highlighted the regional asymmetries in SST anomalies and their atmospheric responses. This suggests that the precise location of equatorial Atlantic warming significantly influences where and how precipitation anomalies manifest in the tropics.

2.2.3 Prediction Skill and Advances in Modeling the Atlantic Niño

Several studies emphasize the crucial role of improved climate models in improving the forecast skill of the Atlantic Niño mode. Incorporating anomaly coupling into models significantly reduces climatological errors in the tropical Atlantic, leading to a better representation of equatorial Atlantic variability and improved forecasting of the Atlantic Niño mode (Counillon, 2021). In particular, the correction of momentum and SST fields exchanged between oceanic and atmospheric models within the anomaly-coupled version of the Norwegian Climate Prediction Model (NorCPM) has been shown to improve forecast skill (Counillon, 2021). This improvement is attributed to the model's increased ability to process ocean observations in the equatorial Atlantic region (Counillon, 2021). Furthermore, the use of high-resolution climate forecasting systems shows improved accuracy in multi-year sea surface temperature (SST) predictions in the tropical North Atlantic (Zhang, 2024). This improvement is due to a stronger response of the surface wind to changes in equatorial SST gradients, enabled by a reduction in the Intertropical Convergence Zone (ITCZ) bias (Zhang, 2024). These advances underscore the importance of model resolution and the accurate representation of ocean-atmosphere interactions for improving forecast skill.

The development and application of multi-model ensembles (MMEs) also contribute significantly to improving forecast skill. Multi-model analyses of the North American Multi-Model Ensemble (NMME) and the Copernicus Climate Change Service (C3S) show a significant improvement in the forecast skill of the Atlantic Niño (Prodhomme, 2020; Wang, 2021). For example, the anomaly correlation coefficient (ACC) in some models reaches up to 0.8 for May start dates (Prodhomme, 2020), exceeding the accuracy of persistence forecasts for earlier start dates (Prodhomme, 2020). Although improvements are evident, persistent warm SST biases and the associated drift continue to pose a challenge in most systems (Prodhomme, 2020). Furthermore, the NMME models show improved forecast skill for Atlantic Niño/Niña events with a lead time of up to five months compared

to previous constraints of two to three months (Wang, 2021). However, a seasonality-dependent forecast skill is observed, with a significant decline in forecast skill in boreal spring, suggesting a "spring predictability barrier" similar to that of ENSO (Wang, 2021).

Hu and Huang (2007a) evaluated the predictive skill of Atlantic SSTs using both coupled models and statistical approaches. They found that ENSO significantly influences predictability in the Atlantic, particularly through lagged correlations and atmospheric teleconnections. However, the most predictable pattern in the Atlantic was largely internal, driven by zonal wind anomalies and local coupling. This highlights the value of regional model adjustments to improve forecast performance.

Counillon et al. (2021) demonstrated that using anomaly coupling in the Norwegian Climate Prediction Model (NorCPM) significantly improves Atlantic Niño prediction skill. By correcting momentum and SST exchanges between model components and enhancing data assimilation of ocean observations, their system reduced climatological errors and better captured the seasonal cycle and thermocline variability, especially in the eastern equatorial Atlantic.

Zhang (2024) investigated the impact of high-resolution coupled prediction systems on SST forecasts and showed that multi-year prediction skill in the tropical North Atlantic improves when ITCZ bias is reduced. This results from a stronger surface wind response to cross-equatorial SST gradients, indicating that model resolution and mean state improvements directly enhance Atlantic Niño forecast skill.

Prodhomme et al. (2020) assessed multi-model ensemble (MME) systems, including the North American Multi-Model Ensemble (NMME) and the Copernicus Climate Change Service (C3S) models. They found that anomaly correlation coefficients (ACCs) reach up to 0.8 for summer events initialized in May, outperforming persistence forecasts. However, seasonal dependence, warm biases, and forecast drift continue to limit performance, especially in boreal spring, consistent with the “spring predictability barrier” known from ENSO forecasting.

Wang et al. (2021) evaluated Atlantic Niño/Niña prediction skill across several NMME models and observed that lead times of up to five months are now achievable, particularly for events peaking in July-August. Nonetheless, they reported a significant drop in skill for boreal spring start dates, with forecasts often failing to capture event onset timing, again emphasizing the challenge of the spring barrier and the need for better initialization of subsurface conditions.

Palmer et al. (2004) developed the DEMETER multi-model ensemble system and highlighted the role of ensemble averaging in enhancing prediction skill for tropical SST anomalies, including those in the Atlantic. Their findings showed that model diversity helps reduce systematic errors. However, performance is still limited by mean state biases, particularly related to the cold tongue, ITCZ position, and wind stress representation in the equatorial Atlantic.

Li et al. (2020) applied statistical models and outputs from the Kiel Climate Model to demonstrate that monthly to seasonal SST prediction in the tropical Atlantic is feasible, particularly when trained on observational and reanalysis data. Their approach outperformed some dynamical models, especially at shorter lead times, suggesting that statistical post-processing and bias correction remain valuable tools for operational Atlantic Niño forecasting.

Kim et al. (2012) assessed retrospective forecasts from the ECMWF System 4 and NCEP CFSv2. They found that while ENSO prediction skill was generally higher than for the Atlantic Niño, some skill exists for predicting Atlantic events up to 2-4 months in advance, particularly during the summer. They emphasized that improving ocean initial conditions, subsurface heat content, and surface flux parameterizations would likely further enhance skill.

2.2.4 Observed weakening in Atlantic Niño Variability and Feedback Strength

Observational and model analyses show a weakening of Atlantic Niño variability, which has been particularly pronounced since the beginning of the 21st century (Tokinaga et al., 2011; Prigent et al.,

2020; Silva et al., 2021; Crespo et al., 2022). This is attributed to a weakening of the associated ocean dynamics, which is expected to further worsen under increased anthropogenic greenhouse effect (Prigent et al., 2024; Yang et al., 2022).

Tokinaga et al. (2011) investigated Atlantic climate variability in the context of anthropogenic warming and found that near-surface latent heat fluxes and changes in cloud cover play an increasingly important role in shaping tropical sea surface temperatures in the Atlantic. Their analysis showed that a long-term weakening of the trade winds and enhanced shortwave downward radiation have altered the ocean surface heat budget. This led to shifts in SST variability patterns and a reduced effectiveness of dynamic ocean-atmosphere feedback over the tropical Atlantic.

Prigent et al. (2020) investigated the Atlantic Niño thermocline feedback using reanalyses and model data. They found that while the Bjerknes feedback remains a dominant driver, its strength has decreased since the early 2000s, particularly in the eastern equatorial Atlantic. This weakening was associated with shallower thermocline anomalies, reduced wind stress variability, and changes in the vertical structure of the ocean, all of which contributed to lower SST variability and reduced predictability of Atlantic Niño events.

Silva et al. (2021) used CMIP5 and CMIP6 results to assess changes in air-sea coupling strength over the equatorial Atlantic. They found that models predict a weakening of the zonal wind-SST coupling under future warming scenarios. They showed that this decrease is associated with a shallower zonal SST gradient and weaker trade winds. Both of these factors reduce the amplification of SST anomalies. This suggests that Atlantic Niño events may become less frequent or less intense in the future.

Crespo et al. (2022) (also cited previously) analyzed the projected future behavior of the Atlantic Niño in climate models. They reported that thermocline feedback and the strength of the surface coupling decrease significantly in both CMIP5 and CMIP6 simulations. Their results showed that

surface-subsurface decoupling, together with increasing stratification in the upper ocean, contributes to a projected reduction of the Niño amplitude in the Atlantic by up to 48%, posing significant challenges for seasonal forecasting and teleconnection capabilities.

Prigent et al. (2024) extended their earlier work by comparing observational diagnostics and idealized model experiments, confirming a post-2000 weakening of the Atlantic Niño system's feedback loop. They observed that the thermocline's influence on SST anomalies has decreased, while surface heat fluxes have become relatively more important. Their findings reinforce the shift toward a more thermodynamically driven Atlantic Niño, with implications for its seasonality, predictability, and response to remote forcing.

Yang et al. (2022) analyzed the relationship between mean state changes and feedback strength in coupled models and observations. They found that models with stronger stratification and weaker thermocline slope simulate weaker air-sea coupling and Atlantic Niño variability. Their study emphasized that background state biases, especially in thermocline structure and wind climatology, are critical for understanding the past and future weakening of feedback mechanisms essential for Atlantic Niño development.

2.3 Impacts of global warming on equatorial Atlantic variability

The impacts of global warming on the variability and predictability of the Atlantic Niño are an important area of research. Modern models predict a weakening of the Atlantic Niño in response to global warming, primarily due to the decoupling of subsurface and surface temperature variability (Crespo, 2022). More than 80% of the models from phases 5 and 6 of the Coupled Model Intercomparison Project predict this weakening under high-emission scenarios (Crespo, 2022). By the end of the century, the variability of the Atlantic Niño could decrease by 14%, and by as much

as 48% when accounting for model errors (Crespo, 2022). This reduction in variability could significantly affect the accuracy of seasonal forecasts in many regions (Crespo, 2022).

Furthermore, the relationship between the Atlantic Niño and precipitation along the Guinean coast, which was typically stable in the 20th century, is weakening in climate projections for the 21st century due to atmospheric stabilization (Worou, 2021). The weakened influence of the Atlantic Niño on precipitation is attributed to reduced SST amplitudes, leading to enhanced upwelling cooling effects (Worou, 2021). A decrease in precipitation is projected with the Atlantic Niño both along the Guinean coast and in the equatorial Atlantic, with greater certainty for the ocean areas (Worou, 2021).

The influence of the Atlantic Niño on ENSO is also modulated by global warming (Wang, 2024). The warmer tropical Atlantic background plays a significant role in increasing local mean rainfall and leading to stronger divergence and near-surface easterlies in the Pacific (Wang, 2024). Even weak warming in the Atlantic from Niño could promote La Niña development through the cross-basin Walker circulation and the Indian Ocean-mediated Kelvin wave response (Wang, 2024). The change in the Atlantic Niño pattern itself leads to weak convective anomalies in the western Atlantic, which cannot trigger a significant atmospheric response in the Pacific (Wang, 2024). This highlights the complex interplay between global warming, cross-basin connections, and the influence of the Atlantic Niño on broader climate patterns, as well as the need to incorporate these changes into forecast models.

Tokinaga et al. (2011) examined observed trends in the tropical Atlantic surface climate. They found that enhanced shortwave radiation, resulting from reduced low-level cloud cover, combined with weakened trade winds, contributed to asymmetric warming in the tropical Atlantic. This pattern led to a flattening of meridional and zonal SST gradients, which undermines coupled feedback such as the Bjerknes and WES feedback and ultimately reduces the amplitude of interannual variability.

Nnamchi et al. (2015) emphasized that SST variability in the tropical Atlantic is not solely driven by dynamic ocean processes but increasingly by thermodynamic influences, particularly surface heat fluxes. Under warming conditions, this shift toward a more thermodynamically dominated system has contributed to the observed decline in Atlantic Niño strength, a trend supported by observations after 2000.

Crespo et al. (2022) conducted a multi-model assessment using CMIP5 and CMIP6 and found that the Atlantic Niño amplitude is projected to decrease under high-emission scenarios. This decline is due to a decoupling of surface and subsurface temperatures caused by increased ocean stratification and reduced vertical heat exchange. They project a 14–48% reduction in event amplitude by the end of the 21st century, raising concerns about the reliability of seasonal forecasts in the region.

Silva et al. (2021) found that the strength of the air-sea coupling in the equatorial Atlantic decreases in future climate projections in both the CMIP5 and CMIP6 models. This weakening is due to shallower zonal SST gradients, weaker trade winds, and increasing stratification in the upper ocean, which reduce the effectiveness of the feedback mechanisms required for event amplification. Prigent et al. (2020, 2024) provided robust evidence for a weakening of the thermocline feedback associated with the Atlantic Niño after 2000. They demonstrated that changes in thermocline structure, wind stress, and surface heat fluxes resulting from warming lead to a more thermodynamically driven regime of SST anomalies. In future scenarios, their modeling suggests a reduced seasonal forecast window for the Atlantic Niño due to altered background conditions and the timing of the feedback.

Yang et al. (2022) analyzed the strength of the feedback in CMIP6 models. They concluded that models with shallower thermocline slopes and stronger stratification in the upper ocean exhibit weaker SST-wind coupling and lower variability of the Atlantic Niño. They concluded that warming-associated mean state changes-particularly weaker easterly winds and stronger thermocline biases-suppress the Bjerknes feedback loop. Lübbecke et al. (2014) found that SST variability in the eastern

equatorial Atlantic has decreased since the early 2000s. They attributed this trend to flattened thermocline gradients, the weakening of cross-equator winds, and increased stability of the overlying atmosphere. All of this has contributed to a less favorable environment for the development of canonical Niño events in the Atlantic.

Richter and Tokinaga (2020) (current synthesis) highlighted that the Cold-Tongen bias and ITCZ misrepresentation in climate models are exacerbated under warming scenarios, leading to a further deterioration in the simulation performance of the Atlantic Niño. These model biases are related to greenhouse-induced mean state changes and increase the uncertainty of future TAV projections.

He et al. (2023) found that greenhouse gas forcing enhances subsurface stratification in the tropical Atlantic, thus reducing the efficiency of equatorial upwelling. Their study showed that dynamical feedback (e.g., the coupling between the thermocline and sea surface temperature) weakens even with continued surface warming. This suggests a future state in which Atlantic sea surface temperature anomalies become weaker and more localized.

Pascale et al. (2022) highlighted the role of increased atmospheric stability. They suppressed convection over the equatorial Atlantic during warming, which reduces the sensitivity of the atmosphere to sea surface temperature anomalies. This thermodynamic suppression contributes to a dampened atmospheric response, limiting the strength of coupled feedback loops, such as the Bjerknes and WES mechanisms.

2.3 Off-Equatorial Variability: Meridional Modes and Remote Influences

Servain et al. (1999) identified the Atlantic Meridional Mode (AMM) as one of the leading modes of SST variability in the tropical Atlantic. They showed that the AMM is characterized by an interhemispheric SST gradient, whose positive phases are characterized by warm anomalies in the Northern Hemisphere and cold anomalies in the Southern Hemisphere. This gradient drives

equatorial winds that modulate upwelling, evaporation, and ITCZ shift, with significant impacts on the Atlantic Niño and regional precipitation.

Chiang and Vimont (2004) developed a dynamical model to understand the AMM as a coupled ocean-atmosphere mode maintained by the wind-evaporation-SST (WES) feedback. They argued that initial SST anomalies in the subtropics induce surface wind anomalies that alter evaporation and enhance the SST signal. This feedback is particularly active during boreal spring, a season when the AMM often peaks and can modulate the background conditions for the onset of the Atlantic Niño through wind-driven changes in the depth of the equatorial thermocline.

Foltz and McPhaden (2010), provided observational evidence that AMM-induced cross-equatorial wind anomalies in boreal spring influence thermocline tilt and SST anomalies along the equator, acting as precursors to Atlantic Niño events. Their results suggest that off-equatorial SST gradients, such as those associated with AMM, play a significant role in preconditioning the equatorial Atlantic, supporting stronger or weaker Bjerknes feedback cycles.

Servain (1991) first discussed the link between interhemispheric SST gradients and ITCZ migration, noting that a northward shift of the ITCZ is often associated with warm northern SST anomalies, leading to enhanced convection over the Sahel and changes in zonal wind stress. This affects not only rainfall variability but also the ocean dynamics that sustain equatorial SST anomalies, indicating a broader regional influence of AMM-like patterns.

Xie (1999) emphasized that the meridional SST gradient, anchored by the AMM, shapes surface wind convergence and the latitudinal position of the ITCZ. He showed that a northward-displaced ITCZ can reduce upwelling and wind stress along the equator, weakening cold tongue development and enhancing the likelihood of Atlantic Niño-like warming, especially when supported by thermocline preconditioning.

Kucharski et al. (2008) linked the AMM to interannual and multidecadal precipitation variability over the tropical Atlantic and West Africa. They demonstrated that positive AMM phases lead to a northward ITCZ displacement, which reduces trade wind strength near the equator, limits upwelling, and promotes equatorial SST warming. Their findings highlighted how AMM contributes to both the initiation and amplification of Atlantic Niño events.

Zhang and Zhao (2015) used coupled models and observational analysis to show that the AMM modulates air–sea coupling strength across the tropical Atlantic. During positive AMM phases, they found enhanced wind stress curl anomalies and eastern basin warming, which reinforces thermocline feedback mechanisms associated with the Atlantic Niño. Their study supports the notion that AMM-related atmospheric anomalies can serve as remote triggers for equatorial SST variability.

Martin-Rey et al. (2012) further demonstrated that the timing of AMM peaks, typically in March-April, is crucial for understanding its influence on the Atlantic Niño. Their study suggested that early-season AMM events, even if weak in magnitude, can initiate wind and thermocline anomalies that grow into full-fledged equatorial warm events, depending on the background state and seasonal coupling window.

CHAPTER THREE

DATA AND METHODOLOGY

3.1 STUDY AREA

The Equatorial Atlantic is a dynamic and complex region of the Atlantic Ocean, spanning approximately 10°N to 10°S latitude and extending longitudinally across the ocean basin. This region is of critical importance in oceanography, climate science, and marine ecosystems due to its distinct oceanographic and atmospheric processes (Carton et al., 2005).

The western boundary of the Equatorial Atlantic is defined by the coastlines of South and Central America, including Brazil, Colombia, and Venezuela. In contrast, the eastern boundary is delineated by the west coast of Africa, including Gabon, Congo, and Angola (Molinari & Johns, 1984). Ocean circulation in the region is influenced by major current systems, such as the North Equatorial Current (NEC) in the north and the South Equatorial Current (SEC) in the south (Stramma & Lutjeharms, 1997).

One of the most striking features of the equatorial Atlantic is the Equatorial Undercurrent (EUC), a subsurface, eastward-flowing current that occurs at depths of 100 to 300 meters (Philander, 1978). The EUC plays a crucial role in transporting heat and nutrients across the equatorial Atlantic, interacting with surface currents to shape the regional oceanographic structure (Lumpkin and Garzoli, 2011). In addition, the eastward-flowing North Equatorial Countercurrent (NECC) separates the NEC from the SEC and significantly influences the transport of warm water and momentum (Grodsky et al., 2012).

This study uses two key index regions to analyze Atlantic Niño variability:

Atl3 region (3°S–3°N, 0°–20°W): Represents the eastern equatorial Atlantic, where SST anomalies determine Atlantic Niño variability.

Western Equatorial Atlantic region (WEA) (3°S–3°N, 40°–20°W): used to compute zonal SST gradients by evaluating the difference in anomalies between the two regions.

These defined regions provide a basis for understanding Atlantic Niño dynamics and the atmosphere-ocean interactions governing its variability, as indicated in Figure 3.1.

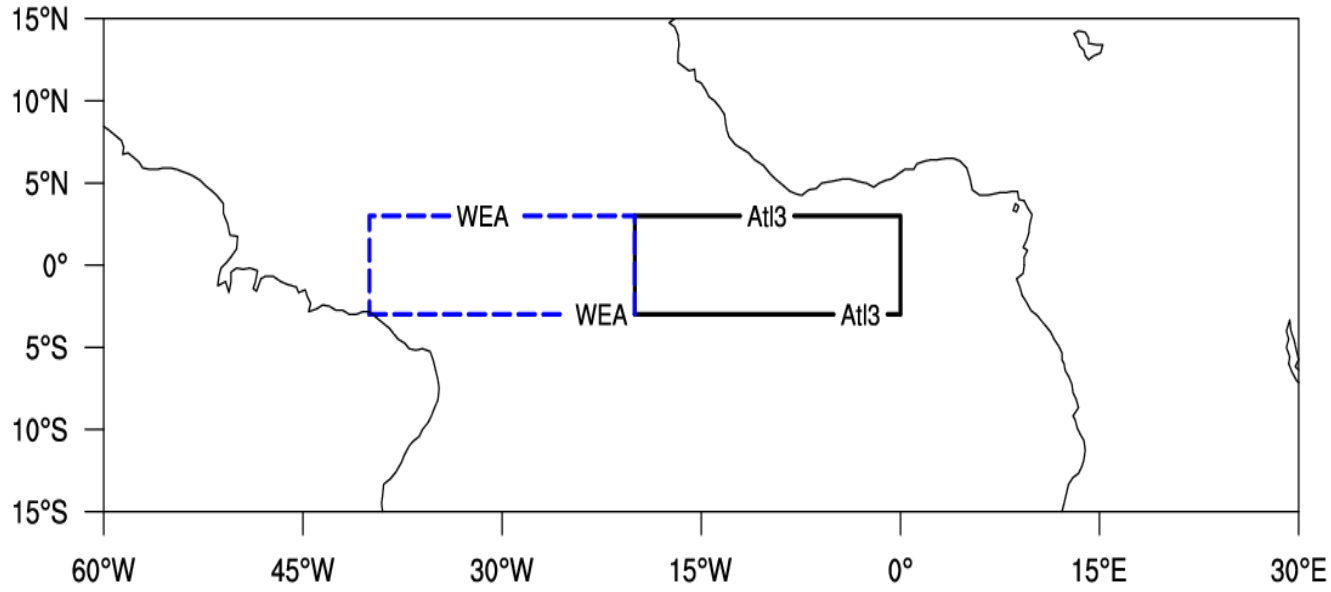

Figure 3.1: Location of Atl3 (3°S–3°N, 0°–20°W) and WEA (3°S–3°N, 40°–20°W), which were used as indices and also used to calculate the zonal gradient as the difference between the anomalies averaged over the two fields. Source (Gyuk et al., 2025)

3.2 STUDY DATA

This study utilizes multiple datasets to analyze the ocean-atmosphere interactions governing Atlantic Niño variability. These datasets include satellite-based products, reanalysis data, seasonal forecast system outputs, and Coupled Model Intercomparison Project Phase 6 (CMIP6) simulations. Key parameters analyzed include sea surface temperature (SST), precipitation, potential temperature profiles, zonal and meridional ocean currents, sea surface height (SSH), sea level pressure (SLP), zonal and meridional wind stress, zonal wind, vertical velocity, and mixed layer depth. All variables are analyzed at monthly and seasonal time resolutions to facilitate assessments of interseasonal and interannual variability.

3.2.1 Observational Data

a) Sea Surface Temperature (SST)

The Bjerknes feedback and air-sea interaction are investigated using monthly gridded sea surface temperature (SST) data. The SST used is from the Hadley Centre Global Sea Ice and Sea Surface Temperature (HadISST) version v1.1, available at a resolution of 10 degrees of longitude and 10 degrees of latitude (Rayner et al., 2003, 2006). It corresponds to monthly mean SST values at 0 °C. The HadISST data are freely available at https://www.metoffice.gov.uk/hadobs/hadisst/.

b) Global Precipitation Climatology Centre (GPCP) Precipitation

This study utilizes the Global Precipitation Climatology Centre (GPCP) version 2.3 dataset (Adler et al., 2003). The GPCP provides monthly precipitation products constructed from global land surface precipitation measurements at a resolution of 2.5° × 2.5°. The GPCP product is available at https://psl.noaa.gov/data/gridded/data.gpcp.html.

3.2.2 Reanalysis Data

a) Global Ocean Data Assimilation System (GODAS)

The NOAA Global Ocean Data Assimilation System (GODAS) v2.0.4 is an ocean analysis and reanalysis system developed by NOAA's National Centers for Environmental Prediction (NCEP). It provides oceanic initial conditions for seasonal and climate forecasts, primarily for the Climate Forecast System (CFS) (Behringer et al., 1998).

The study utilizes sea surface height (SSH), vertical profiles of potential temperature, and zonal and meridional current velocities from the Global Ocean Data Assimilation System, which has a horizontal spatial resolution of 10 degrees longitude by 10 degrees latitude and is available at https://psl.noaa.gov/data/gridded/data.godas.html.

b) NCEP/NCAR Reanalysis

The National Centers for Environmental Prediction (NCEP) reanalysis data were compiled from observations from ground stations, radiosondes, and other data (Kalnay et al., 1996). These data were incorporated into assimilation modeling for the period 1957-1996.

The monthly-averaged data set of sea level pressure and monthly vertical velocity at pressure levels, produced by NCEP/NCAR Reanalysis 1, consists of four daily, monthly, and annual atmospheric model data sets from 1948 to the present, with a horizontal spatial resolution of 2.50 degrees longitude by 2.50 degrees latitude. It is available at https://www.psl.noaa.gov/data/gridded/data.ncep.reanalysis.html.

c) ORAS5 Reanalysis

ORAS5 (Ocean ReAnalysis System 5) is a high-resolution global ocean reanalysis product developed by the European Centre for Medium-Range Weather Forecasts (ECMWF). It provides historical estimates of ocean state using data assimilation techniques (Zuo et al., 2019).

The ORAS5 datasets used include zonal and meridional current velocities, surface momentum flux (τu and τv), mixed layer depth, and potential temperature, with a spatial resolution of 0.25 degrees longitude by 0.25 degrees latitude. The ORAS5 reanalysis datasets are available at https://www.ecmwf.int/en/forecasts/dataset/ecmwf-reanalysis-v5.

d) ERA5 Reanalysis

ERA5 is a global atmospheric reanalysis product of the European Centre for Medium-Range Weather Forecasts (ECMWF) (Hersbach et al., 2020). It provides high-resolution historical weather and climate data. The monthly-averaged ERA5 reanalysis dataset used for the study includes vertical velocity and zonal wind at pressure levels with a spatial resolution of 0.250 degrees longitude by 0.250 degrees latitude.

3.2.3 Seasonal forecast ensemble Data

The seasonal forecast dataset used in this study comes from the 51-member ensemble of the European Centre for Medium-Range Weather Forecasts (ECMWF) Seasonal Forecast System (Hersbach et al., 2020). This system was designed to provide long-range climate forecasts by simulating interactions between the atmosphere, ocean, and land surface. Ensemble members are initialized on the first day of each month under observational initial conditions to ensure a realistic representation of the climate state at the start of each forecast. The forecasts are then integrated for lead times of 1 to 6 months (Johnson et al., 2019). We used the monthly sea surface temperature

(SST) dataset with a spatial resolution of 0.250 degrees longitude by 0.250 degrees latitude. The ECMWF seasonal forecast system datasets are available at https://cds.climate.copernicus.eu/cdsapp#!/dataset/seasonal-monthly-single-levels?tab=form.

3.2.3. CMIP6 AMIP ensemble

Recent changes in the strength of the Bjerknes feedback in the equatorial Atlantic are investigated using multiple general circulation model (GCM) simulations from the Coupled Model Intercomparison Project Phase 6 (CMIP6) (Eyring et al., 2016), obtained from https://esgf-node.llnl.gov/search/cmip6/ for the period 1979-2014, which have the advantage of physically consistent and gap-free data. Details of the models used in this study are summarized in Table 3.1. The experiment considered here is the Atmospheric Model Intercomparison Project (AMIP), which runs atmospheric GCMs and atmospheric general circulation models (AGCMs) with observationally derived SSTs. The fully coupled models suffer from severe atmosphere-ocean biases in the equatorial Atlantic (Richter et al. 2014), while the AMIP simulations based on observed SSTs are less biased.

To assess the strength of the atmosphere-ocean coupling in this study, a multi-model ensemble (MME) of the Atmospheric Model Intercomparison Project (AMIP) was constructed by averaging the outputs of 26 ensemble members. This ensemble-averaging approach helps reduce individual model biases and internal variability, thus isolating the robust features of atmospheric forcing on the ocean surface across models.

Table 3.1. Basic details of 26 models employed in this study from **CMIP6.**

Model Name	Institution, Country	Resolution (lon. x lat.)
ACCESS-CM2	CSIRO-ARCCSS, Australia	192 × 144
ACCESS-ESM1-5	CSIRO, Australia	192 × 144
BCC-CSM2-MR	BCC, China	320 × 160
BCC-ESM1	BCC, China	128 × 64
CanESM5	CCCma, Canada	128 × 64
CAS-ESM2-0	CAS, China	256 × 128
CESM2	NCAR, USA	288 × 192
CESM2-WCCAM	NCAR, USA	288 × 192
EC-Earth3-AerChem	EC-Earth Consortium, Europe	512 × 256
EC-Earth3	EC-Earth Consortium, Europe	512 × 256
EC-Earth3-CC	EC-Earth Consortium, Europe	512 × 256
EC-Earth3-Veg-LR	EC-Earth Consortium, Europe	320 × 160
FGOALS-f3-L	CAS, China	288 × 180
FGOALS-g3	CAS, China	180 × 80
GFDL-ESM4	NOAA-GFDL, USA	288 × 180
GISS-E2-1-G	NASA GISS, USA	144 × 90
INM-CM4-8	INM, Russia	180 × 120
INM-CM5-0	INM, Russia	180 × 120
IPSL-CM6A-LR	IPSL, France	144 × 143
MPI-ESM1-2-LR	MPI-M, Germany	192 × 96
MPI-ESM-1-2-HAM	HAMMOZ, Germany	192 × 96
MRI-ESM2-0	MRI, Japan	320 × 160
NESM3	NUIST, China	192 × 96
NorCPM1	NCC, Norway	144 × 96
NorESM2-LM	NCC, Norway	144 × 96
SAM0-UNICON	SNU, Korea	288 × 192

3.3 METHODOLOGY

3.3.1 Basic statistical principles

3.3.1.1 Correlation and explained variance

Correlation analysis measures the strength and direction of the relationship between two variables. In statistics, the correlation coefficient (r) ranges from +1 to -1, where r = 1 represents a perfect positive relationship, r = -1 represents a perfect negative relationship, and r = 0 represents no linear correlation.

$$r = \frac{n(\sum xy) - (\sum x)(\sum y)}{\sqrt{[n\sum x^2 - (\sum x)^2][n\sum y^2 - (\sum y)^2]}} \quad (3.1)$$

In statistics, three types of correlation are commonly measured: Pearson correlation, Kendall rank correlation, and Spearman correlation.

The explained variance, also known as the coefficient of determination, denoted by R^2 or r^2 (correlation squared), is a number that quantifies the proportion of the variability in the dependent variable that the independent variable can explain. Mathematically, R^2 is expressed as the ratio of the explained variance to the total variance. The coefficient of determination is thus a measure of the proportion of the explained variance.

A higher R^2 value indicates that the independent variable has greater explanatory power than the dependent variable.

3.3.1.2 Climatology, Seasonal Mean and Standardized Anomaly

Three vital statistics are frequently used in the analysis of this work: the climatology, the seasonal mean, and the standardized anomaly. Climatology is defined here as the long-term average of a given variable, often over periods of 20 to 30 years. Climatology can be calculated for different time

periods. For example, a monthly climatology provides a mean for each month, and a daily climatology provides a mean for each day over a given period.

The seasonal mean represents the average value of a given variable over a specific season, typically defined as a three-month period (e.g., June to August for summer). It provides insight into the prevailing climate conditions of that season and is useful for identifying long-term trends, variability, and departures from typical conditions. Seasonal means are widely used in climate studies to smooth out short-term fluctuations and highlight large-scale patterns.

Anomalies, or deviations from the mean, arise from subtracting climatological values from observed data. Standardized anomalies (also called normalized anomalies) are calculated by dividing the anomalies by the climatological standard deviation. They generally provide more information about the magnitude of the anomalies because scattering effects have been removed.

3.3.1.3 Standard Deviation

The standard deviation is a measure of the dispersion of a data set relative to its mean. It quantifies how much individual data points deviate from the mean and provides information about the variability within a data set. A higher standard deviation indicates greater variability, while a lower standard deviation indicates that the values are more closely clustered around the mean.

Mathematically, the standard deviation (σ) is calculated as follows:

$$\sigma = \sqrt{\frac{1}{N}\sum_{i=1}^{N}(X_i - \bar{X}_\iota)^2} \qquad (3.2)$$

where:

X_i represents individual data points,

$\bar{X}$ is the mean of the dataset, and

N is the total number of observations.

3.3.1.4 Climate Indices

Indices are diagnostic tools for describing the state of a climate system. Climate indices are usually presented as time series; each point in time corresponds to an index. An index can be created to describe almost any climate event, for example, the Atlantic Niño/Niña event indices.

3.3.1.5 Index regions

Two Atlantic Nino indices were used in the present study: the Atlantic Nino Index (Atl3), defined as the normalized area-averaged SST anomalies over the eastern region of the equatorial Atlantic (3°N-3°S, 0°-20°W) (Zebiak, 1993), and the zonal gradients, defined as the differences between the area-averaged anomalies over the eastern equatorial Atlantic (3°S-3°N, 0°-20°W) and western equatorial Atlantic (3°S-3°N, 40°-20°W) regions. The western equatorial Atlantic surface wind index (WEA) was calculated as the average of the surface winds over (3°S-3°N, 40°-20°W). Finally, precipitation anomalies over the equatorial Atlantic (3°N-3°S, 5°E-40°W) were averaged, and precipitation anomalies over the Guinean coast (4°N-10°N, 15°W-10°E) were averaged.

3.3.1.6 Bias

Bias refers to the deviation of the statistical mean from the estimated parameter, i.e., the error in estimating a variable. The bias of an estimator is the difference between the observed value of the estimator and its estimated value. An estimator with a bias of zero is considered unbiased. Otherwise, it is considered biased. The bias is calculated using the following equation:

$$Bias(mm) = \frac{1}{N}\sum_{i}^{N}\left(X_{i(est)} - X_{i(obs)}\right)$$

(3.3)

where: N is the number of data pairs

$X_{obs}$is the observed value and $X_{pred.}$is the modelled value at time/place i.

3.3.1.7 Root Mean Square Error (RMSE)

The mean square error (RMSE) (also called root mean square deviation, RMSD) is a commonly used measure of the difference between the values predicted by a model and the values actually observed in the modeled environment. These individual differences are also called residuals, and the RMSE serves to summarize them into a single measure of predictive power. The RMSE of a model prediction with respect to the estimated variable is defined as the square root of the mean square error. The calculated RMSE values have the unit of the variable under consideration and are expressed as follows:

$$RMSE = \sqrt{\frac{1}{N}\sum_{i}^{N}\left(X_{i(pred.)} - X_{i(obs.)}\right)^{2}} \quad (3.4)$$

where

N is the number of data pairs

$X_{obs}$is the observed value and $X_{pred.}$is the modelled value at time/place i.

3.3.1.8 Regression Analysis

Regression analysis is a multivariate statistical technique for estimating relationships between variables. It encompasses numerous techniques for modeling and analyzing multiple variables, focusing on the relationship between a dependent variable and one or more independent variables.

Regression analysis is widely used for prediction and forecasting. Numerous techniques have been developed for conducting regression analysis. Well-known methods such as linear regression and ordinary least squares regression are parametric, as the regression function is defined by a finite number of unknown parameters estimated from the data. Nonparametric regressions, such as the Mann-Kendall trend test and Theil-Sen trend estimation, refer to techniques that allow the regression function to be placed within a fixed set of functions, which can be infinite-dimensional.

Parametric tests, such as first-order regression analysis, make assumptions about the normality of the data distribution; therefore, the results can sometimes be influenced by outliers in the data. They are also prone to gross errors, and the associated confidence interval is sensitive to deviations from normality (Sen, 1968). In contrast, nonparametric tests are suitable for analyzing data that do not follow a normal distribution. Nonparametric methods focus on the location of the probability distribution of the population under study, rather than on specific parameters of the population. The test result is not determined by the total size of the data points, but depends on the ranking of the individual data points. Assumptions about the data distribution are not required for nonparametric tests.

3.3.1.9 Tests for Statistical Significance

Statistical significance assesses whether an observed result is likely to have occurred by chance or represents a meaningful pattern in the data. Significance testing helps determine whether relationships, trends, or anomalies are robust and not due to random variability.

A commonly used approach is hypothesis testing. The null hypothesis (H_0) assumes no real effect, while the alternative hypothesis (H_1) suggests a significant effect. Significance is typically assessed using a p-value, which indicates the probability of achieving the observed result if the null hypothesis

is true. A p-value below 0.05 (5%) is often used as the threshold for statistical significance, although more stringent values (e.g., 0.01 or 0.001) can be applied in high-confidence analyses.

Other common methods for assessing significance in climate research include Student's t-test (for comparing means), Monte Carlo or bootstrapping methods (for robust uncertainty estimation), field significance tests (for evaluating spatially distributed data), and false discovery rate (FDR) correction (to control for multiple testing bias).

For all results of the regression analyses conducted in this study, statistical significance was tested using a two-tailed Student's t-test with a marked 95% confidence level. Statistical tests are reported with $p \leqslant 0.05$, which corresponds to this confidence level. The ±95% confidence limits are given in the explanation of the range. Autocorrelation was accounted for in statistical significance tests for the regression coefficients by adjusting the number of degrees of freedom for the time series pairs according to the method of Bretherton et al. (1999):

$$N = N\frac{(1-r_1 r_2)}{(1+r_1 r_2)} \qquad (3.5)$$

where N is the length of the time series; r_1 and r_2 are the lag-1 autocorrelation coefficients of the time series, respectively; and N* is the adjusted number of degrees of freedom used for determining the statistical significance.

3.3.1.10 Analysis Period

The period of analysis for observations and the reanalysis dataset is 1982-2021.

The CMIP6 AMIP simulations cover the period from 1979 to 2014.

The modeled SST results were converted to a standard grid of $1^0 \times 1^0$ longitudes, and precipitation amounts were converted to $2.5^0 \times 2.5^0$ longitudes, consistent with the observations.

Monthly SST and precipitation anomalies were first calculated for each grid point as the difference between the climatological and the monthly mean for each year. The anomalies were then detrended to remove long-term trends and to focus on the interannual variability. Subsequently, the seasonally averaged anomalies were calculated for the JJA season, that is, when the Atlantic Niño exhibits maximum variability (Morioka et al., 2011; Nnamchi et al., 2011; Nnamchi and Li, 2016).

3.4 Analyses

3.4.1 Linear Correlation and Regression Analyses

Correlation and linear regression techniques will be utilized to examine the relationships between two different variables. The strength of atmosphere-to-ocean Bjerknes feedback will be quantified by the regression of zonal wind stress, precipitation, and sea surface height onto the Atlantic Niño index defined as the SST anomalies averaged in the eastern equatorial Atlantic (3°N-3°S,0°-20°W). This method involves applying a linear equation to the already proposed dataset to establish a relationship between the two variables: the dependent variable and the independent variable.

Equation (3.6) typically represents the linear regression model:

$$Y = a + bX \tag{3.6}$$

where Y is the dependent variable, X is the independent variable, b is the slope of the line, and a is the intercept constant. A positive and negative value of b indicates that the data tend to increase or decrease with time, respectively.

3.4.2 Changes in the atmosphere-to-ocean Bjerknes feedback observed after 2000

To investigate the mechanisms underlying the observed weakening of the atmosphere-ocean Bjerknes feedback in the equatorial Atlantic after 2000, we adopted the methodological framework previously applied to the tropical Pacific by Zheng et al. (2014, 2016) and Li et al. (2024). Their diagnostic approach, developed to assess the westward shift and weakening of the Pacific feedback, is well-suited to isolating the roles of individual atmospheric processes within the coupled system. Here, we apply a similar framework to the tropical Atlantic to evaluate whether comparable atmospheric subprocesses are responsible for the recent weakening observed in this basin.

The original Bjerknes (1969) framework identified a sequence of coupled interactions between sea surface temperature (SST), atmospheric convection, sea level pressure (SLP), and surface wind stress, which together form a positive feedback loop in the tropics. Lin (2007) later elaborated these interactions into three key atmospheric subprocesses:

1. Subprocess 1: dSST/dx → dPrecip/dx - the response of atmospheric deep convection to zonal SST gradients.

2. Subprocess 2: dPrecip/dx → dSLP/dx - the response of zonal SLP gradients to zonal convection gradients.

3. Subprocess 3: dSLP/dx → τx - the response of zonal wind stress anomalies (τx) to SLP gradients.

To assess changes in the strength of each subprocess over time, the linear sensitivity of each relationship was evaluated for two periods: 1979-1999 and 2000-2021, using observational datasets. This approach enables assessment of how the individual components of the feedback loop may have weakened and contributed to the overall reduction in atmosphere-to-ocean coupling.

Here, the monthly anomalies of the observed and simulated data are derived by removing the climatological monthly means and the long-term trends from each calendar month. The long-term trend is calculated by fitting a linear regression model to each variable over time. For the observational datasets, long-term trends and climatological monthly means are calculated for the period 1979-2021, while for the AMIP simulations, they are calculated for the period 1979-2014.

3.4.2.1. The zonal gradient

The zonal gradients in this study are defined as the normalized differences between the area-averaged anomalies over the eastern equatorial Atlantic (Atl3) and the western equatorial Atlantic (WEA). They are calculated as follows:

$$\frac{dX}{dx} = X_{[Atl3]} - X_{[WEA]} \tag{3.7}$$

where X represents the variable of interest (e.g., SST, precipitation, sea level rise). The square brackets [ ] denote area means, and the two abbreviations in the square brackets denote the regions used for the area means. These are (Atl3; 3°S-3°N, 0°-20°W) and (WEA; 3°S-3°N, 40°-20°W), as shown in Figure 3.1. A similar approach has been used to calculate zonal SST in the equatorial Atlantic (Tokinaga and Xie, 2011).

The linear regression method is used to investigate the relationships between two different variables. The strength of the Bjerknes feedback between the atmosphere and the ocean is quantified by regressing the zonal wind stress on the zonal gradient of sea surface temperature (dSST/dx). Firstly, the observed zonal gradient of SST (dSST/dx) was regressed against the observed zonal wind stress anomalies (τ_x) map. Similarly, the observed dSST/dx was regressed against the zonal wind stress ensemble from AMIP/CMIP6 simulations to determine the strength of the atmosphere-to-ocean Bjerknes feedback before and after the year 2000.

We use ordinary least squares to investigate the response between atmospheric subprocesses related to the positive Bjerknes feedback. The results of the three subprocesses are summarized in scatterplots illustrating the relationship between zonal SST gradients and the corresponding response of the zonal precipitation gradient; Subprocess 1: the changes in the zonal SLP gradient caused by changes in the zonal precipitation gradient; Subprocess 2: the changes in the zonal wind stress caused by changes in the zonal SLP gradient; Subprocess 3: The slope of the regression line represents the sensitivity of the variables in each subprocess.

3.4.3 Composite analysis

Categorization of events. To categorize extreme Atlantic Niño/Niña events, the June-August (JJA) mean Atl3 SST anomalies over the period 1982-2021 were first computed. The JJA Atl3-SST anomalies were then normalized to obtain the normalized JJA Atl3-SST index, which captures the interannual variability in the eastern equatorial Atlantic during the boreal summer, that is when Atlantic Niño events typically peak. Events were classified as extreme warm (Atlantic Niño) when the normalized JJA Atl3-SST anomalies exceeded +1.0 standard deviation, and as extreme cold (Atlantic Niña) when they fell below -1.0 standard deviation. This threshold ensures that only the most pronounced SST anomalies, representing the upper and lower extremes of the distribution, are retained for the analysis.

Composite Differences Between Canonical and Non-Canonical Events

To investigate the role of atmospheric preconditioning in the development of Atlantic Niño/Niña events, all identified extreme events were categorized based on the presence or absence of significant atmospheric convection before the peak SST anomalies. This classification is grounded in the

hypothesis that deep convection in the equatorial Atlantic during May, one month before the June SST peak, is a key driver in enhancing warm SST anomalies in the eastern equatorial basin.

Events were initially categorized into two types: canonical and non-canonical. Canonical warm events were defined as those where June SST anomalies were preceded by enhanced positive May precipitation anomalies, indicating strong convection-ocean coupling. Non-canonical warm events lacked this preceding convection signal. Similarly, canonical cold events were identified by negative SST anomalies preceded by negative precipitation anomalies, while non-canonical cold events showed no such antecedent atmospheric signal.

Subsequently, composite differences were computed to examine the structural differences between canonical and non-canonical events. The canonical composite difference was derived by subtracting the mean of canonical cold events from that of canonical warm events. The same procedure was applied to non-canonical events. These composites allow for the isolation of the characteristic patterns associated with each event type and aid in identifying their distinct physical mechanisms. The spatial structures derived from these composites were found to be consistent with those obtained via linear regression analysis, affirming the reliability of the classification and analysis framework.

Predictability of Events:

To assess the predictability of canonical and non-canonical Niño events in the Atlantic, the outputs of a seasonal forecast system are analyzed:

European Centre for Medium-Range Weather Forecasts (ECMWF): A 51-member ensemble initialized on the first day of each month and integrated for lead times of 1 - 6 months for the period 1982 - 2021 (Johnson et al., 2019).

Due to different grid resolutions, the SST outputs of the forecast systems are bilinearly mapped to a common 1° × 1° grid (latitude and longitude) consistent with the HadISST observational dataset.

Predictability Assessment:

The forecast skill of the ECMWF seasonal forecast systems would be evaluated using HadISST as the reference dataset:

Monthly anomalies for both observed and forecast data are derived by removing long-term trends and climatological monthly means from 1982 to 2021.

The ECMWF seasonal forecast system ensemble consists of state-of-the-art operational seasonal forecasts from eight centers, available for lead times of one to six months. Lead times denote the time interval between forecast initialization and the target month. Since this research focuses on the Atlantic Niño, which peaks in June, June was chosen as the target month. A lead time of one month means that the forecast was initialized on May 1, whereas a forecast with a six-month lead time was initialized on December 1.

Seasonal forecast systems composites:

Forecast systems composites for each lead time (1–6 months) are constrained to the observed canonical and non-canonical event years, ensuring alignment between forecast and observational datasets.

Skill Metrics:

Correlation skill and root mean square error (RMSE) are calculated between forecast anomalies and HadISST anomalies for the JJA seasonal average at each lead time.

By constraining the forecast system composites to observational years, we ensure consistency in event timing across datasets, allowing a robust comparison of model predictability for canonical and non-canonical Atlantic Niño events.

The composites are tested for statistical significance using a two-sided *t*-test and the 90% confidence level.

3.4.4 Mixed-layer heat budget

We calculated the heat budget by decomposing the time derivative of the temperature ($\partial T/\partial t$) averaged in the ocean-mixed-layer as follows:

$$\frac{\partial \langle T \rangle}{\partial t} = \underbrace{\left\langle u\frac{\partial T}{\partial x} + v\frac{\partial T}{\partial y}\right\rangle}_{horizontal advection} + \underbrace{\frac{1}{h}|\langle T\rangle - T_{-h}|w_e}_{entrainment} + \underbrace{\frac{Q_{net}}{\rho C_w h}}_{heat flux} + \epsilon \quad (3.8)$$

where T, u, and v are the sea temperature and the zonal and meridional ocean current velocities, respectively. The differential operators (x, y represent zonal and meridional directions, respectively, and t represents time). ρ and C_w are constants representing seawater density (ρ = 103 kg m^{-3}) and specific heat capacity (Cw = 4 × 103 J^{-1} kg^{-1} K), h is the annually varying monthly mean depth of the mixed layer, T_{-h} is the temperature at the base of the mixed layer, w_e is the entrainment velocity (Nnamchi et al., 2021a), and Q_{net} is the net surface heat flux. ϵ is the residual term representing the sum of unresolved physical processes (such as mixing and high-frequency variability not resolved by the monthly mean time series). T, u, and v are based on vertical averages over the depth of the oceanic mixed layer (h). All values are also averaged over the eastern equatorial Atlantic (3°N-3°S, 0°-20°W); this corresponds to the Atl3 region (Zebiak, 1993). The terms on the right-hand side of the equation represent zonal advection, meridional advection, entrainment, heat flux, and error terms, respectively.

CHAPTER FOUR

4 RESULTS AND DISCUSSION

4.1 The ocean-atmosphere coupled processes influencing the Atlantic Niño variability

4.1.1 Coupled variability in the equatorial Atlantic

Figure 4.1 shows the two leading empirical orthogonal functions (EOFs) derived from linearly detrended monthly sea surface temperature anomalies (SSTA) over the tropical Atlantic during the period 1982 - 2021 using the HadISST dataset. The first EOF, which captures the dominant mode of SST variability- commonly referred to as the Atlantic Niño mode explains about 37.7% of the total seasonal SST variance. The second EOF explains 24.3% of the variability, indicating its importance as a secondary, yet substantial, driver of SST variability in the region.

The spatial structure of the leading EOFs is characterized by a zonal pattern of positive SST anomalies centered over the eastern and central equatorial Atlantic, typically associated with the warm phase of the Atlantic Niño. These warm anomalies are flanked by relatively weaker SST anomalies in the far west of the tropical Atlantic. This zonal SST gradient is known to influence atmospheric convection and circulation patterns and thus plays a key role in regional climate variability.

The Atlantic Niño Index (Atl3-SST) is widely used to quantitatively monitor and represent SST anomalies associated with the Atlantic Niño. This index is defined as the area-averaged monthly SST anomaly over the region between 3°S-3°N and 0°-20°W (see the black box in Figure 4.1). This index has been widely used in previous studies (e.g., Zebiak, 1993; Keenlyside & Latif, 2007) to investigate air-sea interactions, particularly the role of oceanic-atmospheric coupling in the equatorial Atlantic.

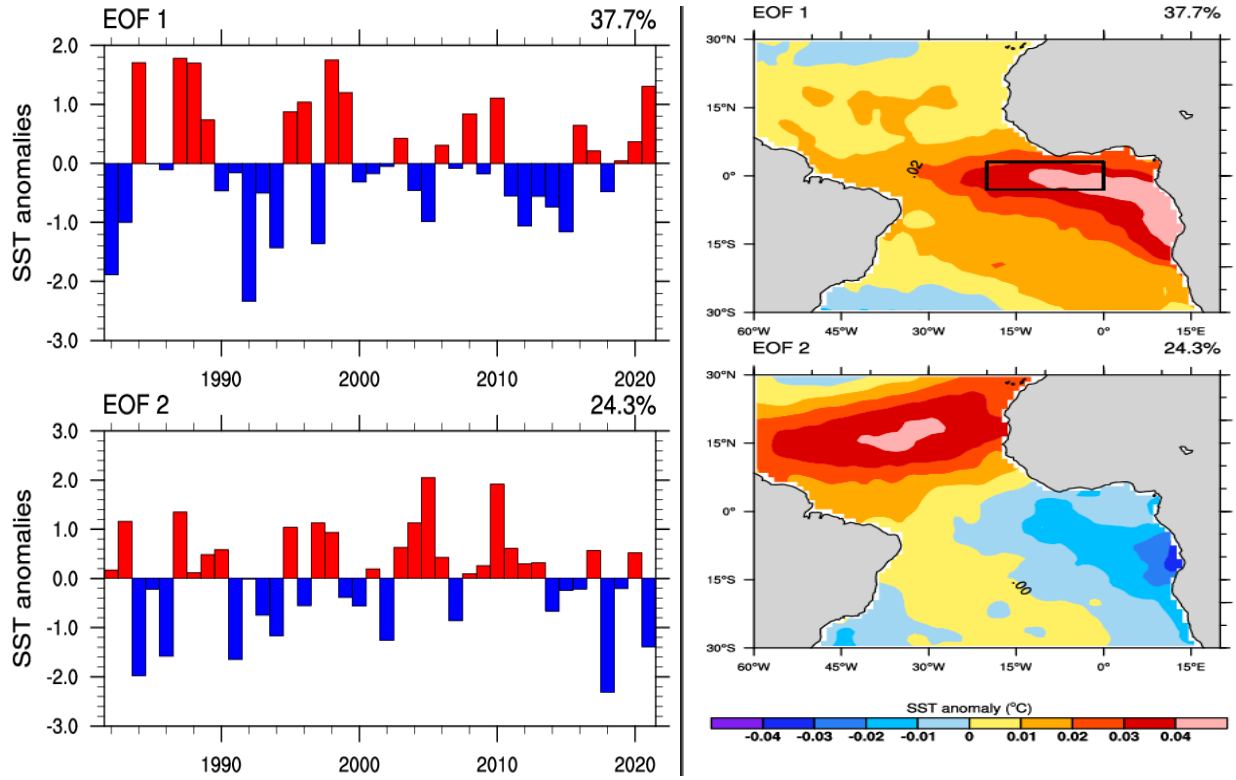

Figure 4.1: Spatial pattern and temporal evolution of sea surface temperature (SST) anomalies in the tropical Atlantic for the period 1982-2021.

4.1.2.1 Bjerknes positive feedback in the equatorial Atlantic

The first element of the positive Bjerknes feedback describes the ocean-atmosphere coupling, in which monthly SST anomalies in the eastern equatorial Atlantic modulate zonal surface wind anomalies over the central and western basin. This mechanism is investigated by regressing monthly SST anomalies in the Atl3, an index used to capture SST variability in the eastern equatorial Atlantic, onto zonal surface wind anomalies (Zebiak 1993; Keenlyside and Latif 2007).

The regression results reveal a characteristic ENSO-like pattern, in which positive SST anomalies in the eastern basin are associated with positive westerly wind anomalies in the west and negative easterly wind anomalies in the east (Figure 4.2). This spatial structure is similar to the Pacific El Niño feedback, in which SST anomalies trigger surface wind responses that amplify the initial SST anomaly. The magnitude of the coupling in the equatorial Atlantic suggests that a 1°C increase in Atlantic sea surface temperature (SST) corresponds to a maximum westerly wind anomaly of about 0.6 to 1.0 m/s, centered primarily in the western equatorial Atlantic (Figure 4.2).

The SST-wind relationship explains only about 21% of the variability in the equatorial Atlantic (Figure 4.2). This suggests that other processes also play a significant role in modulating surface wind anomalies and SST anomalies in the Atlantic.

An analogous regression using zonal surface wind stress instead of surface zonal winds yields similar results with the same spatial response pattern (Figure 4.3). Interestingly, using wind stress results in higher explained variances of 23% (Figure 4.3), likely due to the stronger dynamical connection between surface wind stress and the ocean.In other words, the first element of the positive Bjerknes feedback can only explain 21-23% of the eastern equatorial SST anomalies and the western equatorial wind/wind stress variability. Thus, 79-77% of the equatorial Atlantic variability remains unaccounted for. This suggests that wind stress variability in the Bjerknes feedback-coupled

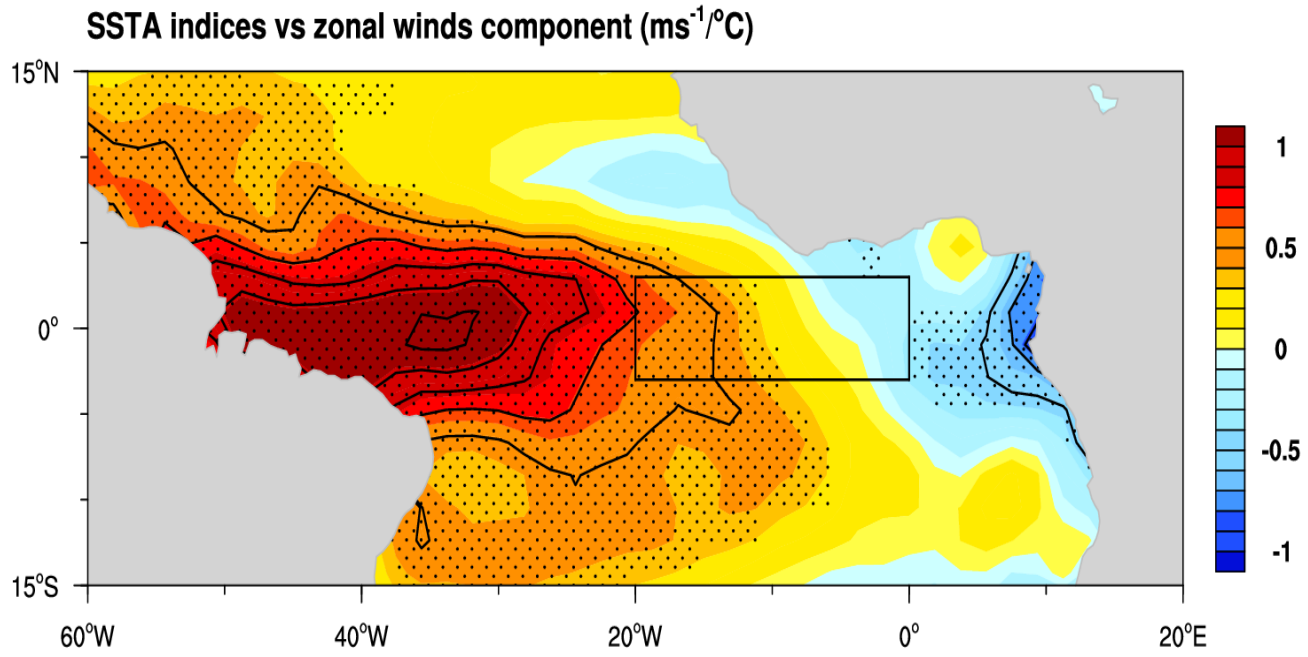

Figure 4.2: Atlantic3 (Atl3) SST anomalies regressed onto the 10-m zonal wind speed. The black contour denotes explained variances at an interval of 21%. Stippling denotes statistical significance at a 95% confidence level. The black solid box indicates the Atl3 region (3°S-3°N, 0°-20°W).

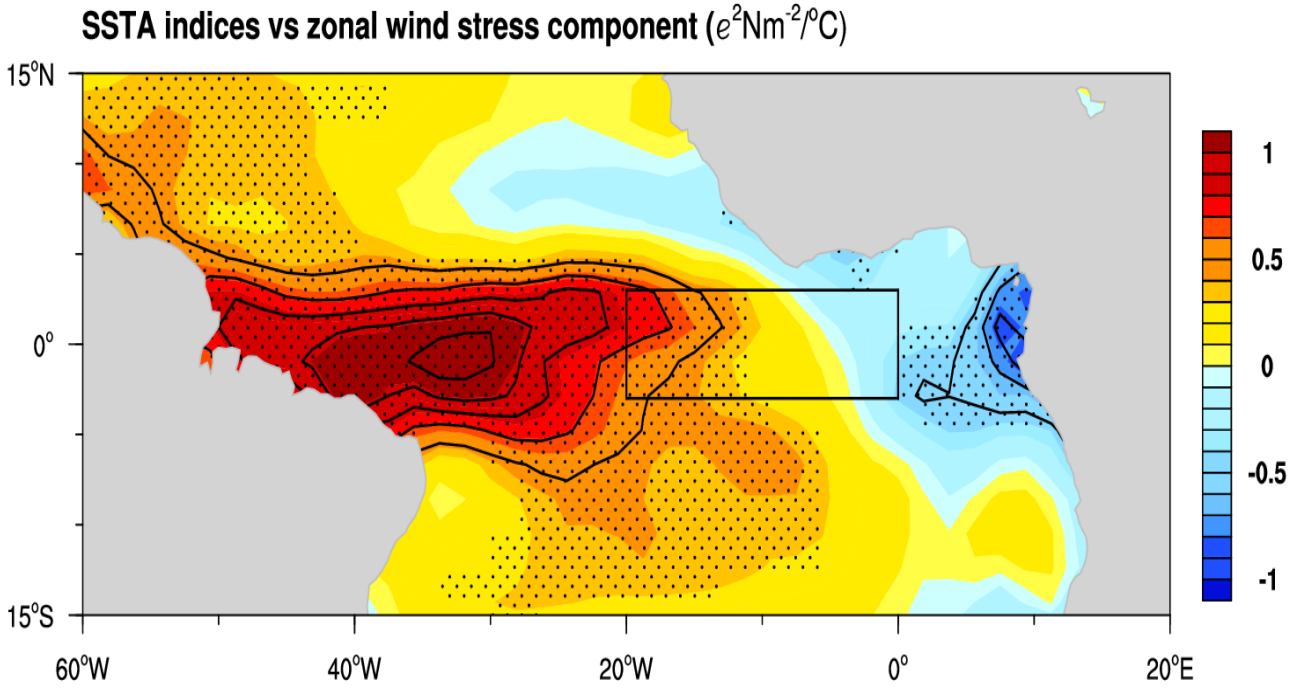

Figure 4.3: Atlantic3 (Atl3) SST anomalies regressed onto the zonal wind stress. Black contour denotes explained variances at an interval of 23%. Stippling denotes statistical significance at a 95% confidence level. The black solid box indicates the Atl3 region (3°S–3°N, 0°–20°W).

atmosphere-ocean anomalies associated with the Atlantic Niño appears to play a less significant role in shaping the atmosphere-ocean coupling in the equatorial Atlantic.

The second component of the positive Bjerknes feedback encompasses the dynamic coupling between the variability of surface winds, or more precisely, wind stress, over the western equatorial Atlantic, and variations in thermocline depth in the eastern equatorial Atlantic.

The regression result shows that westerly wind stress anomalies in the western equatorial Atlantic are associated with increased SSHA and increased HC in the eastern equatorial Atlantic, accompanied by a concurrent decrease in SSHA and HC in the west Atlantic (Figure 4.4). This dipole-like structure reflects the eastward propagation of thermocline and warm-water anomalies. It is consistent with the expected dynamics of equatorial Kelvin and Rossby waves driven by wind perturbations. This spatial pattern is in strong agreement with the analogous positive Bjerknes feedback observed in the Pacific.

However, it is essential to note that the strength of this coupling is comparatively weaker in the equatorial Atlantic. The regression coefficients are smaller, and the variance of the SSHA explained by zonal wind stress anomalies is lower than typically observed in the Pacific. This suggests that the underlying processes of the positive Bjerknes feedback are active in the Atlantic.

This aspect of the feedback describes how westerly wind stress anomalies in the western basin trigger oceanic adjustments in the eastern basin, which in turn amplify the original SST perturbation. An increase in SSHA in the east equatorial Atlantic corresponds to a deepening of the thermocline, which increases the upper heat content of the ocean and supports further warming SST anomalies. Conversely, a decrease in SSHA is associated with a shallowing of the thermocline and lower heat content.

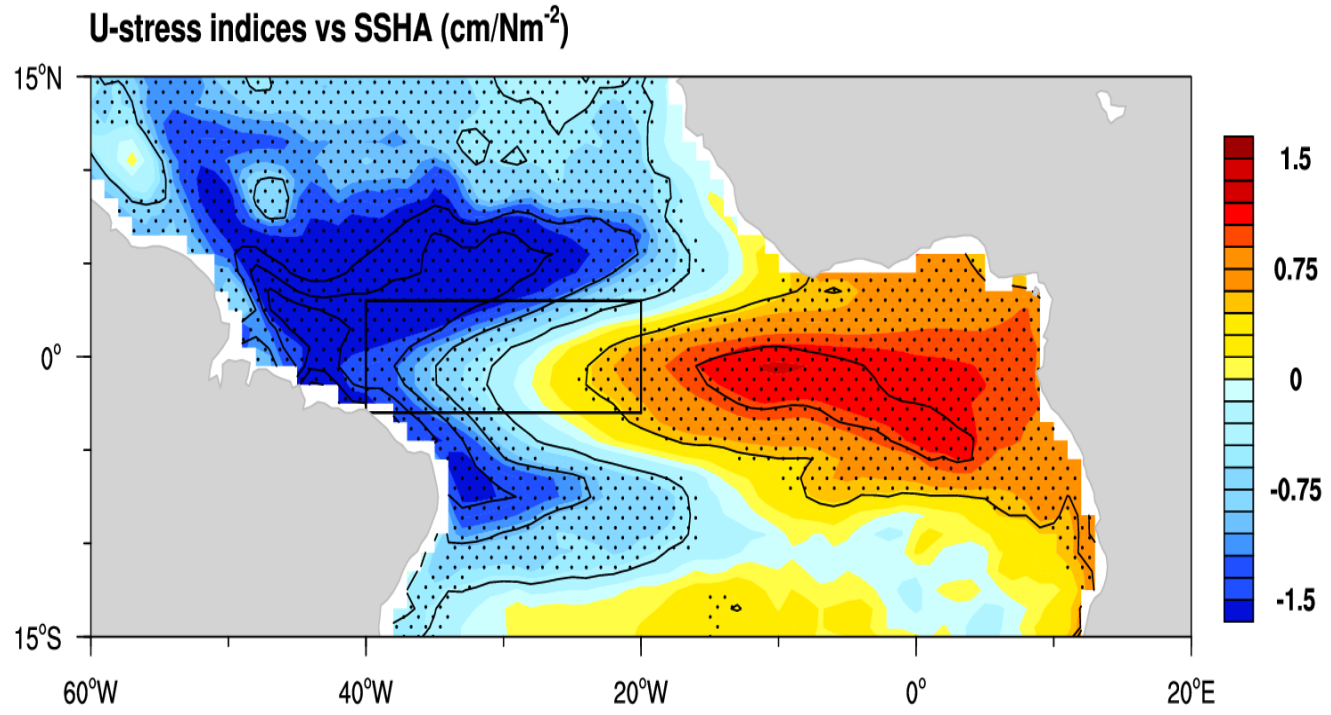

Figure 4.4: Zonal wind stress anomalies regressed on sea surface height anomalies. Black contours indicate explained variances in the 38% interval. Dots indicate statistical significance at the 95% confidence level. The black solid box indicates the WEA region (3°S–3°N, 40°–20°W).

Figure 4.5 shows the regression pattern of Atl3 SST anomalies against the sea surface height anomalies (SSHA). The strongest coupling is evident in the eastern to central equatorial Atlantic, particularly along the western boundaries of Africa, where the regression coefficients are somewhat stronger. This suggests that thermocline depth variability is vital in modulating SST variability in this region.

More importantly, the explained variance of SSHA by SST anomalies in the equatorial Atlantic reaches 37%, suggesting a substantial dynamic coupling between upper ocean and surface temperature variability (Figure 4.5). This result is further supported by a parallel analysis using ocean heat content (HC) anomalies instead of SSHA. Regression of Atl3 SST anomalies onto HC anomalies reveals a very similar spatial pattern and an even higher explained variance of 46% (Figure 4.6). These results confirm that, despite the smaller ocean basin size of the Atlantic compared to the Pacific, the coupling between thermocline variability and sea surface temperature (SST) is robust, particularly in the eastern equatorial Atlantic basin, and forms an integral part of the positive feedback system of the Atlantic Bjerknes feedback.

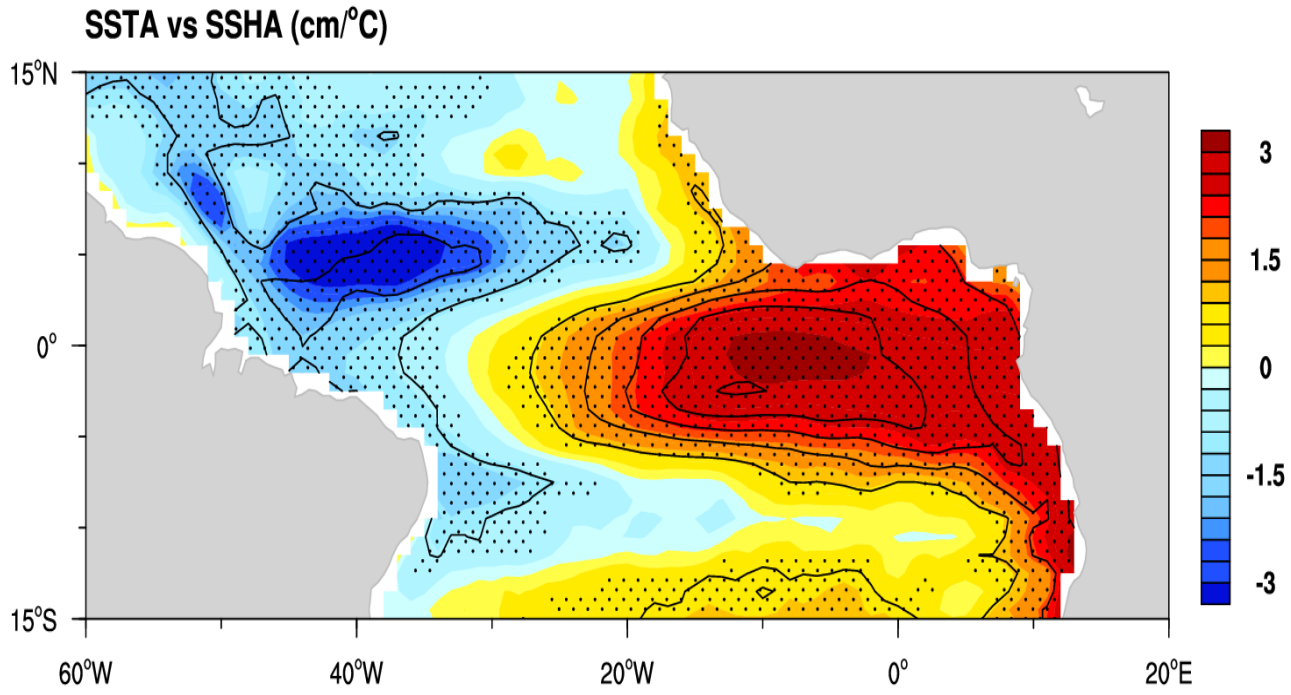

Figure 4.5: The SST anomalies of Atlantic3 (Atl3) were regressed onto the sea surface height anomalies. Black contours indicate explained variances at the 37% interval. Dots indicate statistical significance at the 95% confidence level.

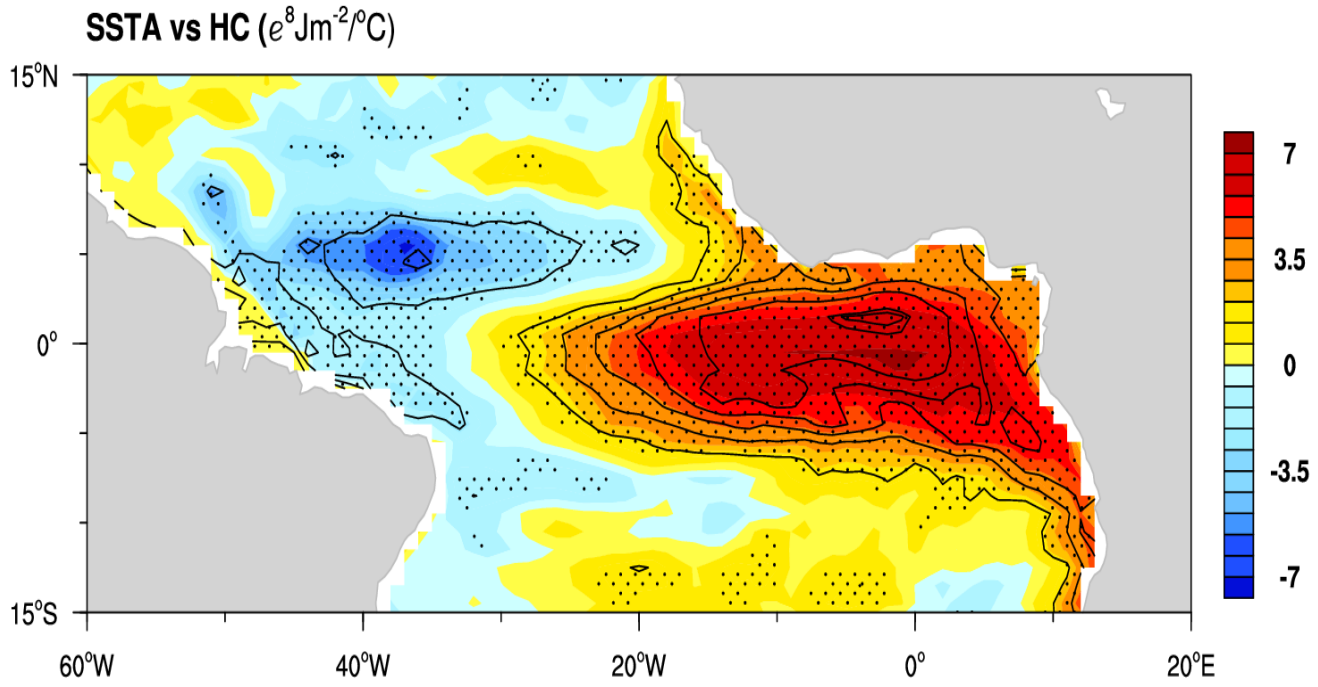

Figure 4.6: Atlantic3 (Atl3) SST anomalies regressed on heat content anomalies. Black contours indicate explained variances within the 46% interval. Dots indicate statistical significance at the 95% confidence level.

Figure 4.7 depicts a clear temporal relationship between oceanic and atmospheric convection variability. The regression result indicates that enhanced precipitation anomalies occur primarily along the western to central equatorial Atlantic (Figure 4.7). This spatial convection pattern indicates a strong atmospheric response to Atl3-SST anomalies, particularly during the developing phase of the Atlantic Niño. The associated explained variance is approximately 36%, suggesting a moderately strong relationship between Atl3 SST anomalies and precipitation variability in this region.

These results support the framework that atmospheric convection-ocean coupling, particularly in the meridional direction, is determined by the northward migration of the ITCZ and thermocline coupled feedback in the zonal direction, which contributes to the development and strengthening of Atl3 SST anomalies in the equatorial Atlantic.

In the equatorial Atlantic, atmospheric deep convection is significantly influenced by the position of the Intertropical Convergence Zone (ITCZ), which acts as a central regulator of tropical precipitation and atmospheric circulation. Variability in the latitudinal position of the ITCZ can significantly alter the spatial structure and strength of the precipitation response to SST anomalies. Such shifts can, in turn, modulate the strength of atmosphere-ocean coupling and the effectiveness of the positive Bjerknes feedback mechanism in maintaining or strengthening Atlantic Niño conditions.

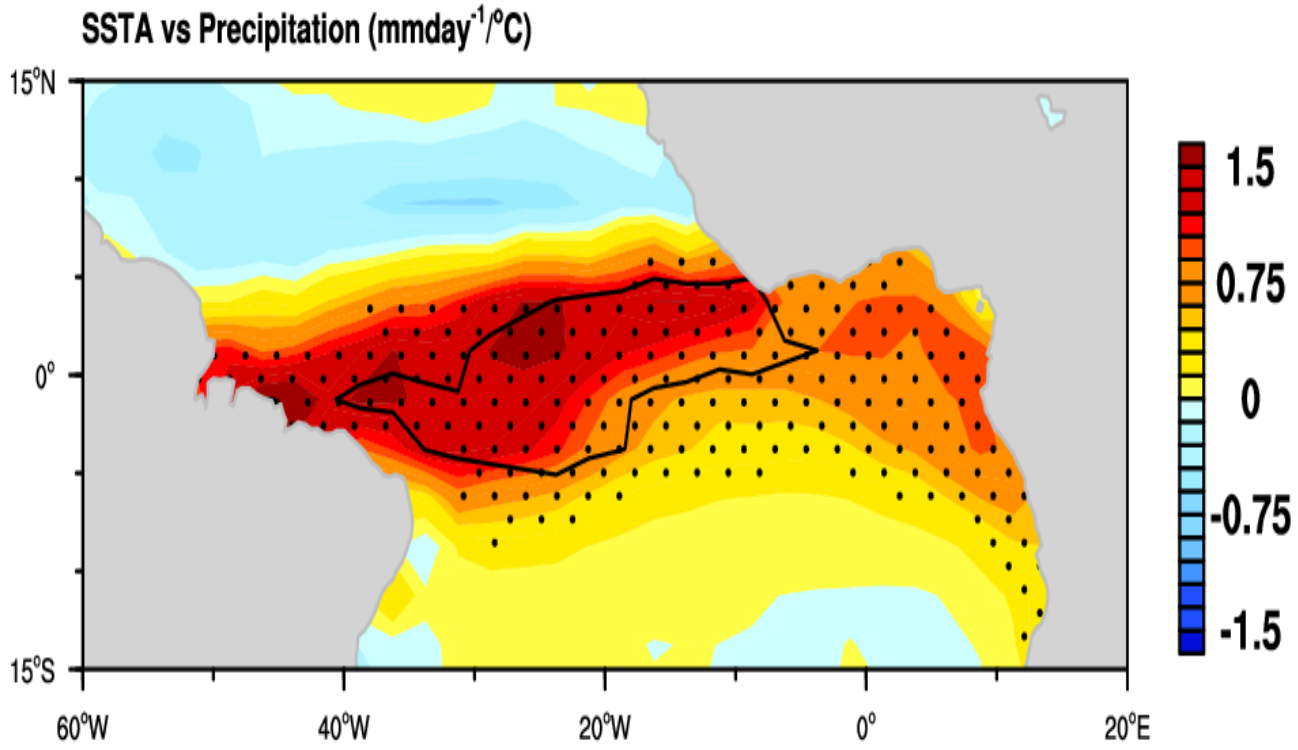

Figure 4.7: Atlantic3 (Atl3) SST anomalies regressed on precipitation anomalies. Black contours indicate explained variances within the 36% interval. Stippling indicates statistical significance at the 95% confidence level.

4.1.2.2 Atmospheric convection-ocean coupling and thermocline coupled feedback in the equatorial Atlantic

4.1.2.2.1 Coupling of convection-ocean coupling

Panels (a), (c), and (e) of Figure 4.8 illustrate the SST anomalies (color shading) and precipitation anomalies (black contours) for April, May, and June, respectively.

In April, positive SST anomalies are centered in the eastern and central equatorial Atlantic, particularly within the Atl3 region (bounded by the gray box), which is referred to as the well-known zonal pattern of SST anomalies during its developing phase (Figure 4.8a; color scale). These warm SST anomalies are accompanied by precipitation anomalies (Figure 4.8a; solid black contours), especially near the equator and enhanced precipitation anomalies west of the Atl3 region, suggesting strong coupling between SST and atmospheric convection.

In May, the relationship strengthens and expands, with the more enhanced SST anomalies also concentrated in the central to eastern equatorial Atlantic. Enhanced precipitation anomalies are also observed near and at the equator. In contrast, reduced precipitation anomalies are observed further north, suggesting a dipolar structure and southward migration of the equatorial Atlantic ITCZ. The strongest precipitation anomalies are observed over the western boundary of the Atl3 box (Figure 4.8c; solid black contours), suggesting that precipitation anomalies in May contribute in setting the background conditions for the development of the Atlantic Niño.

In June, the zonal SST anomaly pattern also showed enhanced SST anomalies in the eastern and central equatorial Atlantic (Figure 4.8c; color scale).

Similarly, the June SST (color scale) and precipitation anomalies (black contours) show the well-known zonal pattern of SST anomalies during the peak phase, as well as enhanced precipitation anomalies concentrated north of the Atl3 box in the equatorial Atlantic (Figure 4.8e; solid black contours).

4.1.2.2.1 Thermocline Feedback and Wind Stress Anomalies

Panels (b), (d), and (f) focus on thermocline feedback by showing SSH anomalies (color shading) and wind stress anomalies (vectors) over the same months.

In April, negative SSH anomalies are evident in the western equatorial Atlantic, while positive anomalies appear in the east, indicating a deepening of the thermocline in the east and shoaling in the west. This east-west dipole is consistent with equatorial wave dynamics and supports the formation of warm SST anomalies via thermocline feedback (Figure 4.8b).

The wind stress (only statistically significant vectors are shown) in April is primarily easterly across the basin, weakening toward the east, which facilitates eastward-propagating Kelvin waves and westerly wind anomalies favorable for further SST warming (Figure 4.8b).

By May, the wind stress anomalies become more coherent and intense, especially along the equator. The SSH gradient strengthens, reinforcing the eastward thermocline tilt Figure 4.8d).

In June, the SSH anomalies reach their peak amplitude, particularly in the eastern basin, with wind stress anomalies indicating further weakening of the trade winds. This pattern supports continued shoaling of the western thermocline and deepening in the east, characteristic of Bjerknes feedback amplification during Atlantic Niño events Figure 4.8f).

The Precipitation anomalies are predominantly northwesterly west of 0^0, and the strongest wind stress anomalies are observed in the very west, where they are nearly westerly. Overall, the wind stress anomalies indicate a weakening of the prevailing southeasterly trade winds. The westward

wind stress anomalies at the equator strengthen the dynamic coupling between the ocean and the atmosphere.

Through these regression analyses, the roles of both oceanic (thermocline feedback) and atmospheric (convection-ocean feedback) processes in sustaining the emergence and intensification of coupled feedback over three key months are examined. The thermocline feedback, through wind-induced SSH anomalies, acts in concert with convective responses to sustain SST anomalies, illustrating the core dynamics behind tropical Atlantic variability. These insights are critical for understanding the mechanisms of interannual climate variability in the tropical Atlantic and improving predictive models of related climatic impacts in the surrounding continents.

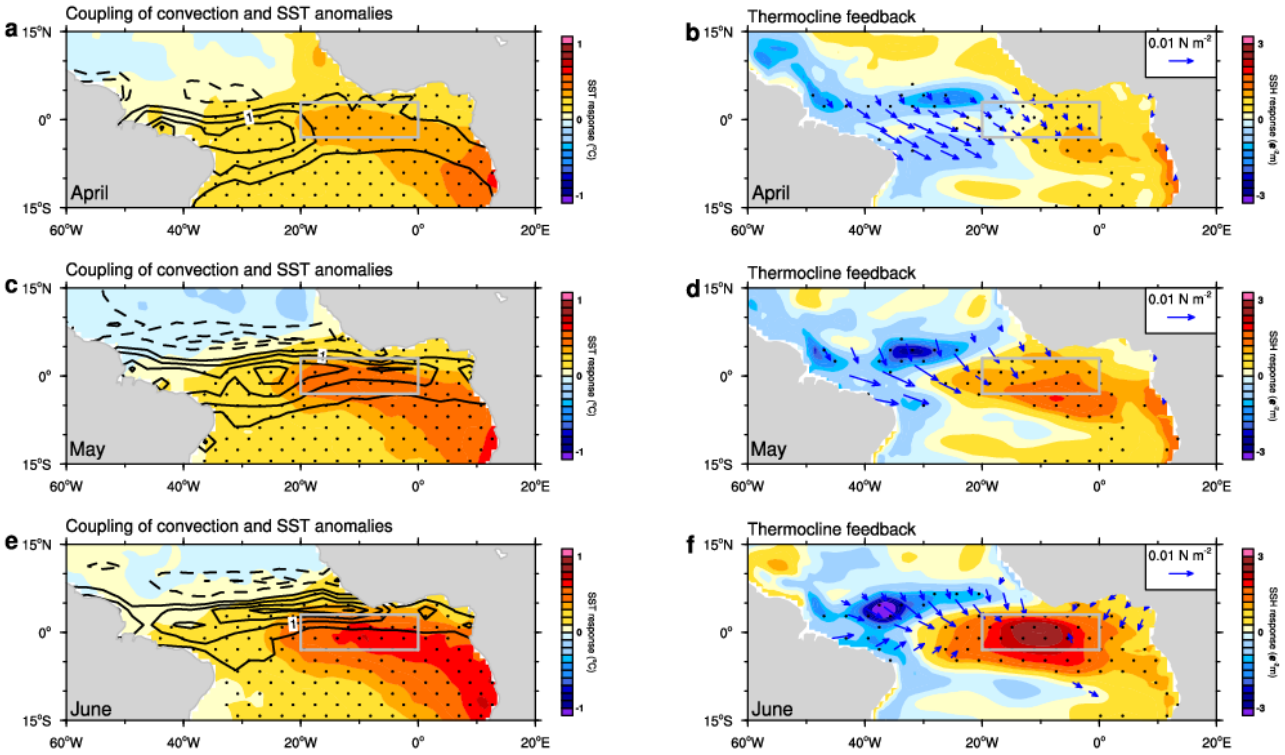

Figure 4.8: Monthly regressions of the normalized Atl3 SST index onto (a, c, e) SST anomalies (color) with precipitation anomalies (contours) and (b, d, f) SSH anomalies (color) with wind stress anomalies (only statistically significant vectors are plotted) for April, May, and June. Dots indicate significance at the 95% level.

Figure 4.9 shows the spatial structure of SST anomalies (shaded colors, in °C) in June regressed onto normalized June Atl3 SST anomalies, alongside the precipitation anomalies (black contours) for May, also regressed onto the same June Atl3 SST index.

The SST response pattern is characterized by a prominent warming signal centered along the equator, particularly between 20°W and the West African coast. The warm SST anomalies indicate a strong zonal SST anomaly pattern, consistent with the peak of the Atlantic Niño event. The warmest anomalies are located near the eastern equatorial Atlantic, just off the West African coast. This warm tongue extends westward, weakening gradually toward the central Atlantic. The magnitude and spatial extent of the anomalies suggest a robust positive SST signal associated with the normalized Atl3 index (Figure 4.9).

The precipitation anomalies in May (black contours) indicate a lagged atmospheric response that precedes the peak SST anomalies in June. An apparent positive precipitation anomaly is observed over the western and central equatorial Atlantic, aligning closely with the region of positive SST anomalies (Figure 4.9). It suggests a feedback mechanism in which early-season precipitation anomalies may contribute to oceanic warming.

The May precipitation anomalies and June SST anomalies coincide, which suggests the presence of a coupled ocean-atmosphere interaction. This analysis indicates that mean atmospheric convection supports the growth of the SST anomalies at short negative lags, consistent with a previous study (Nnamchi et al., 2021).

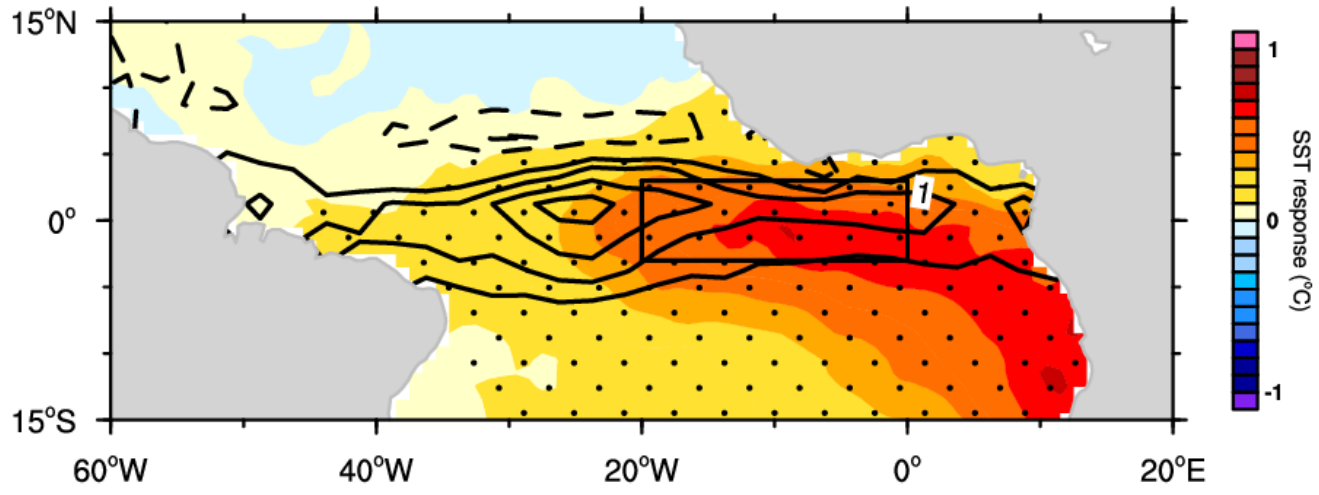

Figure 4.9: The SST (color scale) in June and precipitation anomalies (black contours) in May regressed onto the normalized Atl3 SST anomalies in June. Dots indicate statistical significance at the 95% confidence level.

Figure 4.10 presents the spatial distribution of June sea surface height (SSH) anomalies (color shaded) and wind stress anomalies (blue vectors) in May, regressed onto the normalized June Atl3 SST anomalies.

A prominent feature is the well-developed dipole structure in SSH anomalies centered around the equator. Positive SSH anomalies dominate the central and eastern equatorial Atlantic (between 30°W and 0°), indicating a deepening of the thermocline in this region (Figure 4.10). This is consistent with the peak phase of the Atlantic Niño event, where anomalously warm SSTs emerge due to reduced upwelling and enhanced oceanic heat content.

To the west of the basin, particularly between 50°W and 35°W, a region of pronounced negative SSH anomalies is observed, suggesting shoaling of the thermocline and enhanced upwelling in the western equatorial Atlantic. This west-east SSH gradient across the basin is indicative of a weakened zonal pressure gradient. It supports eastward propagation of equatorial Kelvin waves, which are critical to the development of warm SST anomalies in the Atl3 region.

The overlaid wind stress vectors show the structure of the atmospheric anomalies in the month preceding the peak of SST and SSH anomalies in the Atl3 region. Westerly wind stress anomalies (blue arrows pointing eastward) are observed primarily west of 20°W. These anomalies are consistent with a weakening of the climatological easterly trade winds, which reduces the zonal tilt of the thermocline and favors eastward advection of warm water. The alignment of these wind anomalies with the SSH dipole pattern further supports a Bjerknes-type feedback mechanism, where atmospheric and oceanic anomalies reinforce each other to sustain the development of the Atlantic Niño.

Overall, precipitation variability in May, which is also observed to drive the peak of the Atlantic Niño event in June, has the highest variance, with explained variances reaching about 57% (Figure 4.9). In contrast, the thermocline-coupled feedback loop explains only about 52% of the variation (Figure 4.10).

These results are consistent with a previous study (Nnamchi et al., 2021) and suggest that atmospheric deep convection at short time lag (negative lag) contributes to the growth of Atl3 SST anomalies. Therefore, the zonal thermocline feedback and the meridional migrations of atmospheric deep convection associated with the Atlantic Niño event play a critical role in shaping atmosphere-ocean coupling in the Atlantic. Consequently, understanding the dynamics and patterns of Atlantic Niño variability, which is influenced by short-lag atmospheric convection, could significantly improve seasonal climate forecasts in the tropical Atlantic.

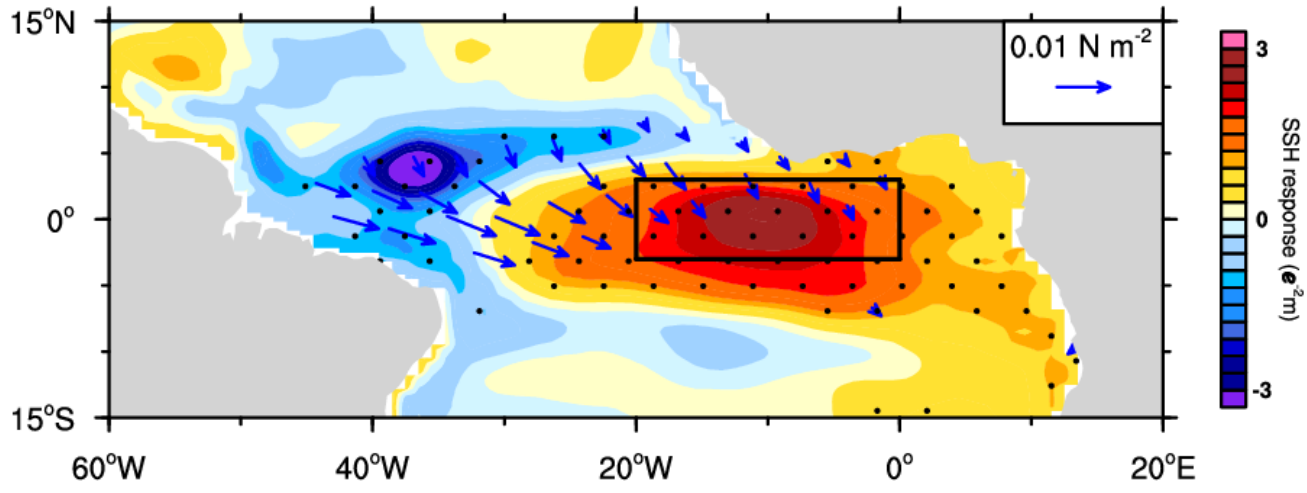

Figure 4.10: The June SSH (color scale) and May wind stress anomalies (only statistically significant vectors are shown) regressed on the normalized Atl3 SST anomalies in June. Dots indicate statistical significance at the 95% confidence level.

4.2 Mechanisms potentially driving the weakened atmosphere-to-ocean Bjerknes feedback

4.2.1 Observed weakening of the atmosphere-to-ocean Bjerknes feedback

Figure (4.11) shows the zonal wind stress-SST gradient coupling over the equatorial Atlantic, across two periods: the earlier period (1979-1999) and the more recent period (2000-2021 for observations, 2000-2014 for models).

During the period (1979-1999), a strong positive zonal wind stress response to SST gradients across the equatorial Atlantic is observed, particularly concentrated in the western to central basin (Figure 4.11a). This positive coupling indicates that during warm SST anomalies (Atlantic Niño events), westerly wind anomalies are enhanced, consistent with a robust atmosphere-ocean feedback that reinforces SST anomalies through changes in surface wind stress.

In contrast, during the period (2000-2021), the strength and spatial extent of the wind stress-SST gradient coupling have significantly weakened, particularly in the western to central basin (Figure 4.11b). The spatial pattern of the regression shows a weakened wind stress response to SST gradients, implying a reduced efficiency of the atmosphere-to-ocean coupling in recent decades.

During the period (1979-1999), pronounced positive feedback is evident over the western equatorial Atlantic, with the strongest regression values concentrated near the continental boundary (Figure 4.11a). This indicates a robust wind stress response to SST gradients, consistent with an active Bjerknes feedback loop. In contrast, the feedback mechanism appears to weaken substantially in the post-2000 period (2000-2021), particularly in the western basin (Figure 4.11b). The spatial pattern of the regression illustrates a diminished wind stress response to SST gradients, implying a reduced efficiency of the atmosphere-to-ocean coupling during this later period.

To better quantify these changes, the regression results were averaged across the equatorial Atlantic band (3°S-3°N). The resulting time series (Figure 4.12e) clearly illustrates the weakening of the

atmosphere-to-ocean feedback after 2000, characterized by both a reduced wind stress response in the western basin in recent decades. These findings suggest a decline in the ability of surface wind stress to respond to SST anomalies and reinforce them through thermocline adjustment, a key process underpinning the development of Atlantic Niño events.

Further insight is provided by comparing observations with outputs from the AMIP multi-model ensemble mean (MME) (Figure 4.11c-d). While the AMIP MME underestimates the overall magnitude of the atmospheric response to the SST gradient in both periods, it successfully captures the observed weakening after 2000, especially over the western equatorial Atlantic. The MME regression pattern for the post-2000 period (Figure 4.11d) reproduces the reduced wind stress response and weakened SST gradient observed in the data, with a slight westward shift and slightly stronger amplitude in some regions (Figure 4.12f). This consistency between models and observations confirmed that the atmosphere-to-ocean coupling strength has diminished in recent decades, potentially contributing to changes in Atlantic Niño variability and predictability.

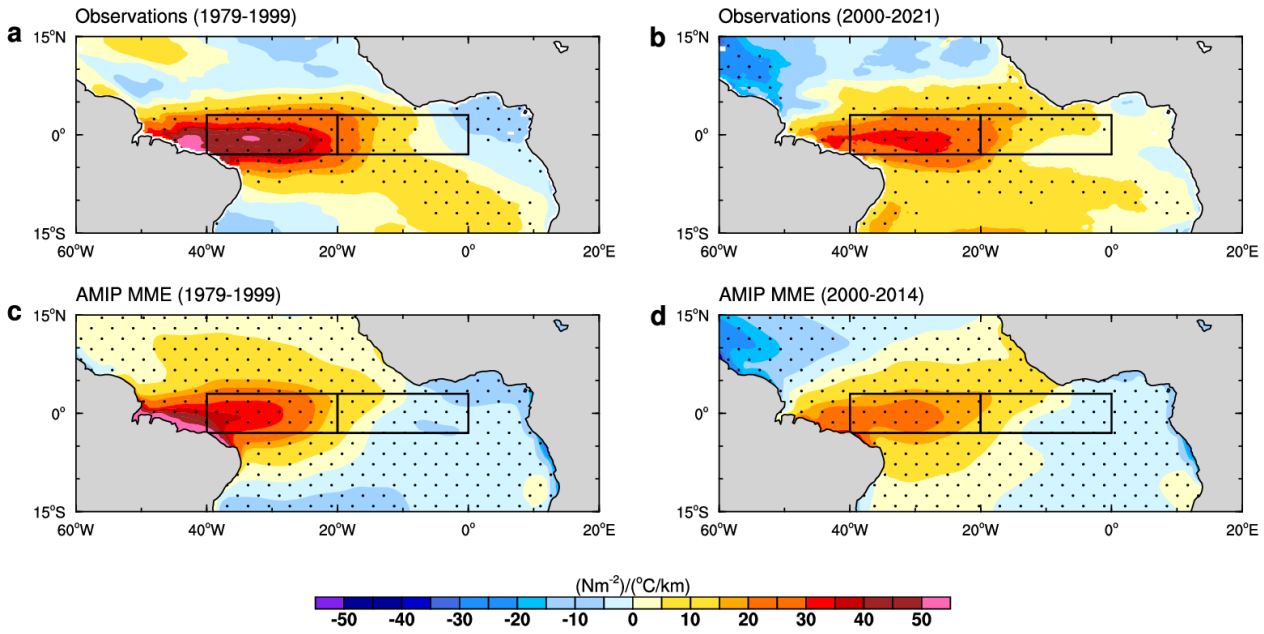

Figure 4.11: Regression pattern of zonal wind stress anomalies onto zonal gradient of sea surface temperature (SST) dSST/dx in observations for the periods (a) 1979-1999 and (b) 2000-2021. Regression pattern of anomalous zonal wind stress onto the zonal gradient of (SST) dSST/dx in the AMIP multi-model ensemble (MME) for the periods (c) 1979-1999 and (d) 2000-2014.

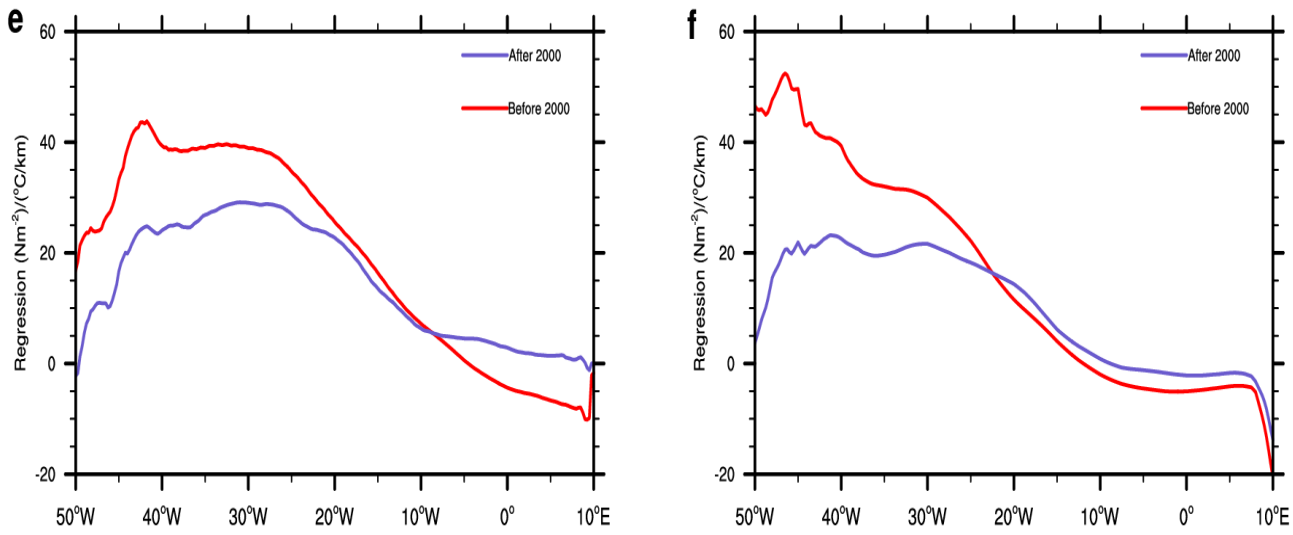

Figure 4.12: Regression of anomalous zonal wind stress onto the zonal gradient of dSST/dx, averaged between 3°S and 3°N. The red and blue lines represent the periods 1979-1999 and 2000-2021, respectively, in the observations panels (e) and (f) for the AMIP MME, but for the periods 1979-1999 and 2000-2014.

4.2.2 Mechanisms Potentially Driving the Weakened Atmosphere-to-Ocean Bjerknes Feedback

Subprocess 1: SST Gradient to Precipitation Gradient (dSST/dx → dPrecip/dx).

Figure 13a is a scatter plot that illustrates the relationship between zonal gradients of SST (dSST/dx) and zonal gradients of precipitation (dPrec/dx) over the equatorial Atlantic, for two distinct periods: before 2000 (black dots) and after 2000 (red dots).

The positive slopes in both periods confirm that stronger SST gradients are associated with enhanced precipitation gradients, reflecting the fundamental role of SST patterns in modulating atmospheric convection and rainfall over the tropical Atlantic.

As shown in Figure 4.13a, there is a notable difference in the strength of this relationship between the two periods. The slope of the regression line before 2000 is 1.34 mm/day/deg (with a statistically significant p-value of ~1.4e-07), indicating a relatively strong sensitivity of precipitation gradients to SST gradients. After 2000, the slope weakens to 0.72 mm/day/deg, with a higher p-value (0.021), suggesting a reduced atmospheric response to the same SST forcing. This substantial reduction indicates that for a given SST gradient, the atmospheric response in terms of convection and precipitation has become less effective after 2000. A weaker SST-precipitation relationship implies a reduced ability of oceanic anomalies to trigger atmospheric feedback, thereby weakening the first link in the Bjerknes feedback chain. This is consistent with the observed and simulated weakening of the Atlantic Bjerknes feedback (Figure 4.11).

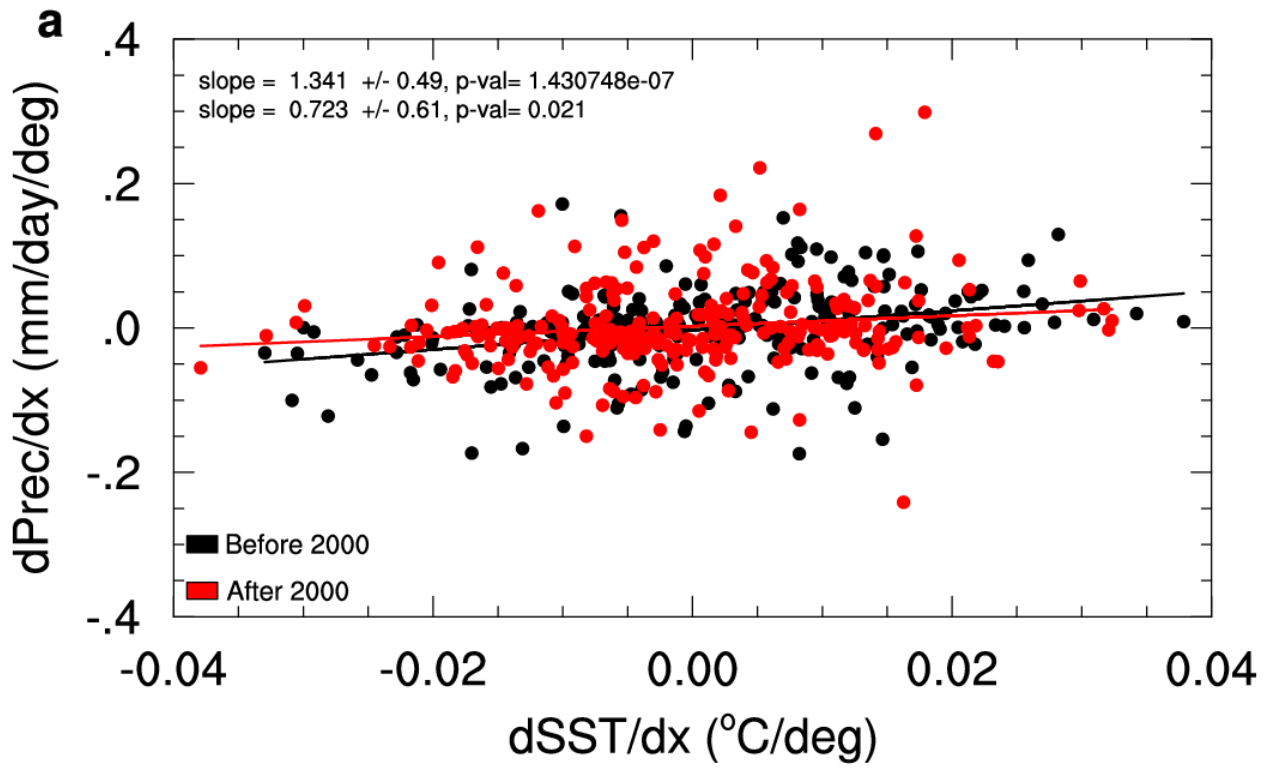

Figure 4.13: Scatter diagram and the corresponding linear fitting lines (with the values of the slope plus and minus the 95% confidence values from the Student's t test) between (a) zonal gradient of sea surface temperature and zonal gradient of precipitation anomalies during the period of 1979-1999 (black) and 2000-2021 (red).

Subprocess 2: Precipitation Gradient to SLP Gradient (dPrecip/dx → dSLP/dx)

This sub-process shows how the precipitation gradient influences the zonal distribution of sea level pressure. The analysis revealed a moderate weakening in this relationship between the two periods (Figure 4.14b). The sensitivity of SLP gradients to precipitation gradients decreases from 0.047 hPa per mm/day in 1979-1999 to 0.028 hPa per mm/day in 2000-2021. This decline indicates that atmospheric pressure systems have become less responsive to precipitation anomalies, further contributing to a disruption in the atmosphere-ocean feedback loop. Such a weakening may be related to changes in tropospheric stability or moisture availability, which affect the ability of convection to modulate pressure gradients.

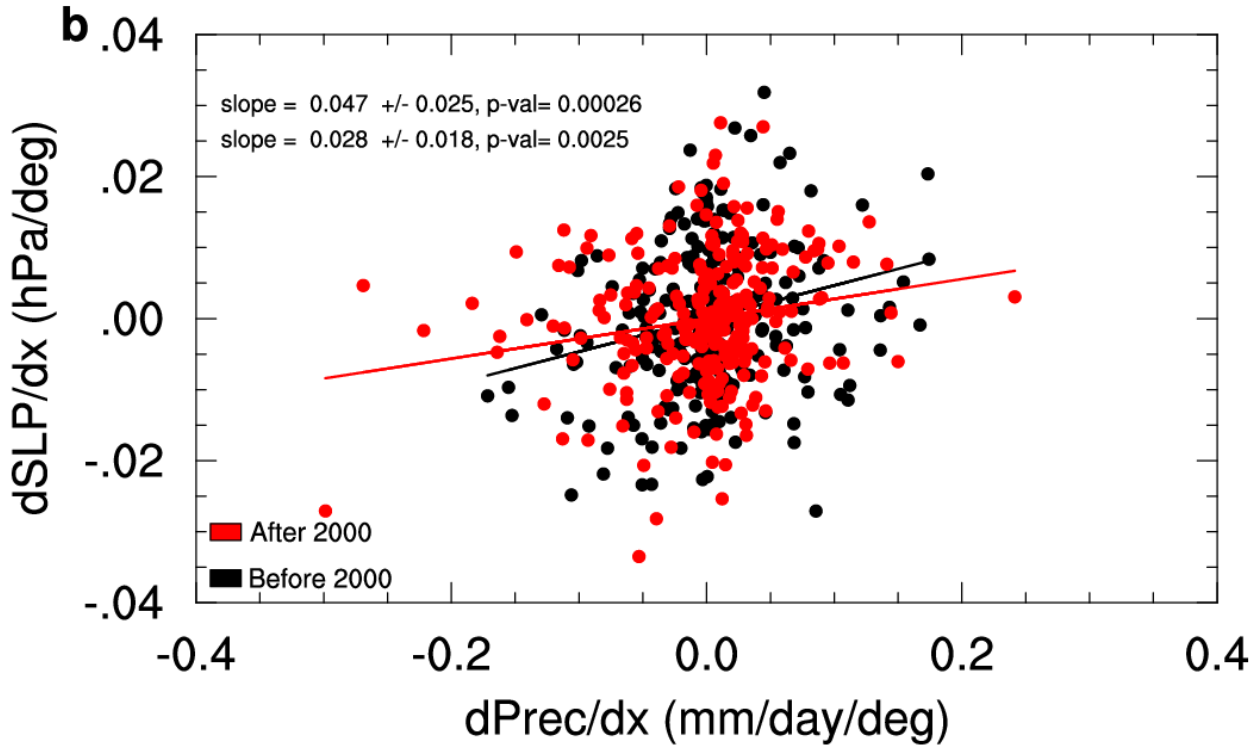

Figure 4.14: Scatter diagram and the corresponding linear fitting lines (with the values of the slope plus and minus the 95% confidence values from the Student's t test) between (b) zonal gradient of precipitation and zonal gradient of sea level pressure (SLP) anomalies during the period of 1979-1999 (black) and 2000-2021 (red).

Subprocess 3: SLP Gradient to Zonal Wind Stress ($dSLP/dx \rightarrow \tau x$)

The final subprocess connects pressure gradients to the surface wind stress response, which is critical for driving oceanic adjustments, such as thermocline feedback and SST anomalies. Unlike the previous two subprocesses, this component shows no noticeable difference over the two periods (Figure 4.15c). The regression slope remains relatively stable: -0.297 ± 0.074 $(N/m^2)/(hPa/°)$ during 1979-1999 and -0.300 ± 0.072 $(N/m^2)/(hPa/°)$ during 2000-2021. This suggests that the dynamical relationship between SLP gradients and surface wind stress has remained stable, and that the weakening of the Bjerknes feedback is primarily from precipitation and pressure response processes, rather than in the mechanical wind stress response.

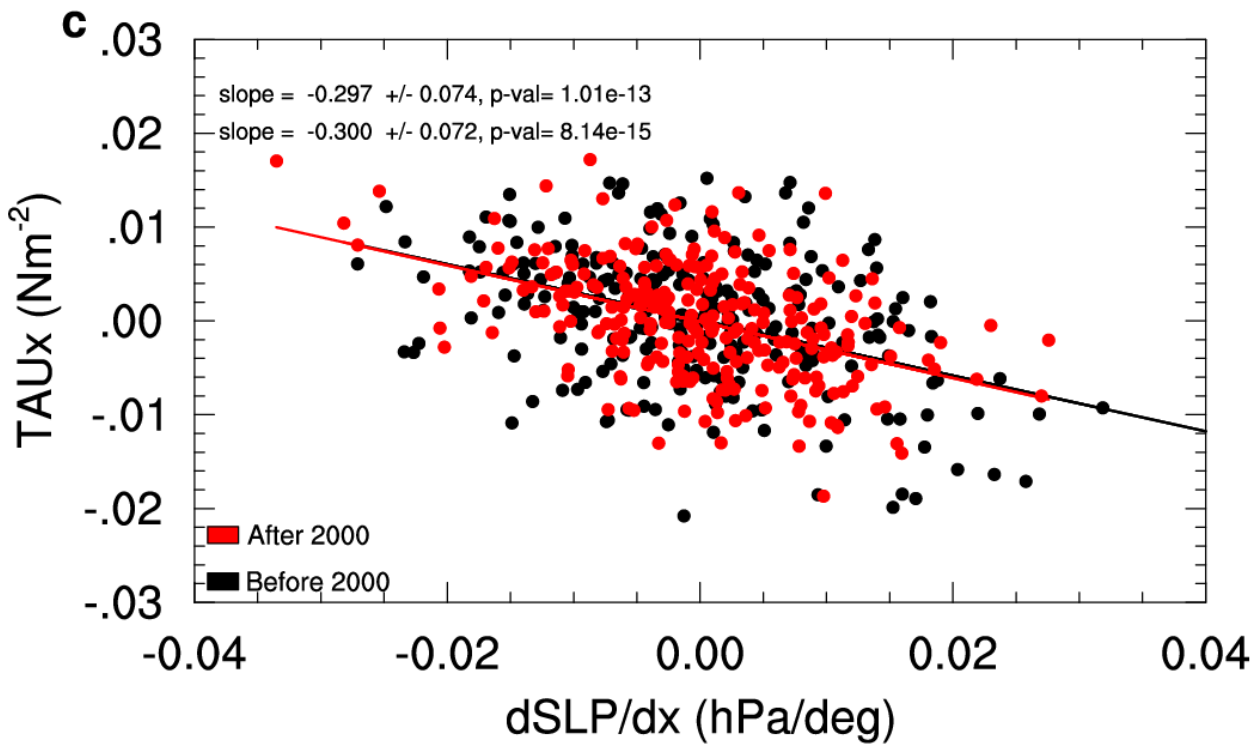

Figure 4.15: Scatter diagram and the corresponding linear fitting lines (with the values of the slope plus and minus the 95% confidence values from the Student's t test) between (c) zonal SLP gradients and area-averaged zonal wind stress anomalies during the period of 1979-1999 (black) and 2000-2021 (red).

4.2.3 Weakening of the Atmospheric Response

To further investigate how Subprocess 1 has evolved, this section examines the precipitation anomalies and vertical velocity (omega) anomalies. At the same time, Subprocess 2 is explored through the analysis of sea level pressure (SLP) responses to zonal precipitation gradients.

Results indicate a significant weakening of the atmosphere-to-ocean coupling after 2000. The precipitation response to the normalized zonal SST anomalies gradient, averaged over the equatorial Atlantic (3°S-3°N), reveals a notable reduction in coupling strength after 2000. Before 2000, observational data show a strong sensitivity of precipitation anomalies to SST gradients, again with peak value centered between 35°W and 32°W (Figure 4.16a, red solid curve). This pattern is effectively captured by the AMIP MME (red dashed curve), further validating the model's ability to replicate the atmospheric processes associated with the atmosphere-ocean feedback. After 2000, both observational and AMIP MME results display a flattened response curve, reflecting a weakened precipitation sensitivity to SST forcing (blue solid and dashed curves, Figure 4.16a). This implies that changes in SST gradients no longer induce a strong convective response, as was the case in the earlier period.

Similarly, the SLP response to zonal SST anomalies gradient before 2000 (solid red line), shows a clear peak in vertical ascent centered around 30°W, indicating that positive zonal SST gradients are associated with enhanced convective activity and upward motion in the central basin. This pattern aligns well with the canonical structure of Atlantic Niño events, during which SST anomalies induce deep convection and atmospheric uplift in the eastern equatorial Atlantic. After 2000 (solid blue line), the pattern shifts eastward, and the magnitude of upward motion increases slightly between 20°W and 0°, suggesting a spatial reorganization and intensification of the convective response associated with zonal SST gradients in recent decades.

In contrast, the AMIP simulations (dashed lines) capture the general structure but underestimate the strength of vertical motion in both periods. Before 2000 (dashed red), the modeled ascent is weaker and more spatially smoothed, failing to reproduce the sharp peak observed in the data. After 2000 (dashed blue), while the pattern does show some eastward extension of upward motion, its amplitude remains significantly damped compared to observational counterparts.

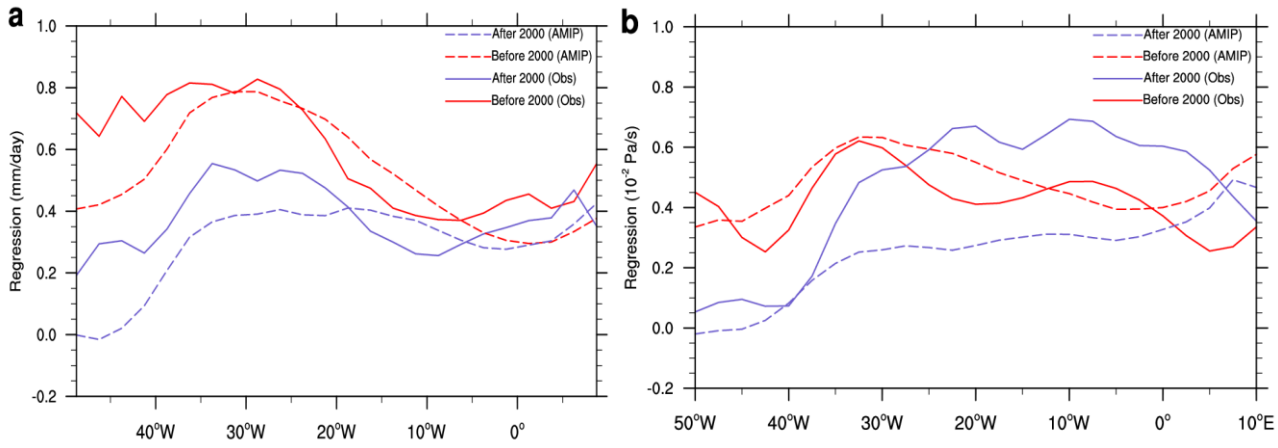

Figure 4.16: Regression of anomalous vertical velocity at the 500-hPa pressure level onto the normalized zonal gradient of SST anomalies, averaged between 3°S and 3°N (a). Regression of anomalous precipitation onto the normalized zonal gradient of SST anomalies, averaged between 3°S and 3°N (b).

Figure 4.17 presents the regression patterns of anomalous vertical velocity at the 500 hPa pressure level with respect to the normalized zonal gradient of SST anomalies over the tropical Atlantic. Negative vertical velocity anomalies typically indicate upward motion, often associated with deep convection and enhanced precipitation (Huang & Xie, 2015).

During the 1979-1999 period (Figure 4.17a), the vertical velocity anomalies show a more spatially moderate upward vertical velocity pattern across the equatorial Atlantic. A pronounced zone of anomalous upward motion is located over the western equatorial Atlantic, consistent with the region of weakened atmosphere-ocean feedback.

Between 2000 and 2021, the strength of the upward motion response exhibits a more spatially extensive pattern, particularly concentrated in the central to eastern basin of the equatorial Atlantic (Figure 4.17b). The spatial extent of ascent increases, and the vertical velocity anomalies strengthen, indicating an increase in atmospheric sensitivity to SST gradients in the recent decades in the eastern basin. The AMIP MME partially captures these observed patterns, although the models tend to underestimate the intensity of the vertical velocity anomalies relative to observations.

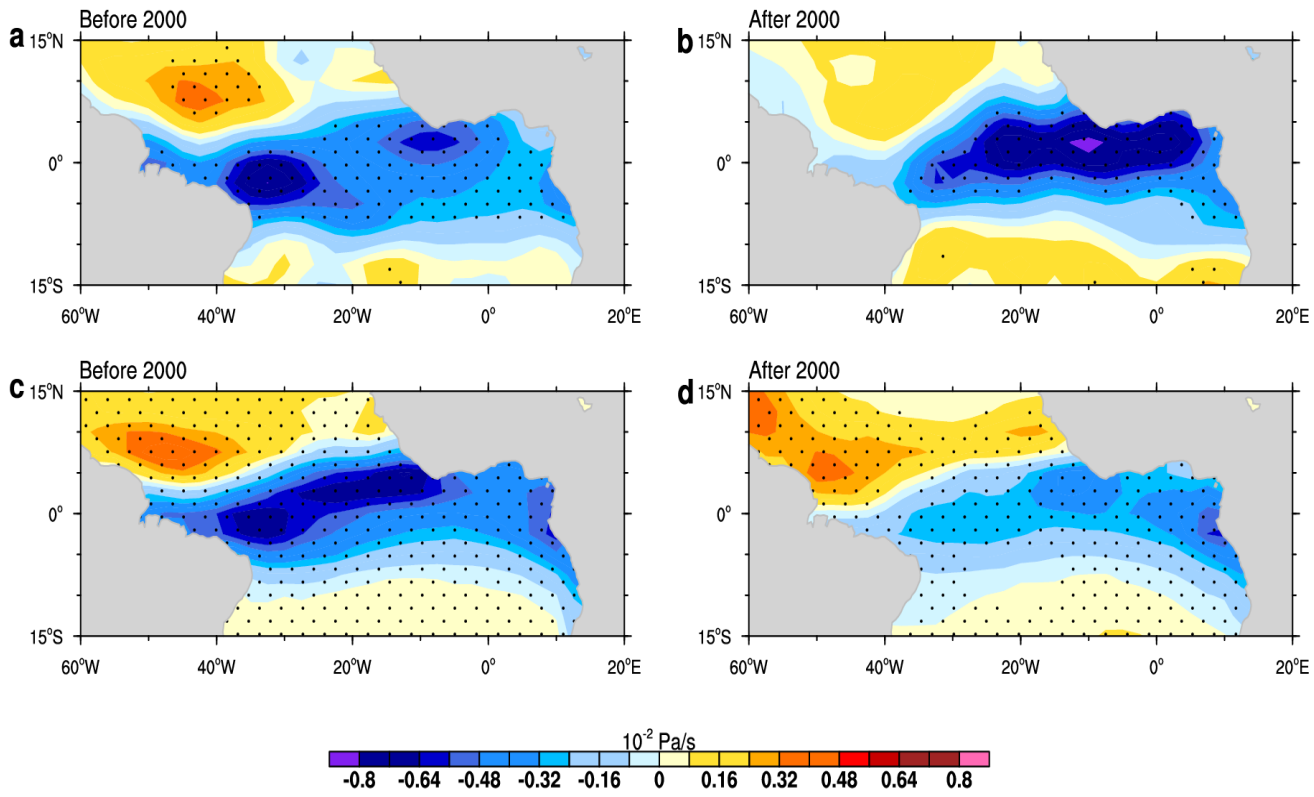

Figure 4.17: Regression patterns of anomalous vertical velocity at 500-hPa pressure level onto the normalized zonal gradient of sea surface temperature in observations for the periods (a) 1979-1999 and (b) 2000-2021. As in panels (a) and (b), but for the CMIP6 AMIP MME for the period (c) 1979-1999 and (d) 2000-2014. Stippling denotes statistical significance at the 95% confidence level.

Figure 4.18 illustrates the regression patterns of anomalous precipitation against the normalized zonal gradient of SST anomalies for the two distinct periods.

In the 1979-1999 period (Figures 4.18a and 4.18c), both observations and AMIP MME exhibit a robust positive zonal precipitation gradient in response to SST anomaly gradients. The result shows a dipolar structure with enhanced positive precipitation anomalies located close to and around the equator, and reduced precipitation further north, suggesting a southward migration of the ITCZ. The largest precipitation anomalies are observed to be concentrated over the western equatorial Atlantic, while suppressed precipitation anomalies appear over the eastern basin.

In contrast, during the 2000-2021 (observations) and 2000-2014 (models) periods (Figures 4.18b and 4.18d), there is a marked weakening of the dipolar structure of precipitation anomalies. Also, the amplitude of the precipitation anomalies diminishes over the western equatorial Atlantic. This weakening is evident in both observations and models, although the models tend to underestimate the strength of the observed anomalies again.

The results in (Figure 4.17 and Figure 4.18) show that the increase in vertical motion does not translate to a corresponding enhancement in precipitation, as the precipitation anomalies during 2000-2021 are substantially weaker than those observed during 1979-1999. This decoupling suggests a potential weakening in the linkage between vertical motion and precipitation, which may contribute to the reduced effectiveness of the Bjerknes feedback during recent decades.

The equatorial Atlantic is strongly influenced by the seasonal migration and intensity of the Intertropical Convergence Zone (ITCZ), a key driver of tropical atmospheric convection. Variations in the ITCZ's position or strength may influence the observed changes in omega and precipitation patterns. For example, during 1979-1999, enhanced precipitation and stronger vertical motion are both concentrated along the western boundary of the basin, reinforcing zonal asymmetries critical for feedback development. In contrast, during 2000-2021, although omega anomalies remain

enhanced across the basin, the associated rainfall response is spatially weaker and more diffuse. These observations point to a weakening of the atmospheric branch of the Bjerknes feedback, particularly the processes connecting SST gradients, vertical motion, and precipitation, thereby contributing to the overall reduction in atmosphere-ocean coupling after 2000.

The AMIP MME reproduces the general zonal pattern, though with slightly weaker magnitude and reduced spatial extent compared to observations. The better agreement in this period suggests that the AMIP MMEs are capable of simulating the precipitation-to-SST gradient coupling under the pre-2000 climate conditions.

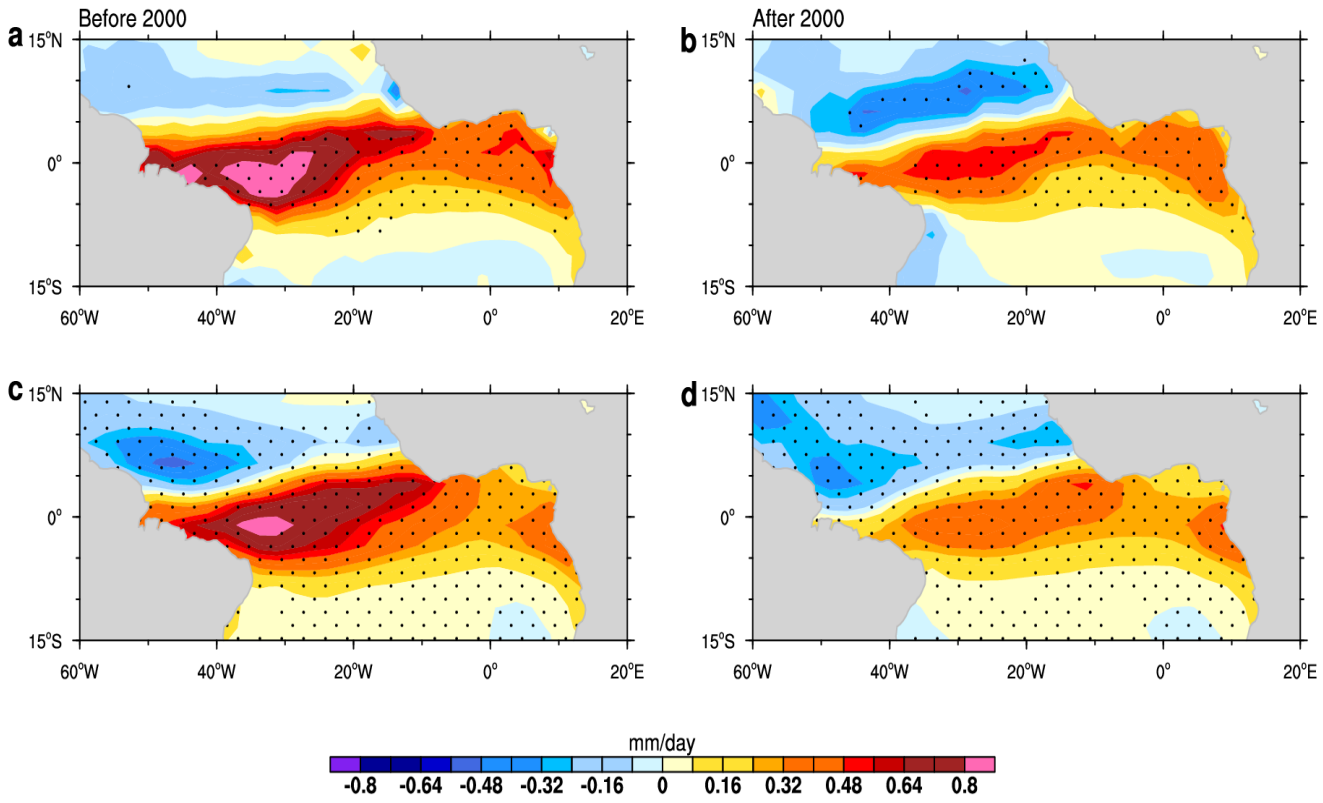

Figure 4.18: Regression patterns of anomalous zonal precipitation gradient onto the normalized zonal gradient of sea surface temperature anomalies in observations for the periods (a) 1979-1999 and (b) 2000-2021. As in panels (a) and (b), but for the CMIP6 AMIP MME for the period (c) 1979-1999 and (d) 2000-2014. Stippling denotes statistical significance at the 95% confidence level.

4.2.4 Reduced Sensitivity of Sea Level Pressure to Precipitation Gradients

Figure 4.19 illustrates the regression patterns of anomalous zonal sea level pressure (SLP) onto the normalized zonal gradient of precipitation anomalies over the tropical Atlantic for the two periods.

During the observational period before 2000 (Fig. 4.19a), a strong positive zonal SLP gradient anomaly is observed over the equatorial Atlantic, particularly between 10°S and 10°N, with the maximum response centered around 10°W to 0°W. This pattern suggests that increased zonal precipitation gradients are associated with reinforced east-west SLP gradients, consistent with enhanced zonal atmospheric circulation responses during this period. After 2000 (Fig. 4.19b), the intensity of this response appears to weaken and shift westward, with a broader but less coherent structure. The reduction in magnitude and spatial coherence after 2000 could indicate a decoupling of the zonal SLP-precipitation relationship, potentially linked to long-term climate shifts or changes in Atlantic mean state dynamics.

In the AMIP MME simulations, a similar spatial structure is observed during the period (1979-1999, Fig. 4.19c), but with slightly weaker magnitudes and a more westward-shifted core compared to observations. The models broadly capture the positive SLP response east of the equatorial Atlantic, though with less spatial detail. However, the after-2000 simulation period (2000-2014, Fig. 4.19d) exhibits a notable reduction in SLP anomalies, aligning with the observed weakening trend but underestimating its spatial pattern.

Overall, the regression patterns reveal a temporal weakening in the relationship between zonal precipitation gradients and SLP gradients after 2000 in both observations and model simulations. This suggests a potential shift in the coupling between Atlantic rainfall and atmospheric circulation.

The observed weakened zonal precipitation (Figure 4.18b), particularly over the western equatorial Atlantic, indicates that SST-induced convection has become less effective in generating zonal asymmetries in precipitation. As a result, the atmospheric response in terms of zonal SLP gradients

is also diminished. Regression results of SLP response to zonal precipitation gradient confirm this reduction in sensitivity, with a lower slope after 2000, as shown in Figure 4.14. The weakened SLP response suggests that precipitation anomalies no longer drive pressure gradients as effectively as they did in the earlier period, thereby affecting the feedback loop.

The reduction in SLP sensitivity to zonal precipitation gradients limits the development of wind stress anomalies that are essential for sustaining the coupled ocean-atmosphere feedback. In the classical Bjerknes framework, convection-induced low pressure in the central and eastern equatorial Atlantic facilitates westerly wind anomalies, which in turn deepen the thermocline in the east and sustain SST anomalies. However, with a weaker zonal precipitation gradient and reduced SLP response, this chain of processes is disrupted. Consequently, the atmosphere becomes less responsive to SST anomalies, undermining the efficiency of the atmosphere-to-ocean coupling and contributing to the overall weakening of the Atlantic Bjerknes feedback after 2000.

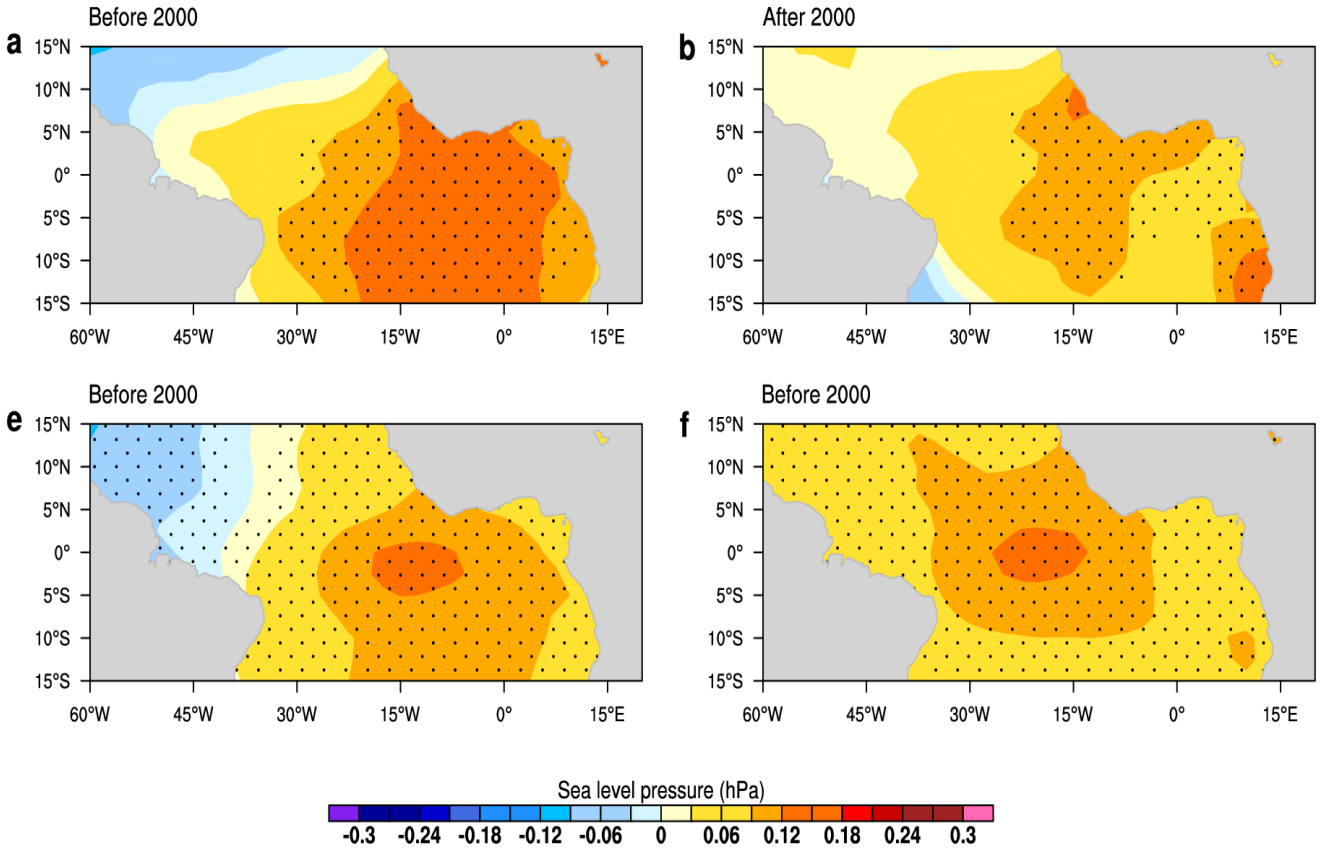

Figure 4.19. Regression patterns of anomalous SLP onto the normalized zonal gradient of precipitation anomalies in observations for the periods (a) 1979-1999 and (b) 2000-2021. As in panels (a) and (b), but for the AMIP MME for the period (c) 1979-1999 and (d) 2000-2014. Stippling denotes statistical significance at the 95% confidence level.

4.3 Characterization and evolution of extreme Atlantic Niño events

4.3.1 Identification and Definition of Extreme Atlantic Niño Events

Using this criterion discussed in the methods section, a total of nine extreme warm events were identified: 1984, 1987, 1988, 1995, 1996, 1998, 1999, 2008, and 2021. Similarly, eight extreme cold events were recorded in 1982, 1983, 1992, 1994, 1997, 2005, 2012, and 2015.

Figure 4.20a presents the monthly evolution of the nine extreme warm SST anomalies. A consistent warming trend is observed from March through June in most warm event years, with peak SST anomalies typically reached in June or July, as seen in years such as 1988, 1995, 1996, and 2021. The amplitude of warming varies significantly across different years, with 1984 and 1988 exhibiting the strongest peaks, approaching or exceeding +1°C (Figure 4.20a). Following July, SST anomalies in most cases show a gradual decline, generally returning toward neutral conditions by November-December (Figure 4.20a).

In contrast, cold events show SST anomalies dipping below zero during the March-June period, with a minimum often reached in June. Recovery typically begins in July, with most years returning to neutral or weakly positive SST anomalies by September or October (Figure 4.20b). The year 1992 stands out for its particularly sharp cold anomaly in June, when SST anomalies dropped below -1°C (Figure 4.20b).

Precipitation anomalies exhibit a strong positive peak from March to May in many warm event years, such as 2008 and 1996, followed by a noticeable decline during June and July. April and May display the greatest variability, with some years, including 1988 and 2008, recording precipitation anomalies exceeding +3 mm/day. After June, the anomalies become more mixed and generally tend toward neutral conditions.

Cold years exhibit pronounced negative precipitation anomalies from March to June, with some years, such as 1983 and 2005, experiencing lows below -2 mm/day. Similar to warm years, the most extreme anomalies are concentrated within the March-June window, after which precipitation values generally normalize toward zero. Despite significant spatial variability among cold years, the seasonal pattern of suppressed rainfall during this period remains consistent.

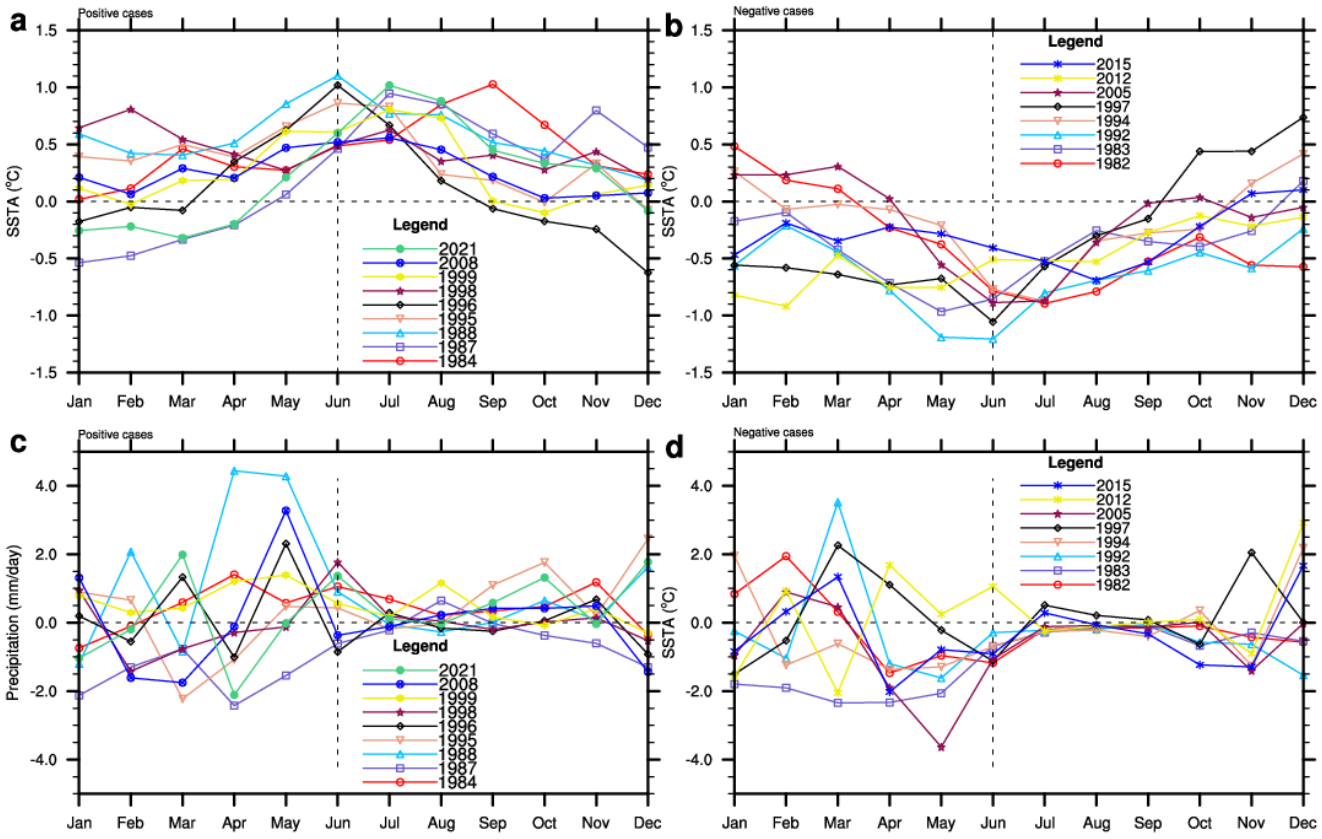

Figure 4.20: a. Annual cycle of the identified nine years of extreme warm events averaged over Atl3 region. b. Annual cycle of the identified eight years of extreme cold events averaged over the Atl3 region. Annual cycle of the associated precipitation anomalies of the identified nine years of extreme warm events, defined over the entire equatorial Atlantic region (3°N–3°S, 5°E–40°W). d. Annual cycle of the associated precipitation anomalies of the identified eight years of extreme cold events, defined over the entire equatorial Atlantic region (3°N–3°S, 5°E–40°W).

Figure 4.21 shows the spatial distribution of the composite mean SST anomalies associated with Atlantic Niño (panel a) and Atlantic Niña (panel b) events. These composites are constructed by averaging SST anomalies during identified event years, offering a climatological view of SST patterns associated with each event type.

In the case of Atlantic Niño events (Figure 4.21a), the SST anomalies exhibit a pronounced warming centered along the equatorial Atlantic, extending from approximately 30°W to 10°E, with peak anomalies exceeding +0.6°C. The warming pattern is strongest near the eastern equatorial Atlantic, particularly off the coast of West Africa. This region, often referred to as the "Atl3 box," is known for its key role in inter-annual climate variability within the tropical Atlantic. The positive SST anomalies are primarily confined to the equatorial region.

Conversely, Atlantic Niña events (Figure 4.21b) are characterized by negative SST anomalies across a similar spatial extent, with the strongest cooling also concentrated in the eastern equatorial Atlantic. The peak cold anomalies surpass -0.6°C, forming a mirror image of the Atlantic Niño structure. These negative anomalies reflect enhanced upwelling and oceanic cooling processes, often linked to stronger easterly winds and reduced convection in the region and adjacent continents.

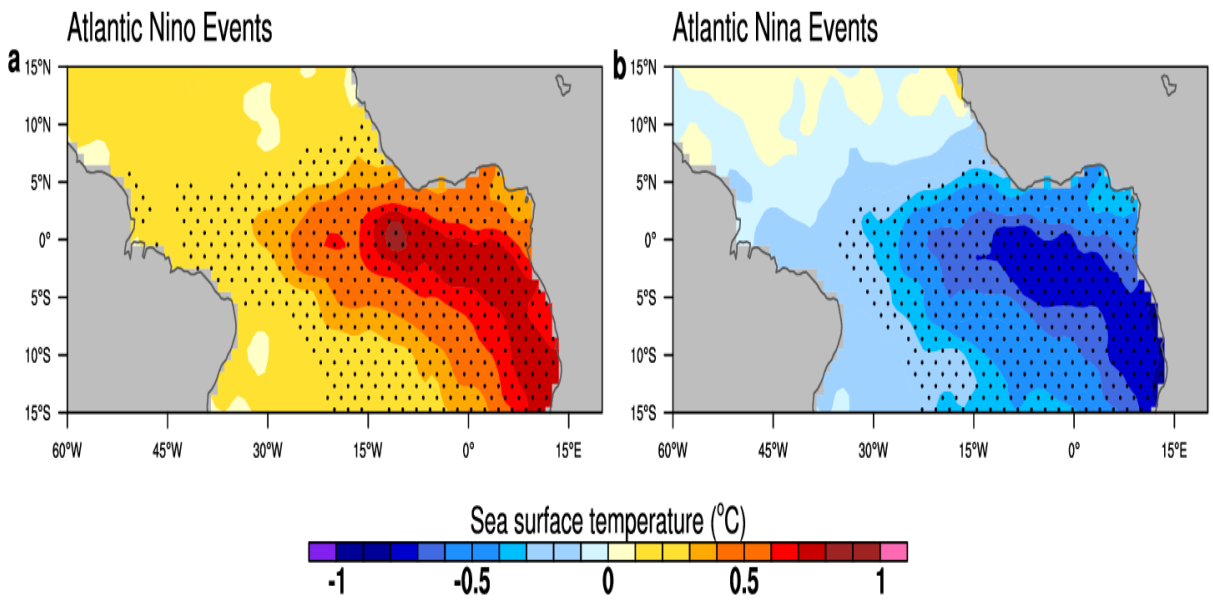

Figure 4.21: Spatial distribution of the composite mean of all event years for Atlantic Niño events (a) and Atlantic Niña events (b) from observation. Dots indicate statistical significance at the 90% confidence level.

4.3.1.1 Composite categorization of Events

Using the criteria outlined in the Methods section, the following canonical and non-canonical events were identified:

Canonical warm events occurred in 1988, 1995, 1996, 1999, and 2008 (Figure 4.22a),

Canonical cold events were recorded in 1982, 1983, 1992, and 2005 (Figure 4.22b),

Non-canonical warm events occurred in 1984, 1987, 1998, and 2021 (Figure 4.23a),

Non-canonical cold events occurred in 1994, 1997, 2012, and 2015 (Figure 4.23b).

For each category, the corresponding precipitation anomalies are also shown in the lower panels of Figures 4.22 and 4.23.

In the warm events (Figure 4.22a), all canonical warm years exhibit positive SST anomalies during the boreal spring to early summer months, peaking prominently around June. The year 1988 exhibits the most sustained warming throughout the year, while 1995 and 1996 demonstrate the sharpest increases in SST anomalies during late spring and early summer, before declining into negative anomalies.

In contrast, the cold events (Figure 4.22b) show sustained negative SST anomalies across all canonical cold years, with SST anomalies reaching their lowest around May to June. The year 1992 features the most pronounced cooling, with anomalies nearing -1.5°C. Notably, the cold events also demonstrate a stronger persistence of negative anomalies beyond mid-year, indicating more prolonged ocean-atmosphere feedback mechanisms during La Niña-like conditions in the tropical Atlantic.

During warm events (Figure 4.22c), precipitation anomalies show significant month-to-month variability, particularly from February to June. For instance, 1988 and 2008 exhibit pronounced positive precipitation anomalies (about 4 mm/day) during April and May, aligning with peak SST warming in June, consistent with the earlier hypothesis.

Conversely, cold events (Figure 4.22d) are associated with largely negative precipitation anomalies across the same region. The 1992 and 1983 events display substantial drying during the boreal spring, with precipitation anomalies below -2 mm/day in several months, notably March to May. These results corroborate the link between cold SST anomalies and suppressed convective activity, indicative of drier-than-normal conditions over the Atlantic basin.

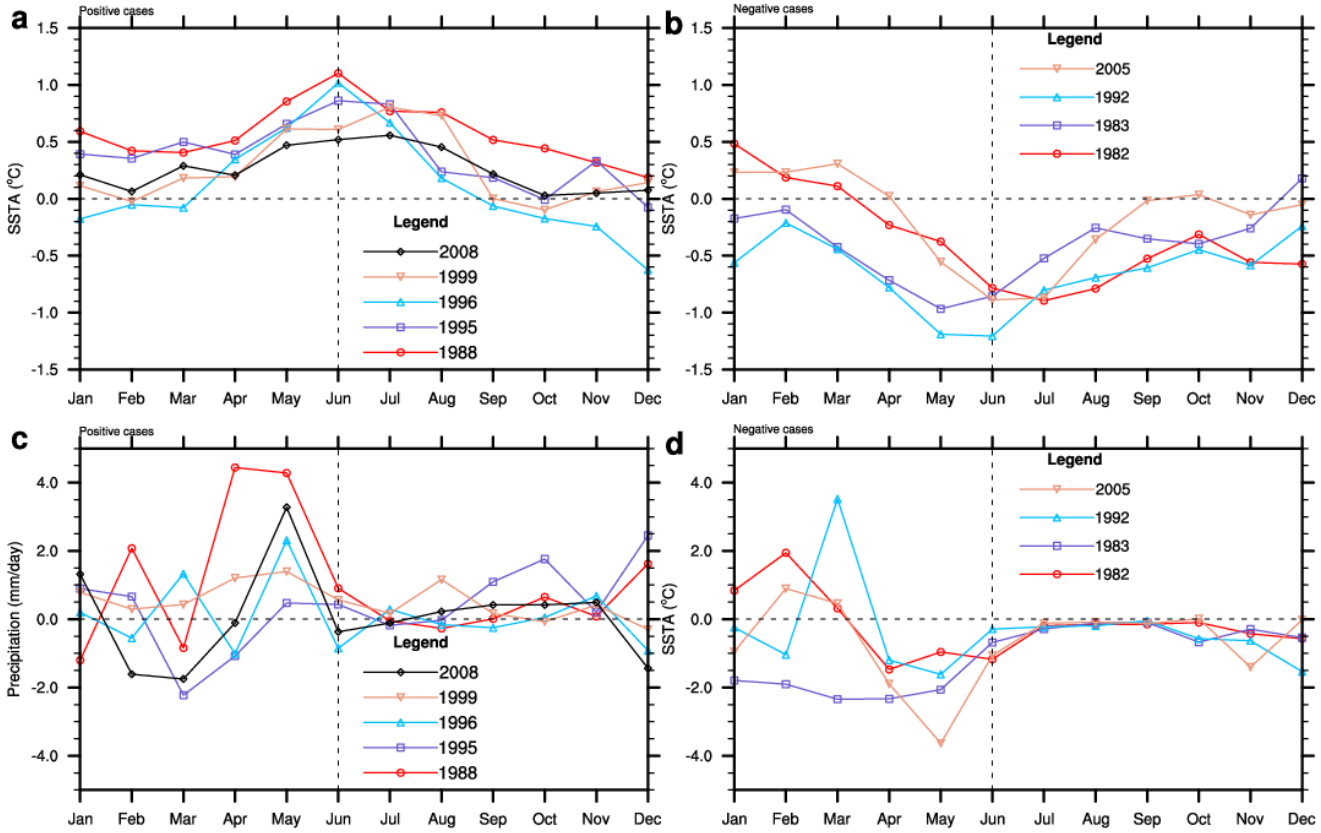

Figure 4.22: a. Composite event years for canonical warm events averaged over Atl3 region. b. Composite event years for canonical cold events averaged over Atl3 region. c. Composite event years of associated precipitation anomalies for canonical warm events, defined over the entire equatorial Atlantic region (3°N-3°S, 5°E-40°W). d. Composite event years of associated precipitation anomalies for canonical cold events, defined over the entire equatorial Atlantic region (3°N-3°S, 5°E-40°W).

In the non-canonical warm events (Figure 4.23a), the selected years show a more gradual warming trend, particularly from March through August. Unlike canonical events that typically peak in May–June, these non-canonical cases show persistent moderate warming well into the late boreal summer (July-October). For instance, 1984 and 2021 show peak anomalies between July and October, suggesting a temporal shift in the SST warming phase. The earlier rise in SSTs in 1998, however, indicates some inter-event variability within the non-canonical events. These patterns suggest that non-canonical warm events may be influenced by different forcing mechanisms or feedback compared to their canonical counterparts.

In contrast, the non-canonical cold events (Figure 4.23b) show a less coherent cooling pattern compared to canonical cold events. The years 1994, 1997, 2012, and 2015 feature sustained negative SSTAs from January through June, with 1997 showing the most persistent and pronounced cooling. After June, SSTs in most years begin to recover toward neutral or slightly positive anomalies, reflecting a shorter duration of cold anomalies.

During non-canonical warm events (Figure 4.23c), precipitation anomalies are less spatially and temporally coherent than those observed in canonical warm cases. While 1984 and 2021 show some periods of enhanced rainfall (e.g., May-June for 2021 and August-October for 1984), the variability among the events is higher. The year 1998, for example, shows a sharp spike in June but relatively dry anomalies earlier in the year. These fluctuations suggest that the atmospheric response to non-canonical warming may be more localized or weaker.

In the case of non-canonical cold events (Figure 4.23d), the precipitation response is again highly variable. Most years, such as 1994 and 1997, feature periods of strong drying in March to May, yet positive anomalies also appear intermittently (e.g., late in 2012). This inconsistent rainfall response contrasts sharply with the widespread drying seen in canonical cold events.

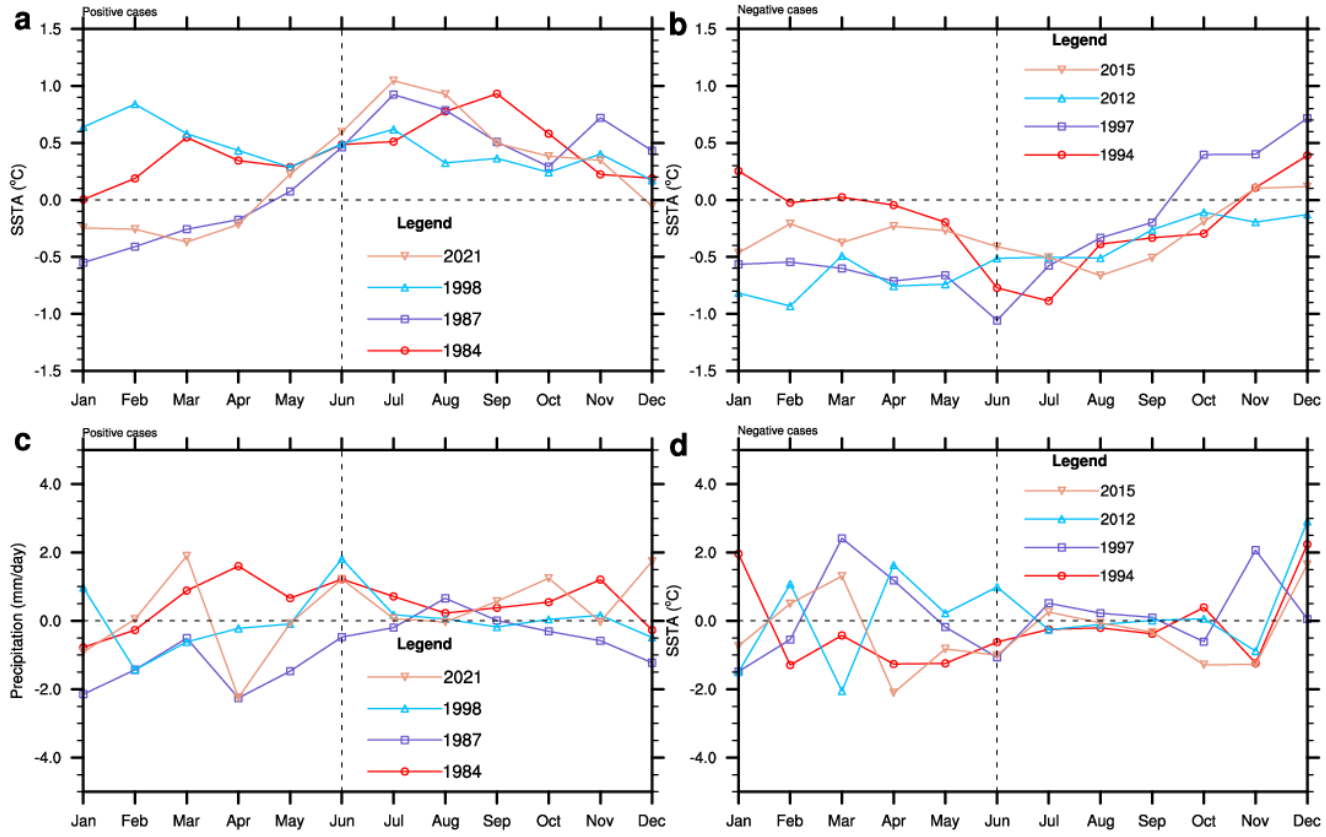

Figure 4.23: a. Composite event years for non-canonical warm events averaged over Atl3 region. b. Composite event years for non-canonical cold events averaged over Atl3 region. c. Composite event years of associated precipitation anomalies for non-canonical warm events, defined over the entire equatorial Atlantic region (3°N-3°S, 5°E-40°W). d. Composite event years of associated precipitation anomalies for non-canonical cold events, defined over the entire equatorial Atlantic region (3°N-3°S, 5°E-40°W).

4.3.1.2 Composite Structure of differences between canonical and non-canonical events

Figure 4.24a shows the composite evolution of cold tongue SST anomalies for the difference between canonical and non-canonical events.

The composite difference in canonical Atlantic Niño events exhibits a pronounced warming pattern, with SST anomalies maximum in June at approximately +0.8°C. The SST anomalies show two maxima, one in June and one in November, with SST variability being significantly larger in June than in November (dashed red curve, Figure 4.24a). The temporal evolution suggests a well-defined seasonal structure, consistent with the known peak in boreal summer.

In contrast, composite differences in non-canonical events also exhibit warming but with a more gradual onset and a slightly lower peak of around +0.7°C in July (dashed blue curve, Figure 4.24a). Importantly, non-canonical events exhibit less month-to-month variability and a broader peak phase, suggesting differing dynamical or thermodynamic forcing mechanisms compared to canonical events.

The composite difference of canonical events is associated with a pronounced increase in precipitation during the April to June period, peaking at nearly 1.8 mm day^{-1} in May (dashed red curve, Figure 4.24b). This peak precedes the maximum SST anomalies in June. This supports the hypothesis that mean atmospheric convection endorses the growth of warm SST anomalies with short negative lags.

Composite difference of non-canonical events exhibits a more muted and less coherent precipitation response. Although a slight increase in rainfall is evident in May and June (maximum of ~0.6 mm day^{-1}), these anomalies are generally weaker and not statistically significant throughout most of the year (dashed blue curve, Figure 4.24b). Furthermore, negative precipitation anomalies emerge toward the end of the year, contrasting with the positive anomalies of the difference in canonical

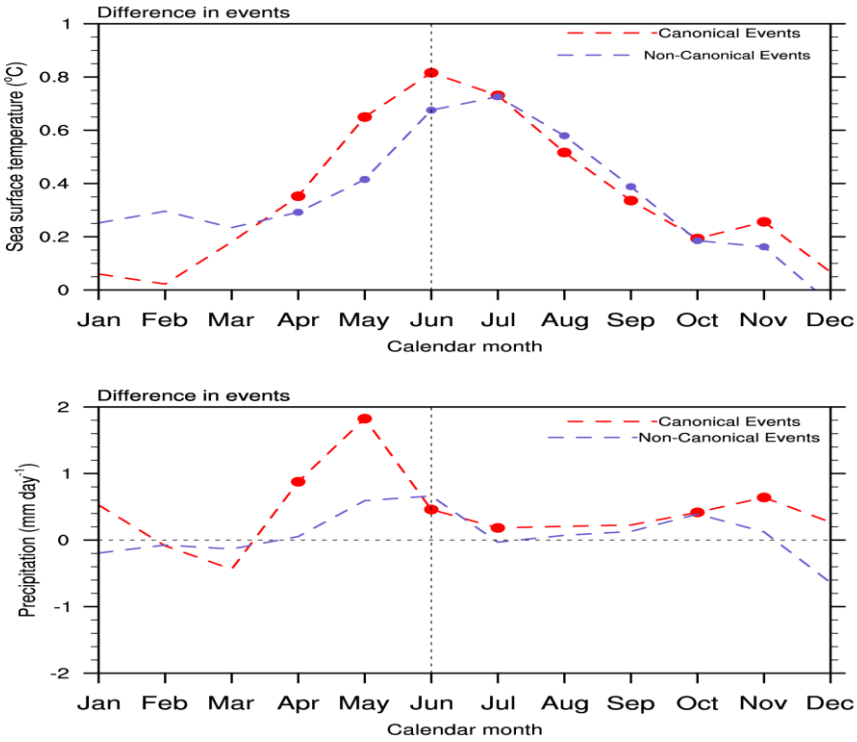

Figure 4.24: a. Composite evolution of average Niño events in the Atlantic, defined as the cold tongue SST index. Evolution of the difference in canonical events (red), difference in non-canonical events (blue). b. Composite evolution of average precipitation anomalies, defined over the equatorial Atlantic region (3°N–3°S, 5°E–40°W). Evolution of the difference in canonical events (red), difference in non-canonical events (blue). Dots indicate values significant at the 90% confidence level.

events. This suggests that the growth of Atlantic July SST is not supported by convection in the atmosphere.

Figure 4.25 presents the spatial patterns of averaged JJA SST anomalies and associated precipitation anomalies in preceding May.

In difference in canonical events, a pronounced positive SST anomaly is evident in the equatorial Atlantic, extending from the Gulf of Guinea westward. This warming exceeds +0.5°C in some regions. These SST anomalies are accompanied by opposite-sign SST anomalies in the southwest extratropical Atlantic, suggesting an apparent dipole pattern in the equatorial Atlantic (Figure 4.25a). Additionally, a distinct negative SST anomaly appears simultaneously along the central and eastern equatorial Pacific, suggestive of La Niña-like conditions (Figure 4.25a).

In contrast, the difference in non-canonical events shows a strong positive SST anomaly in the equatorial Atlantic, spatially resembling the difference in canonical events. The warm SST anomalies associated with the difference in non-canonical events in the equatorial Atlantic are characterized by widespread warm SST anomalies in the tropical Atlantic (Figure 4.25c). The observed Pacific cooling in difference in canonical events appears to be less intense in difference in non-canonical events (Figure 4.25c).

In difference in canonical events, the May precipitation anomalies are significantly enhanced at the equator, suggesting a seasonal southward migration of the ITCZ (Figure 4.25b). This is because precipitation anomalies are more likely to occur near the equator than in the ITCZ (Richter et al., 2020; Richter et al., 2017; Lübbecke and McPhaden, 2012). Strong negative anomalies occur around Indonesia and the Maritime Continent, aligned with the La Niña-like SST anomalies. Slight negative anomalies are observed in northern South America.

In contrast, the Atlantic precipitation anomalies associated with non-canonical events are less intense compared to those during canonical events. Negative precipitation anomalies persist near the Maritime Continent, reinforcing a strong and consistent atmospheric response.

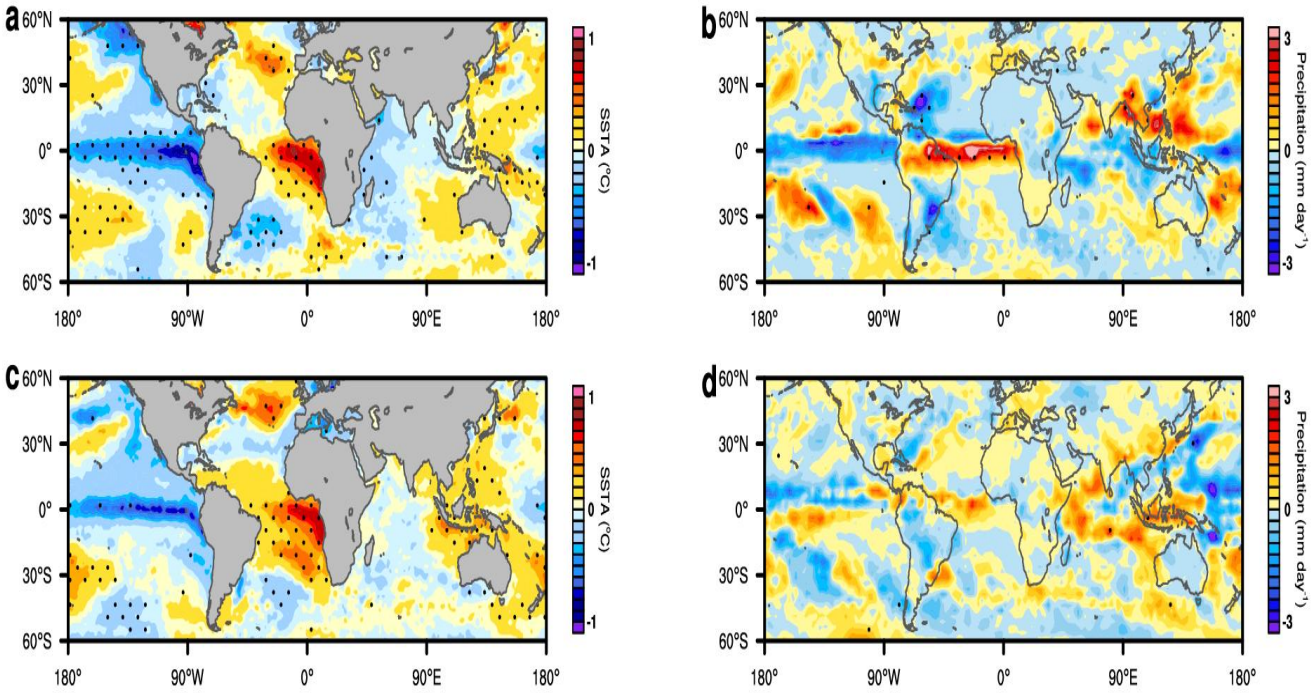

Figure 4.25: Composite maps showing JJA SST anomalies (a and c) and May precipitation anomalies (b and d). Dots indicate statistical significance at the 90% confidence level.

4.3.2 Spatio-temporal evolution of key ocean-atmosphere variables

The difference between canonical and non-canonical Atlantic Niño events shows a clear distinction in convection-ocean coupling and thermocline feedback, as illustrated in the longitude-time composite analysis (Figure 4.26).

For the difference in canonical events, the evolution of warm SST anomalies is characterized by the early development of SST anomalies in April, reaching a maximum in June, and then decaying in July and August across the central and eastern equatorial Atlantic (Figure 4.26a). This pattern closely resembles the early-terminating variety of warm SST anomalies discussed elsewhere (Vallès-Casanova et al., 2020).

Associated with the warm SST anomalies in different canonical events is enhanced precipitation, particularly concentrated between 300W and 200W, reaching its maximum in May but quickly diminishing in June (Figure 4.26b).

The SSH anomalies, which serve as a proxy for the thermocline, show a major peak in June and complete termination in July (Figure 4.26c). The stronger positive SSH anomalies observed between 20°W and 0° in June are consistent with the Bjerknes feedback. This sequence of well-defined eastward propagation of positive anomalies beginning around May, preceding the SST peak, suggests ocean dynamical preconditioning of surface warming. The concurrent negative SSH anomalies in the western basin imply a tilt of the thermocline, consistent with canonical equatorial wave dynamics.

Supporting this, the vertical structure of subsurface potential temperature (Figure 4.26d) shows a deepening of the thermocline (positive anomalies) in the east and shoaling (negative anomalies) in the west during the peak months. This zonal thermocline tilt is indicative of a strong, coupled feedback process between the atmosphere and ocean, driven by wind-forced Kelvin and Rossby waves, which contributes to the canonical Atlantic Niño pattern.

Ocean warming is most pronounced below the surface, particularly at depths between 40 and 80 m, and maximum warm SST anomalies occur between 20°W and 0°. These areas are located near the thermocline defined by the 20°C isotherm (Figure 4.26d).

In contrast, the evolution of warm SST anomalies during non-canonical events is characterized by a gradual increase in SST anomalies, beginning in April, peaking in July, and decaying in August and September (Figure 4.26e). SST anomalies during these events are generally weaker and more localized compared to their canonical counterparts, with maximum warming confined more to the western-central basin (around 20°W).

Precipitation anomalies associated with non-canonical events (Figure 4.26f) are characterized by dry precipitation and lack apparent spatial or temporal coherence. This suggests a weaker coupling between ocean surface conditions and atmospheric convection during these events.

The longitude-monthly map of the sea surface height anomalies (SSHA) of the non-canonical events shows that the SSHA feedback is very weak (Figure 4.26g). Ocean warming is most pronounced between 15 and 35 m depth, above the thermocline defined by the 20°C isotherm (Figure 4.26i). The cross-section also shows that the warmest SST anomalies occur between 10°W and 9°E, with no thermocline extending deeper (Figure 4.26i).

SSH anomalies (Figure 4.26g) show only deviations from the climatology, with limited eastward propagation or zonal gradient and a very weak thermocline feedback.

This absence of a pronounced thermocline tilt is further reflected in the vertical ocean temperature anomalies (Figure 4.26i), which show a weaker and more diffuse thermal structure. The subsurface warming is shallow and lacks the clear east-west asymmetry seen in canonical events, implying a reduced role of oceanic wave dynamics and weaker feedback mechanisms.

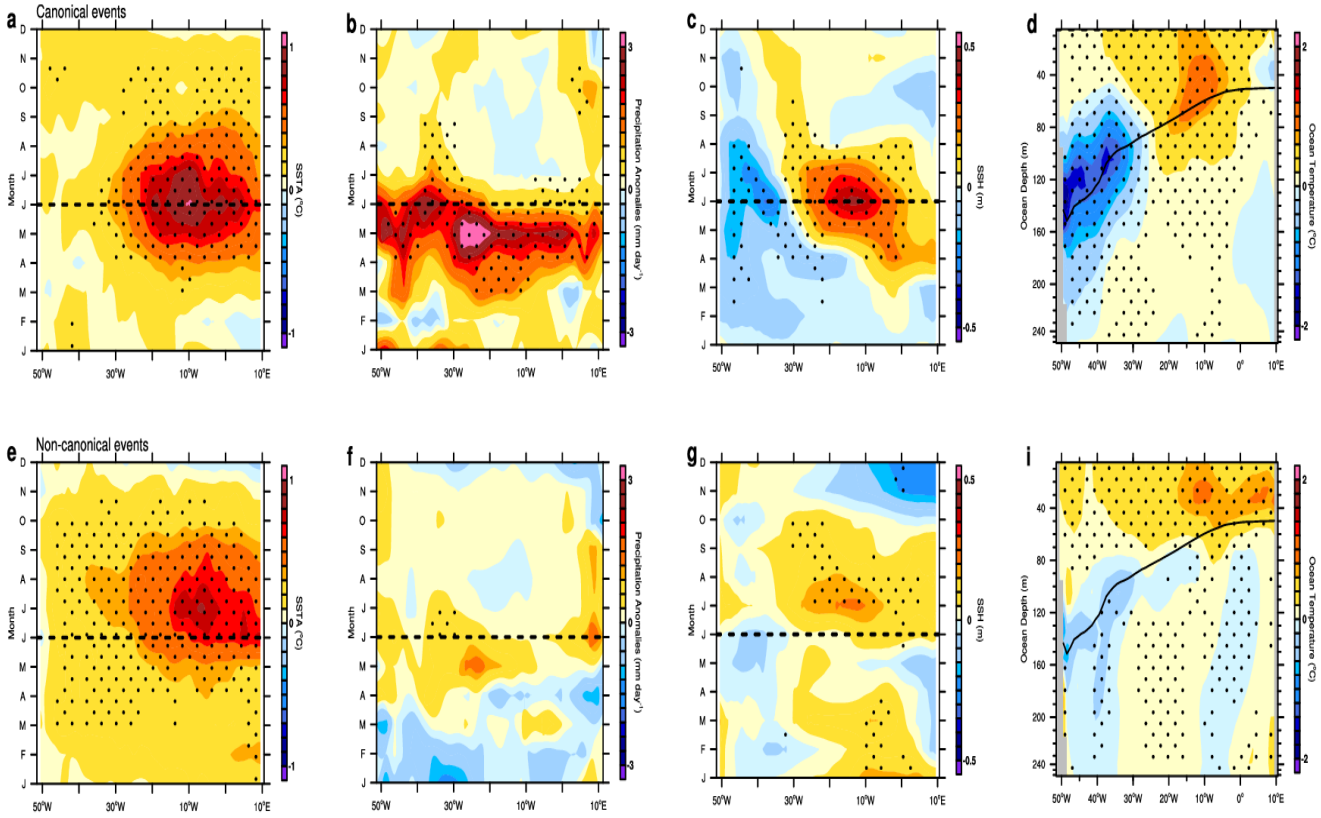

Figure 4.26: Composite means of canonical and non-canonical events in longitude-time maps over the equatorial Atlantic from 3°S to 3°N with SST anomalies (a and e), precipitation anomalies (b and f), SSH anomalies (c and g), and potential temperature (d and i). Dots indicate statistical significance at the 90% confidence level.

4.3.3 Ocean–Atmosphere Processes Underlying Event Growth

4.3.3.1 Ocean-mixed-layer heat budget

To determine the oceanic processes that govern the growth and decay of SST anomalies associated with non-canonical events, the ocean mixed-layer heat budget was computed (Figure 4.27). This approach allows a direct comparison of the roles of surface heating, advective heat transport, and entrainment processes between canonical and non-canonical events.

The time derivative of the mixed-layer temperature ($\partial T/\partial t$) for canonical events exhibits a pronounced maximum warming tendency in May in all reanalyzed data, indicating strong surface heating during the preconditioning phase (Figure 4.27). This warming rapidly diminishes by June, coinciding with the peak of SST anomalies, and transitions to a cooling tendency with a minimum in July.

The entrainment term (1/h[T-T_h]) for canonical events shows a strong contribution to the mixed-layer heat budget. In the GODAS dataset, entrainment peaks in June, whereas in ORAS5, it peaks slightly earlier in May, highlighting its critical role during the early stages of summer (Figure 4.27). This difference in timing between GODAS and ORAS5 likely reflects variations in the representation of thermocline depth and vertical velocity fields between the two reanalyses, which can affect the timing and magnitude of entrainment processes. After the peak, entrainment contributes weakly negatively to the heat budget in August. It transitions to a weak positive contribution in October, indicating a seasonal modulation of vertical mixing and the gradual decay of surface temperature anomalies during the later phases of the events.

The horizontal temperature advection term ($u\partial T/\partial x + v\partial T/\partial y$) during canonical events exhibits negative values throughout the boreal summer, with a minimum in June in the GODAS dataset. In contrast, the ORAS5 dataset shows a very weak positive horizontal advection in June, followed by a

sharp decline to negative values in July. These differences highlight potential sensitivities in the representation of horizontal heat transport between datasets, particularly during the peak phase of Atlantic Niño development (Figure 4.27).

The tendency associated with the net surface heat flux in canonical events, another key contributor to the mixed-layer heat budget, closely reflects the seasonality of the heat storage term. Notably, the net surface heat flux remains negative throughout the boreal summer, reaching its minimum in July (Figure 4.27). This indicates that surface heat flux acts as the primary damping mechanism during June and July, precisely when SST anomalies reach their peak intensity. The fact that SST anomalies continue to strengthen during this period, despite the damping by surface heat fluxes, underscores the dominant role of ocean dynamical processes such as entrainment and horizontal advection in sustaining the warming.

The residual term (ϵ) in the heat budget analysis, which captures both errors in the datasets and the effects of unresolved processes such as vertical mixing and small-scale turbulence, is relatively small in the GODAS dataset but noticeably larger in the ORAS5 dataset for canonical events. In GODAS, the residual reaches its maximum positive value in July, while in ORAS5, it peaks in June (Figure 4.27). Importantly, these peaks coincide with the period when SST anomalies are strongest, suggesting that uncertainties or missing processes become more influential during the peak development of Atlantic Niño events. The smaller residual in GODAS implies a higher level of confidence in the closure of the heat budget in this data set. In comparison, the larger residual in ORAS5 indicates greater uncertainty, particularly during critical phases of SST anomaly development.

In contrast, the mixed-layer heat budget terms for non-canonical events display distinct characteristics compared to canonical events. The temperature tendency term peaks in June across all reanalysis datasets, then rapidly declines to near-zero or negative values. The entrainment term,

however, reaches its maximum contribution in July in all datasets, indicating a delayed role of vertical processes relative to the surface warming. Similarly, the horizontal advection term peaks in June and subsequently decreases to zero or negative values, highlighting a brief but essential contribution early in the summer. The net surface heat flux continues to act as the primary damping mechanism during June and July, counteracting the growth of SST anomalies. Lastly, the residual term remains relatively stable throughout the season, reaching its maximum in August across all datasets. This suggests that unresolved processes or data uncertainties have a more moderate influence during the evolution of non-canonical events compared to canonical events.

A comparison of the mixed-layer heat budgets between canonical and non-canonical events reveals essential differences in their underlying dynamics. For canonical events, ocean dynamical processes-particularly entrainment and horizontal advection terms play a leading role in driving SST anomalies, with entrainment peaking early in the season and supporting sustained warming despite damping by surface heat fluxes. In contrast, non-canonical events exhibit a more surface-driven evolution, with temperature tendencies and horizontal advection peaking sharply in June before rapidly diminishing. The delayed peak in entrainment during non-canonical events suggests a less efficient coupling between the ocean and atmosphere. Additionally, the residual term is relatively small and stable during non-canonical events, indicating fewer unresolved processes compared to canonical events, where uncertainties peak during maximum SST anomalies. These differences highlight that ocean processes more dynamically sustain canonical Atlantic Niño events, whereas non-canonical events are more transient and sensitive to atmospheric forcing.

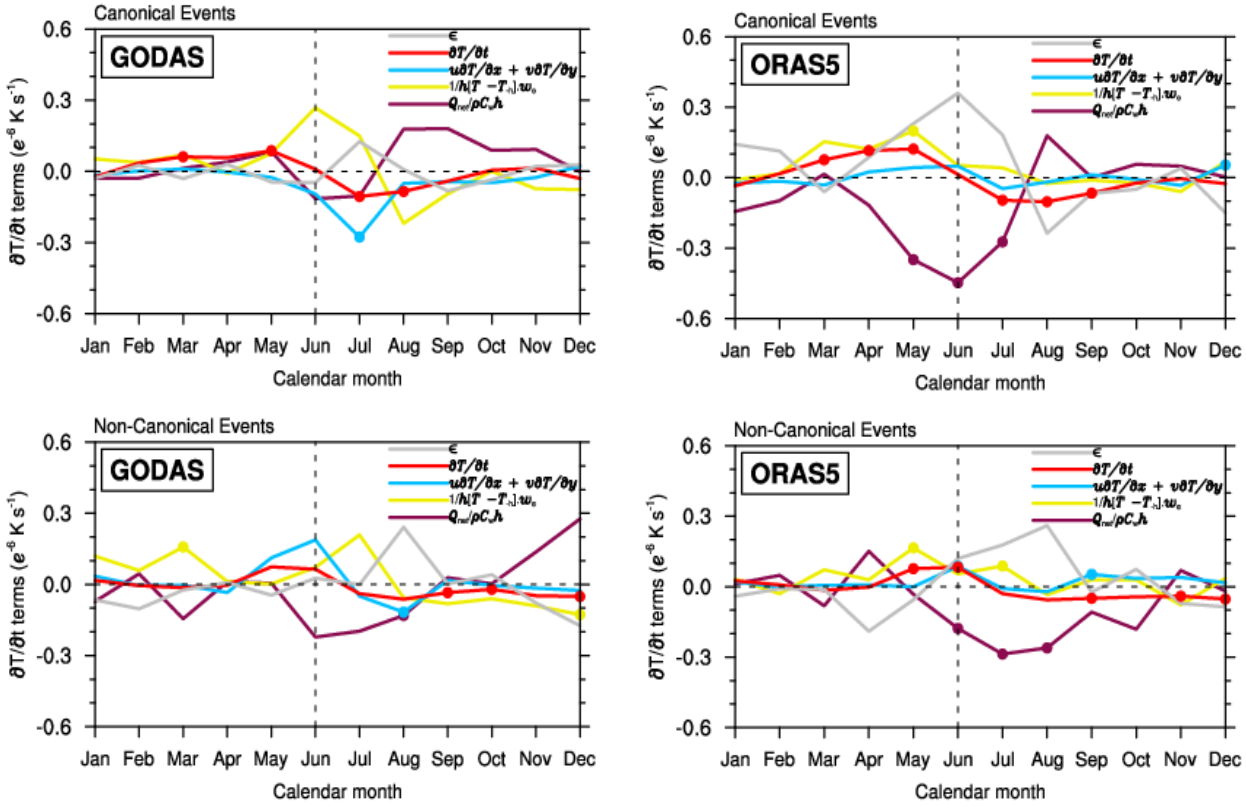

Figure 4.27: Composite of the ocean-mixed-layer heat budget terms for the canonical and non-canonical events in the different ocean reanalysis datasets, indicated in the top-left corner of each panel. Dots denote statistical significance at the 90% confidence level. For all terms, positive (negative) values mean heating (cooling) of the ocean-mixed-layer.

4.3.3.2 Walker circulation

Here, the anomalies in the Walker circulation associated with canonical and non-canonical Atlantic Niño events are examined to understand better the mechanisms driving their evolution are examined. Figure 4.28 presents vertical cross-sections of the vertical velocity anomalies, averaged over the equatorial band (5°N-5°S), for the seasons of June-August (JJA) and April-June (AMJ). For canonical events (Figure 4.28a), the presence of robust La Niña-like SST anomalies in the Pacific (Figure 4.25a) is associated with strong subsidence anomalies across the central and eastern Pacific (90°W-180°E) and pronounced upward motion anomalies over the equatorial Atlantic (80°W-30°E), indicative of intensified deep convection. This enhanced convection is sustained by warm SST anomalies and reduced trade winds, strengthening the Bjerknes positive feedback mechanism. Additional upward motion over the western Pacific (95°E-130°E) and subsidence over the central Pacific (150°E-180°E) further reflect inter-basin teleconnections that reinforce Atlantic Niño development.

In contrast, non-canonical events (Figure 4.28b) display similar overall subsidence patterns but with noticeably weaker magnitudes. Stronger subsidence over the central Atlantic suggests a more localized and less organized atmospheric response. Upward motion over the eastern Atlantic is also weaker, consistent with reduced SST-convection coupling, a weaker Bjerknes feedback, and consequently lower event intensity and predictability.

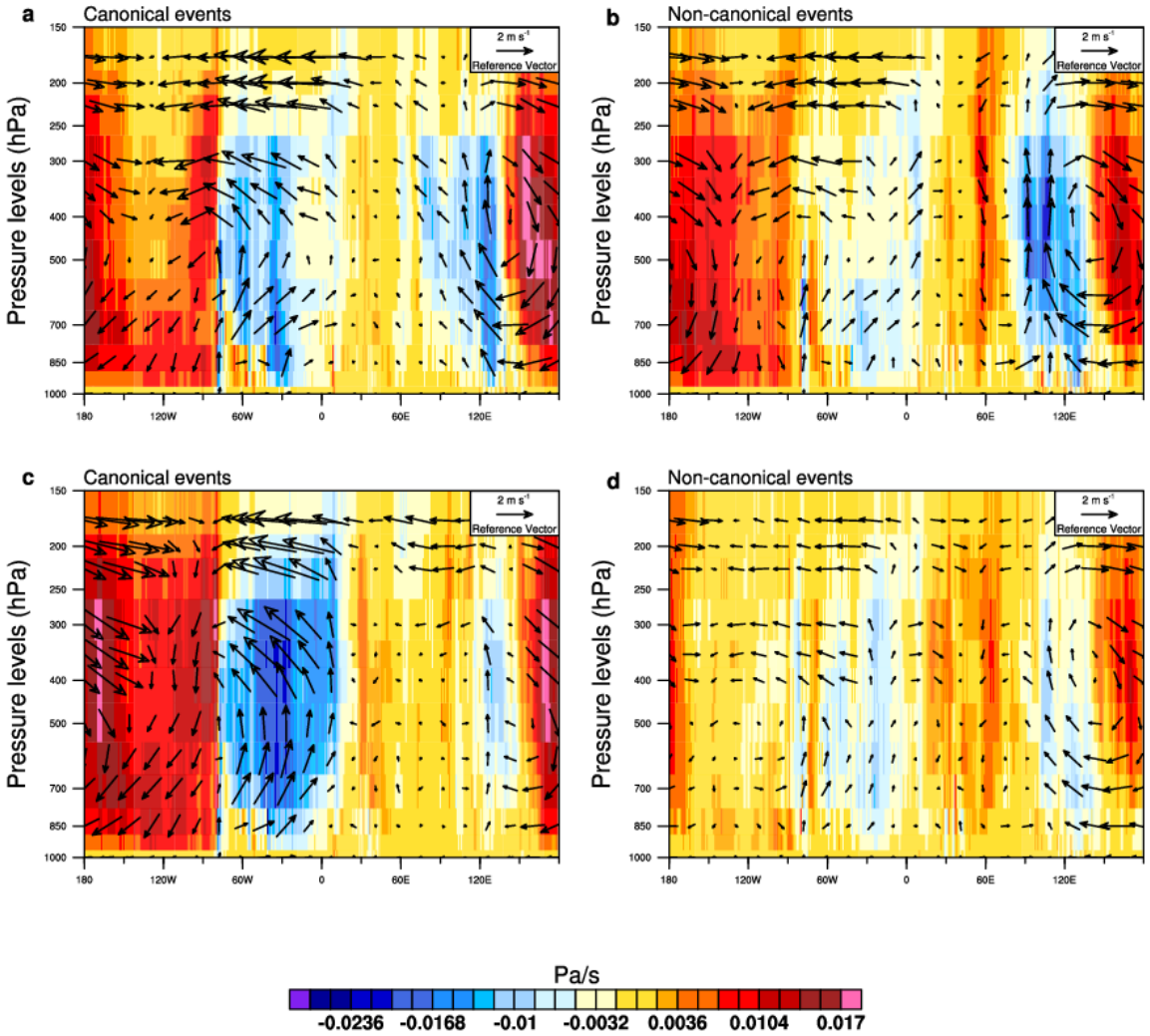

Figure 4.28: Composites of wind (vectors, m/s) and vertical velocity anomalies (shading, −100 × Pa/s) averaged over 5°N–5°S for (a, c) canonical and (b, d) non-canonical events during JJA and AMJ

4.3.3.3 Atlantic–Pacific inter-basin interactions

Figure 4.29 shows the monthly evolution of sea surface temperature (SST) anomalies associated with canonical Atlantic Niño events, from January to December. Warm SST anomalies initially emerge around the Benguela Niño region in March and April, intensifying toward the peak phase of the Atlantic Niño in May and reaching a maximum in June. These anomalies decay rapidly, disappearing by August. Notably, canonical events are preceded by a double-dip La Niña-like pattern in the Pacific earlier in the year, highlighting the potential influence of inter-basin teleconnections (Figure 4.29).

In contrast to canonical events, non-canonical events (Figure 4.30) begin their development in June, with no significant warming observed in the preceding months. The SST anomalies peak in July and dissipate rapidly by September. Interestingly, following the decay of these Atlantic Niño events, the Pacific Ocean exhibits anomalously cold SSTs of comparable magnitude, suggesting that non-canonical events may be associated with an El Niño-to-La Niña phase transition. This distinct seasonal evolution underscores the importance of separating canonical and non-canonical events in understanding Atlantic Niño dynamics.

These contrasting patterns highlight the importance of distinguishing between canonical and non-canonical Atlantic Niño events. Canonical events exhibit an early onset and strong coupling between SST and convection. They are often linked to persistent La Niña conditions in the Pacific, suggesting a robust inter-basin influence that amplifies their predictability and dynamical structure. In contrast, non-canonical events are more abrupt, lack clear atmospheric precursors, and are associated with transitional phases of ENSO, particularly El Niño-to-La Niña shifts. The weaker SST-convection coupling and shorter lifespan of these events imply that internal Atlantic processes, rather than sustained external forcing, play a more dominant role.

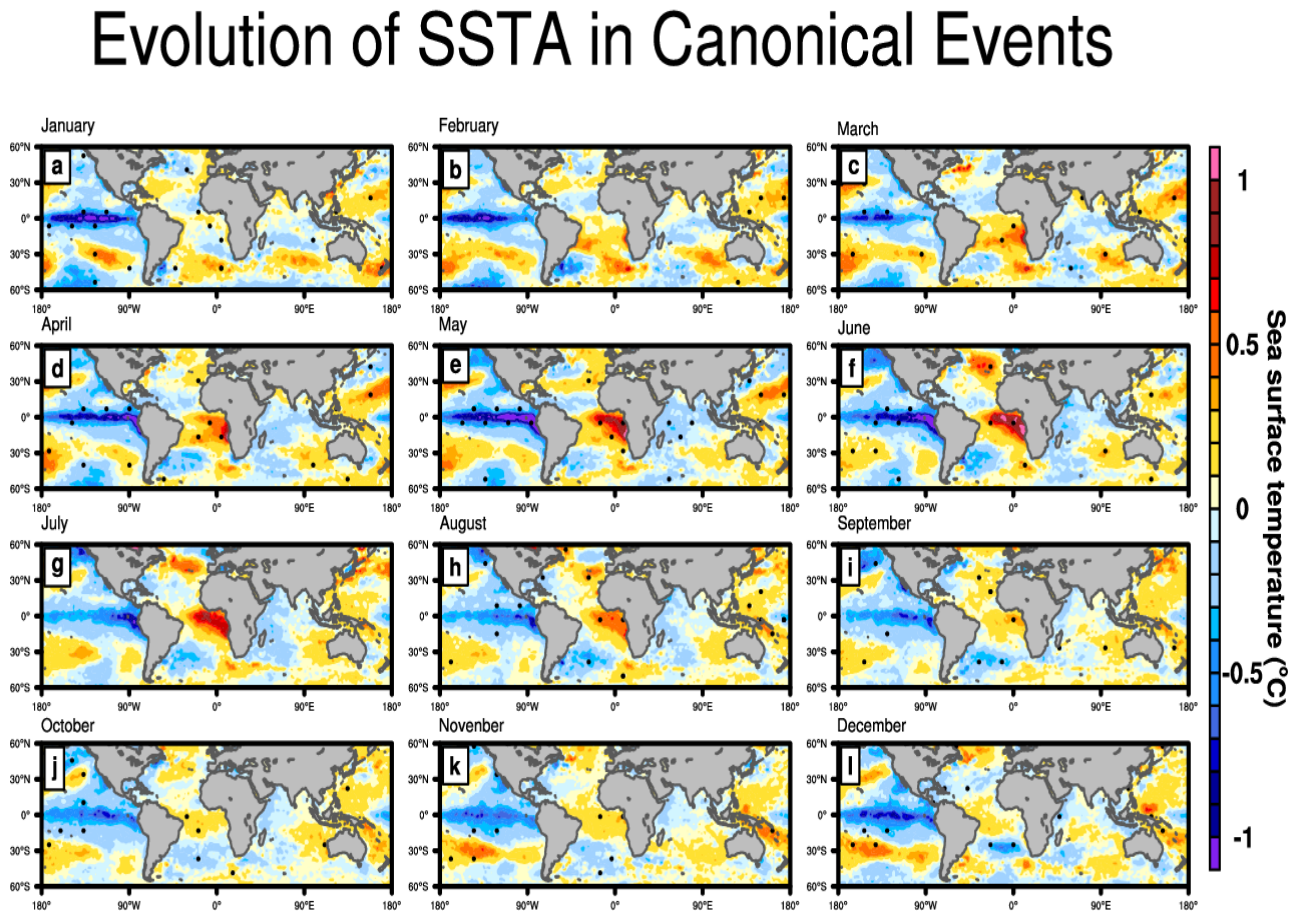

Figure 4.29: Composite mean of canonical event evolution maps of monthly SST anomalies derived from observed negative events of canonical events. Stippling denotes statistical significance at a 90% confidence level.

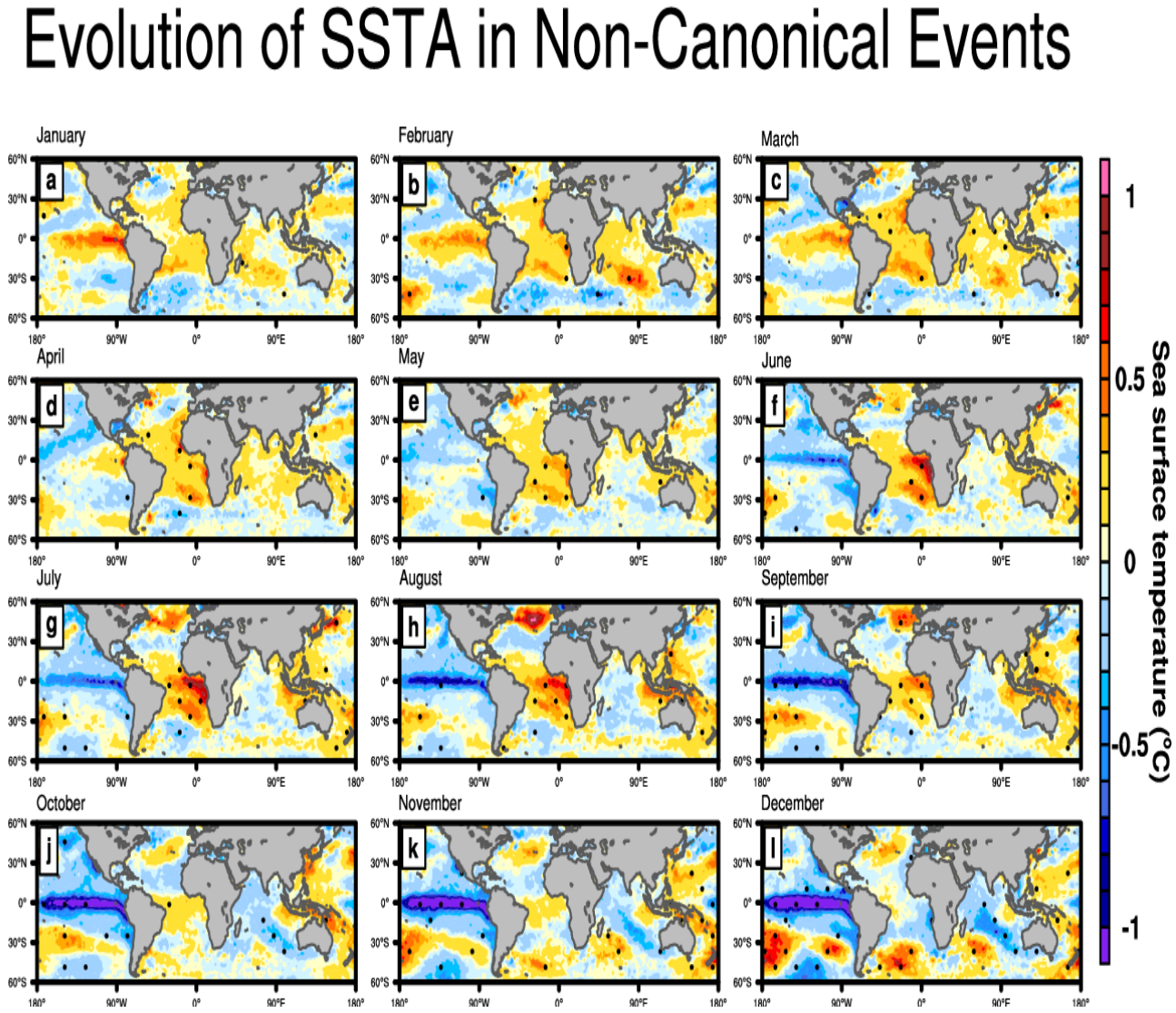

Figure 4.30: Composite mean of non-canonical event evolution maps of monthly SST anomalies derived from observed negative events of canonical events. Stippling denotes statistical significance at a 90% confidence level.

4.4 Seasonal Predictability of Atlantic Niño Events

4.4.1 Predictability of Canonical and Non-Canonical Atlantic Niño Events

Figure 4.31 illustrates the performance of the ECMWF seasonal forecast system in capturing the spatial and temporal evolution of the two different types of SSTA in the equatorial Atlantic (canonical and non-canonical Niño events). First, the composite average of the SSTA was computed for both event types using the ECMWF system's forecast outputs, averaged between 3°S and 3°N and with lead times of one to six months.

The forecast system demonstrates considerable ability to reproduce key features of the warm events, but significant differences between the two types are evident. In particular, canonical Niño events in the eastern equatorial Atlantic exhibit a more sustained SSTA warming signal, which the ECMWF system captures more consistently, particularly at lead times of one to three months. In contrast, non-canonical events are characterized by a westward shift or more diffuse SSTA warming with predictive power typically limited to lead times of about one month.

A comparison with observed SST patterns from satellite-based datasets (Figure 4.26a,e) shows a close agreement in the spatial structure and timing of SSTA evolution during canonical events. This agreement is significantly weaker in non-canonical events, suggesting that the predictability of Atlantic Niño events in the ECMWF system strongly depends on the event type. The improved model performance for canonical events highlights the importance of a well-developed ocean-atmosphere coupling and the presence of a strong thermocline feedback, which are less pronounced in non-canonical cases.

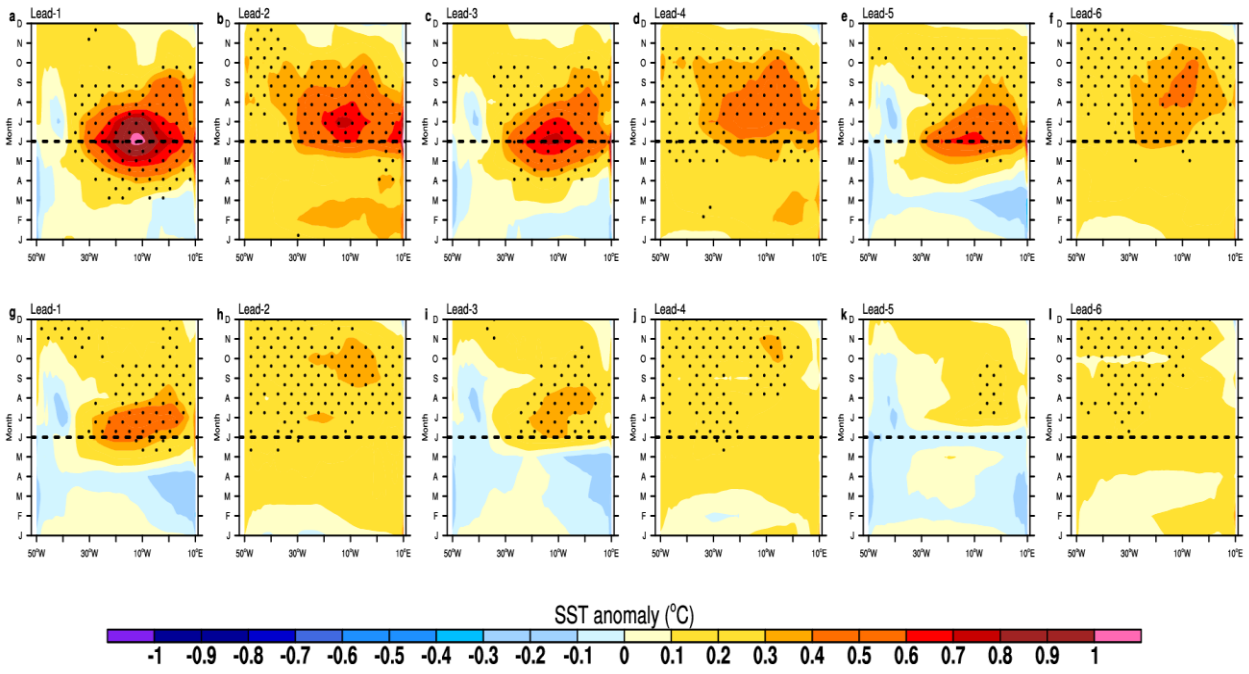

Figure 4.31: Composite mean of canonical and non-canonical events longitude-time maps across the equatorial Atlantic 3°S to 3°N showing SST anomalies monthly evolution from ECMWF prediction systems at 1-6months lead time. Stippling denotes statistical significance at 90% confidence level.

A further analysis of the forecast systems for the two event types was performed by averaging the SST anomalies over the Atlantic cold tongue region for both observations and ECMWF forecasts over lead times of one to six months (Figure 4.32a,b). This comparison allows a more detailed assessment of the monthly evolution of SST anomalies during canonical and non-canonical Atlantic Niño events.

For canonical events, the ECMWF seasonal forecast system successfully captures the monthly evolution of SST anomalies up to four months lead times. Still, it tends to underestimate the amplitude of the SSTA. The model accurately tracks the phase and timing of anomaly development, indicating a relatively high predictability for this event type. In contrast, non-canonical events are less well reproduced, as the forecast system only exhibits a realistic structure and monthly evolution up to a lead time of two months. Furthermore, the model fails to maintain the anomaly pattern, likely due to weaker ocean-atmosphere coupling and more localized or stochastic forcing mechanisms.

A direct comparison with satellite-based SSTA observations confirms an explicit agreement in the temporal evolution of canonical events, particularly regarding the onset and peak phases of SSTA. This agreement applies to non-canonical events.

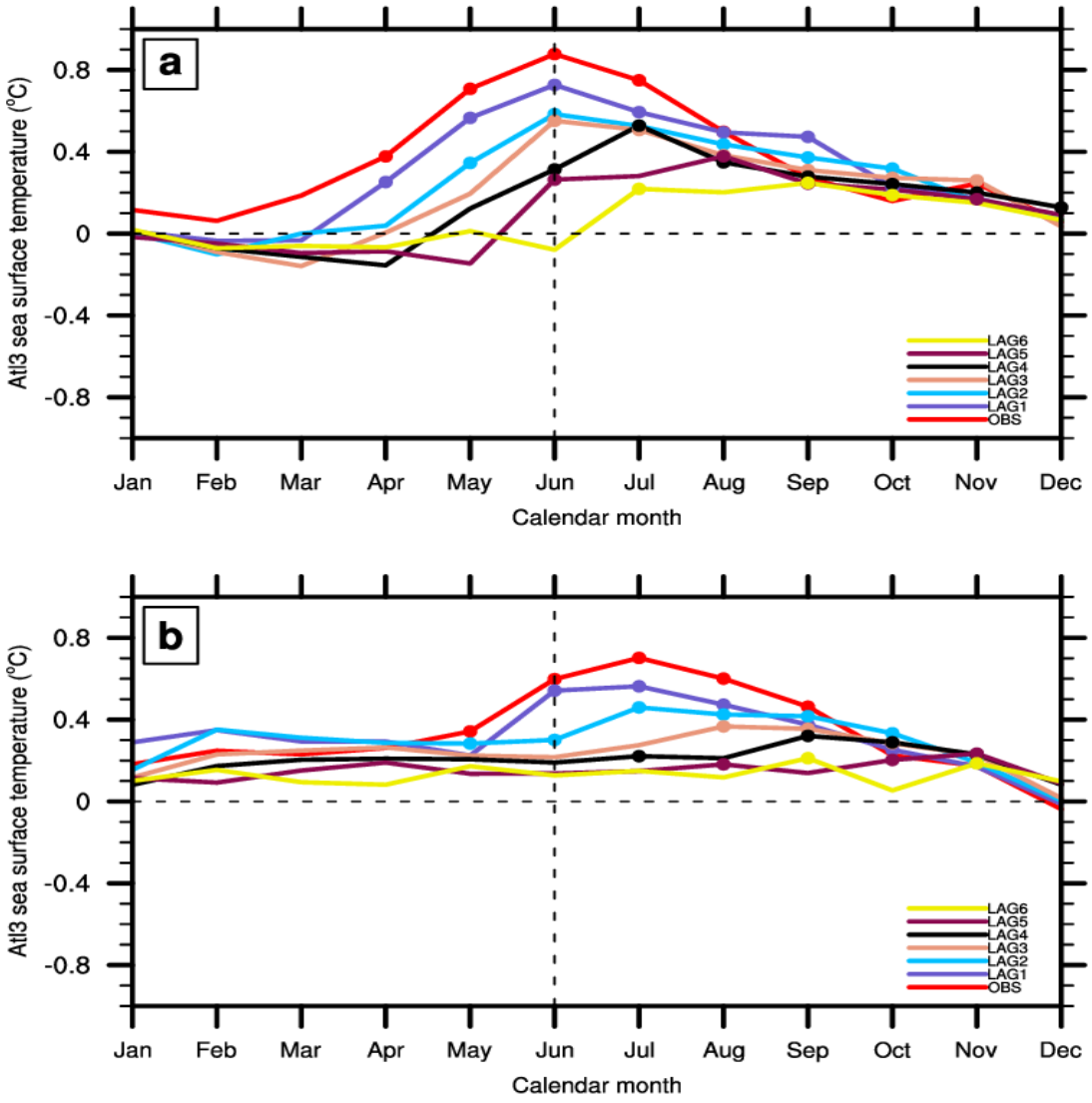

Figure 4.32: a. Composite mean of canonical events, defined as Atl3-SST anomalies. b. Composite mean non-canonical events showing SST anomalies, monthly evolution of observations, and ECMWF prediction systems at 1-6 months lead time. Dots denote values significant at the 90% confidence level.

4.4.1 Prediction skill of events from the ECMWF ensemble

To quantitatively assess the predictive skill of the ECMWF seasonal forecast system, anomaly correlation coefficients (ACCs) and root mean square errors (RMSE) were computed by comparing model outputs with satellite-based SSTA observations. The analysis was performed using seasonal means, with monthly SST anomalies averaged over the boreal summer season (June-July-August, JJA), which corresponds to the peak of Atlantic Niño development.

Figure 4.33 illustrates the seasonal ACCs for lead times ranging from one to six months, separately for canonical and non-canonical Atlantic Niño events.

For canonical events, the model exhibits strong positive ACCs in the Atlantic Niño region from the 1- to 4-day lead times. This indicates a high agreement between predicted and observed seasonal SST anomalies. However, the accuracy decreases from the lead time of 5-6.

In contrast, positive ACCs for non-canonical events are generally restricted to lead times of 1-2, with spatial coherence and magnitude decreasing significantly from lead time 3. This suggests that non-canonical events are less predictable, likely due to their more localized structure.

Overall, the results confirm that the ECMWF seasonal forecast system exhibits higher forecast performance for canonical Atlantic Niño events, with skillful predictability of up to three to four months. For non-canonical events, forecast skill is limited to shorter lead times of approximately one to two months.

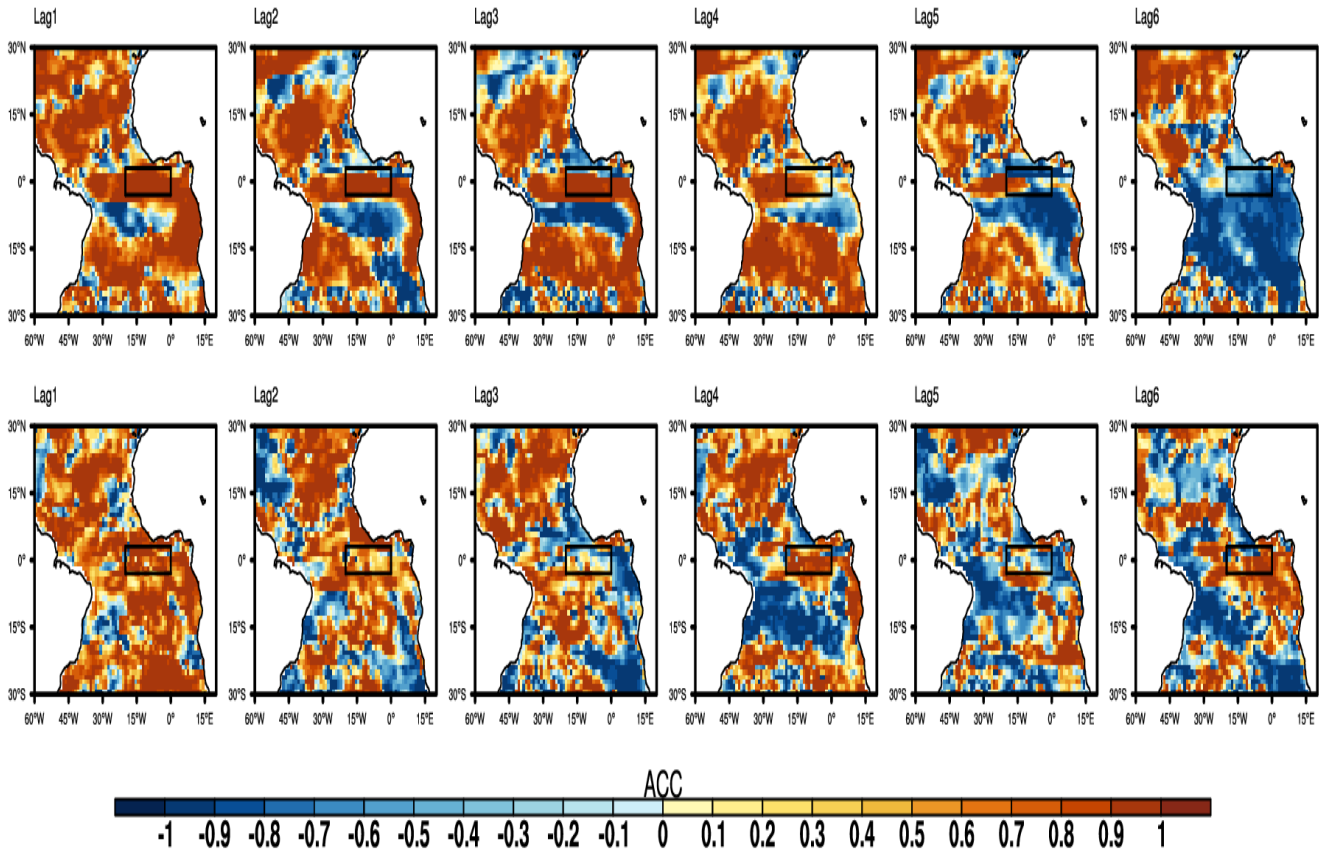

Figure 4.33: Anomaly correlation coefficients between predictions and observations 3-month averaged during the (JJA) seasons at 1-6 months Lead time.

However, RMSE results further confirmed the ACC results of canonical events with values closer to zero from Lead time1 to Lead time4 in the Atlantic Niño region (black box). Values closer to one were observed at Lead time5 and Lead time6 (Figure 4.34).

From the perspective of RMSE, better prediction of non-canonical events was observed at 1-2-months-Lead time with the RMSE (Figure 4.34).

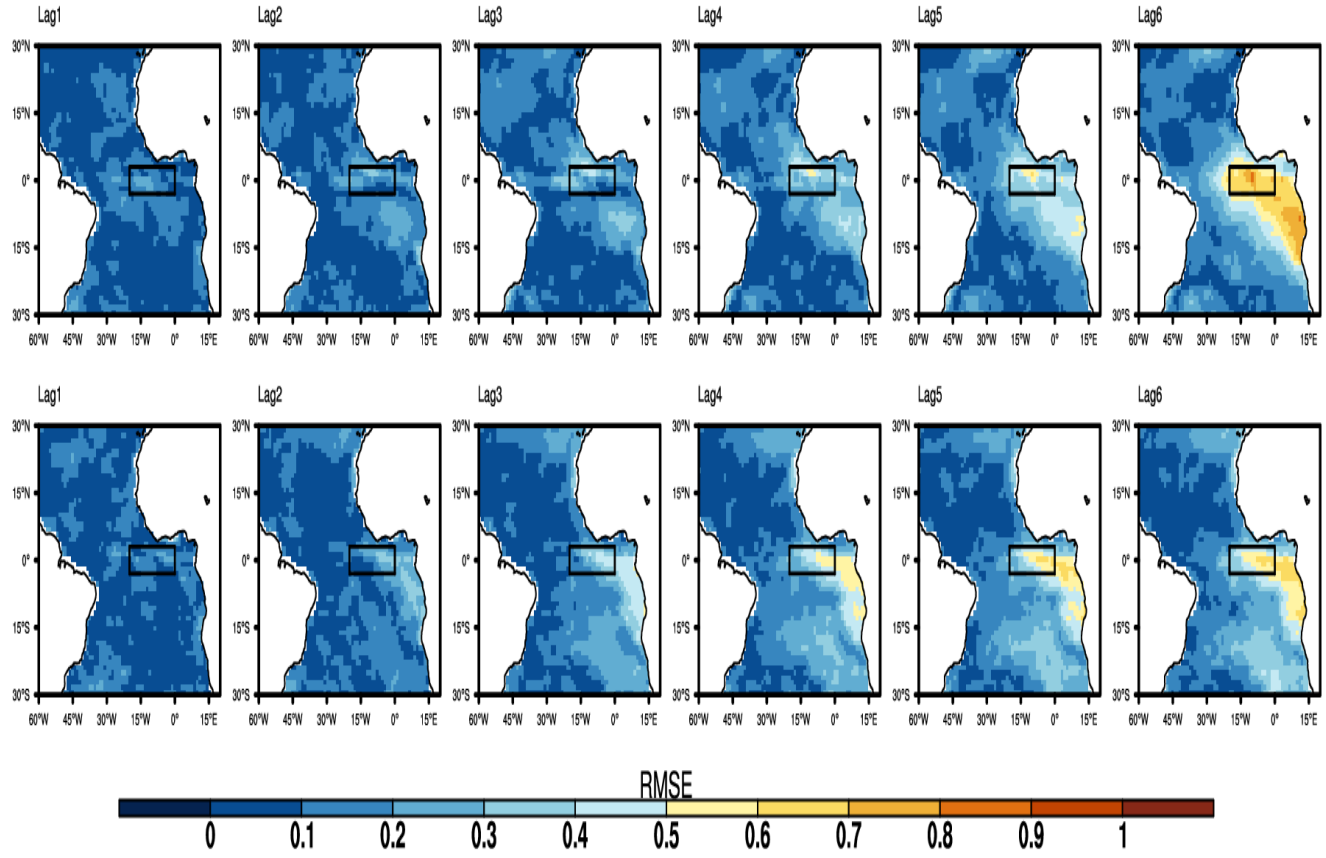

Figure 4.34. Root mean squared error between predictions and observations, 3-month averaged during the (JJA) seasons at 1-6months Lead time.

Additionally, the composite mean of the canonical and non-canonical SST anomalies over the Atl3 region for both observations and the ECMWF seasonal prediction systems at 1-6 lead times is shown in Figure 4.35.

The canonical events are clearly predictable with significant correlations at all 1–6-month lead times available in the ECMWF seasonal forecast archive (Figure 4.35). Note that this assessment of statistical significance is only nominal, as the autocorrelation between the two fields (Bretherton et al., 1999) has not been accounted for. More importantly, there is a clear qualitative difference between the canonical and non-canonical events (Figure 4.35), and the latter type of events do not show any correlation skill. For the canonical events, the correlation skill does

not change much with lead time, but the RMSE increases progressively from about 0.15°C at lag-1 month to 0.61°C at lead time-6 months, indicating increasing uncertainty with lead time.

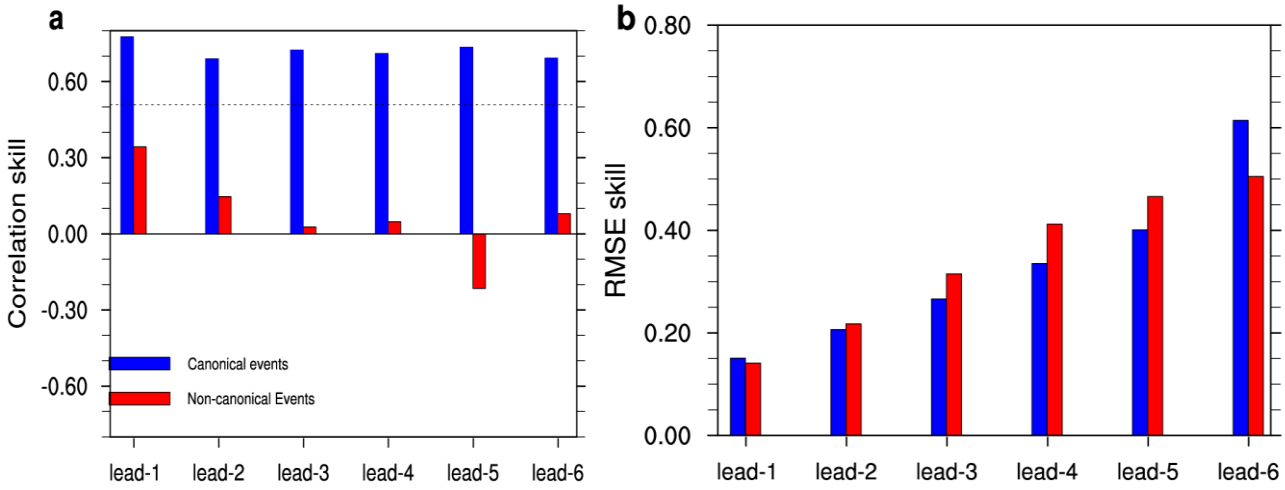

Figure 4.35. Prediction skill of the Atlantic Niño during JJA for different lead times. (a) Correlation skill between forecast anomalies and observed anomalies (HadISST) for canonical and non-canonical events at lead times (1 to 6). The dashed line indicates statistical significance at the 90% confidence level. (b) Root mean square error (RMSE) between forecast anomalies and observed anomalies for canonical and non-canonical events over the same lead times.

CHAPTER FIVE

5.0 CONCLUSION AND RECOMMENDATION

5.1 CONCLUSION

This research investigated the mechanisms governing Atlantic Niño variability and its predictability in the equatorial Atlantic. It specifically addressed four major objectives: (i) evaluating the coupling between sea surface temperature (SST), atmospheric convection, and thermocline variability known as the Bjerknes positive feedback, a mechanism that drives Atlantic Niño; (ii) identifying and analyzing key processes underlying the observed weakening of the atmosphere-to-ocean Bjerknes feedback since the 2000; (iii) assessing the role of atmospheric deep convection in preconditioning the development of Atlantic Niño events; and (iv) determining the predictability of Atlantic Niño events using ECMWF's seasonal forecast systems from SEAS5. The findings significantly broaden our understanding of the mechanisms driving Atlantic Niño events, the dynamics of the Atlantic Niño, and offer insights for improving seasonal climate prediction in the tropical Atlantic.

5.1.1 Atlantic Niño Variability and Coupled Ocean-Atmosphere Processes

The Atlantic Niño remains the leading mode of interannual SST variability in the equatorial Atlantic, sustained primarily through the Bjerknes positive feedback. This positive feedback involves interactions among eastern equatorial SST anomalies, western equatorial Atlantic zonal wind stress, eastern equatorial Atlantic thermocline depth, and equatorial Atlantic atmospheric convection. However, the analysis revealed that this classical Bjerknes positive feedback accounts for only 21-23% of the eastern equatorial Atlantic SST variability, suggesting that coupling in the Atlantic is weaker than in the Pacific. Notably, atmospheric convection (particularly precipitation variability) linked to the northward migration of the Intertropical Convergence Zone (ITCZ) plays a vital role in

setting the background condition for the development of SST anomalies in the eastern equatorial Atlantic. These results highlight the importance of precipitation variability in the meridional direction in modulating equatorial zonal Atlantic SST variability.

5.1.2 Post-2000 Weakening of the Bjerknes Feedback

Another major outcome of this study is the identification of a significant post-2000 weakening in the atmosphere-to-ocean Bjerknes feedback. This weakening is primarily attributable to a reduced sensitivity of precipitation anomalies to zonal SST gradients (Subprocess 1), with a moderate decline in the response of zonal sea level pressure to precipitation anomalies (Subprocess 2). In contrast, the mechanical coupling between sea level pressure gradients and zonal wind stress (Subprocess 3) has remained relatively stable.

The diminished response in Subprocess 1 likely reflects a weakened convective sensitivity associated with changes in ITCZ positioning, which may enhance large-scale atmospheric subsidence and suppress precipitation. The moderation in Subprocess 2 may be linked to a slowing Atlantic Walker circulation, further weakening the feedback loop. While the Bjerknes feedback remains partially functional, its reduced efficiency implies weaker SST variability and reduced predictability of Atlantic Niño events.

These findings are supported by CMIP6 AMIP simulations, which successfully capture the general trend of weakening Bjerknes feedback from atmosphere to ocean. However, they tend to underestimate the coupling strength in the equatorial Atlantic. This highlights the model biases in the region.

5.1.3 Preconditioning Role of Atmospheric Convection

Atmospheric deep convection in May (with precipitation anomalies serving as a proxy for diabatic heating) was shown as critical in preconditioning SST anomalies that typically peak in June. Regression analysis indicates that precipitation explains a larger percentage of explained variance in May (57%) of SST variability compared to zonal wind stress, with an explained variance of 52%. This preconditioning sets the stage for the development of El Niño events in the Atlantic, with the ITCZ's northward shift and associated convective processes acting as key modulators of SST interannual variability.

5.1.4 Categorization and Predictability of Canonical and Non-Canonical Events

Atlantic Niño events were further categorized into canonical and non-canonical types based on the presence or absence of atmospheric preconditioning. Canonical events, which feature enhanced convection (precipitation anomalies) in May and strong subsurface coupling, exhibit early SST onset, more intense anomalies, and delayed precipitation impacts along the Guinea Coast. These events tend to be preceded by La Niña-like SST anomalies in the tropical Pacific and are more predictable, with lead times of up to four months. In contrast, non-canonical events lack a clear atmospheric precursor, exhibit weaker coupling with subsurface processes, and typically show delayed SST peaks, emerging in July. These events are less predictable, with skill generally limited to 1-2 months. The non-canonical events lead to the emergence of La Niña-like variability in the tropical Pacific.

Importantly, this study clarifies the longstanding debate on Atlantic-Pacific linkages. It shows that canonical Atlantic Niño events are more likely influenced by antecedent Pacific variability. In contrast, non-canonical events can serve as precursors to La Niña conditions in the subsequent boreal

fall and winter. Thus, whether the Atlantic Niño leads or lags ENSO depends critically on the event type, offering a new framework for understanding Atlantic-Pacific teleconnections.

5.2 RECOMMENDATION

The equatorial Atlantic, as well as its interaction with the equatorial Pacific, is subject to decadal modulations and external forcing (Martín-Rey et al., 2014, 2018; Nnamchi et al., 2020; Park et al., 2023; Wang et al., 2024). In particular, the Atlantic Niño is projected to become weaker in a warming climate (Crespo et al., 2022; Worou et al., 2023; Yang et al., 2022, 2024). Thus, how these modulations affect the canonical versus non-canonical Atlantic Niño–ENSO needs to be addressed in further studies. In this regard, model biases in the region and ocean observational uncertainty demand enhanced efforts.

Future work could also consider the seasonal predictions in the tropical Atlantic with greater emphasis on the role of atmospheric convection, particularly the preconditioning effects of deep convection during boreal spring in driving Atlantic Niño variability to enhance forecast skill.

Additionally, this study highlights the need to distinguish between canonical and non-canonical Atlantic Niño events systematically. Such categorization can help in understanding Atlantic-Pacific teleconnections and in refining seasonal predictions of regional climate impacts, including those affecting the West African monsoon.

Finally, the reported weakening of the Bjerknes positive feedback observed after 2000 raises questions about the stability of atmosphere–ocean coupling under climate change. Long-term monitoring and targeted model experiments, especially those using high-resolution and convection-permitting simulations, are recommended to understand the dynamics of the tropical Atlantic better. More work needs to be done to better understand the recent weakening of the atmosphere-ocean

Bjerknes positive feedback; these efforts will support more accurate seasonal forecasts and inform climate adaptation strategies in vulnerable regions dependent on Atlantic climate variability.

5.3 THE CONTRIBUTION OF THE RESEARCH TO KNOWLEDGE

This study contributes to the scientific understanding of the tropical Atlantic climate system in the following key areas: First, it improves knowledge of the drivers and mechanisms responsible for sea surface temperature (SST) variability in the eastern equatorial Atlantic cold tongue region. By investigating the role of atmospheric convection-ocean coupling, and thermocline feedback coupling processes

Second, the research improves our understanding of the predictability of the Atlantic Niño mode in seasonal forecast systems, particularly those of the European Centre for Medium-Range Weather Forecasts (ECMWF). By assessing forecast skill, lead-time constraints, and the dynamic representation of coupled processes, the study identifies key factors influencing successful forecasting.

Finally, the study sheds light on the teleconnections between the Atlantic Niño and other tropical basins, particularly the Pacific. This is particularly relevant for improving seasonal rainfall forecasts in West Africa, where the Atlantic Niño significantly influences the West African monsoon.

References

Adler, R. F., et al. (2003). The Version-2 Global Precipitation Climatology Project (GPCP) Monthly Precipitation Analysis (1979–Present). Journal of Hydrometeorology, 4(6), 1147–1167. https://doi.org/10.1175/1525-7541(2003)004<1147:TVGPCP>2.0.CO;2.

Bayr, T., Dommenget, D., & Latif, M. (2020). Mean state biases in the tropical Atlantic in CMIP5 models and their impact on ENSO teleconnections. *Climate Dynamics, 54*(3–4), 1819–1835. https://doi.org/10.1007/s00382-019-05097-3.

Behringer, D.W., M. Ji, and A. Leetmaa (1998) An improved coupled model for ENSO prediction and implications for ocean initialization. Part I: The ocean data assimilation system. Mon. Wea. Rev., 126, 1013-1021.

Bellenger, H., Guilyardi, E., Leloup, J., Lengaigne, M., & Vialard, J. (2014). ENSO representation in climate models: From CMIP3 to CMIP5. *Climate Dynamics, 42*(7–8), 1999–2018. https://doi.org/10.1007/s00382-013-1783-z

Biasutti, M., D. S. Battisti, and E. S. Sarachik (2004), Mechanisms controlling the annual cycle of precipitation in the tropical Atlantic sector in an atmospheric GCM, J. Clim., 17(24), 4708–4723.

Bjerknes, J. (1969). Atmospheric teleconnections from the equatorial Pacific. Monthly Weather Review, 97, 163–172.

Bourlès, B., Lumpkin, R., McPhaden, M. J., Hernandez, F., Nobre, P., Campos, E., Yu, L., Planton, S., Busalacchi, A. J., Moura, A. D., Servain, J., & Trotte, J. (2008). The PIRATA program: History, accomplishments, and future directions. *Bulletin of the American Meteorological Society*, *89*(8), 1111–1125. https://doi.org/10.1175/2008BAMS2462.1.

Boyd, P. W., Newton, P. P., & Parslow, J. S. (1992). Spatial and temporal variability in plankton biomass and productivity in the subtropical convergence zone of the South Atlantic Ocean. Journal of Plankton Research, 14(5), 681–698. https://doi.org/10.1093/plankt/14.5.681

Brandt, P., Funk, A., Hormann, V., Dengler, M., Greatbatch, R. J. & Toole, J. M. (2011). Interannual atmospheric variability forced by the deep equatorial Atlantic Ocean. Nature, 473, 497–500, doi:10.1038/nature10013.

Brierley, C., & Wainer, I. (2018). Inter-annual variability in the tropical Atlantic from the Last Glacial Maximum into future climate projections simulated by CMIP5/PMIP3. Climate of the Past, 14(10), 1377-1390.

Cai, W., Borlace, S., Lengaigne, M., Piao, S., Collins, M., Vecchi, G., … England, M. H. (2019). Increasing frequency of extreme El Niño events due to greenhouse warming. *Nature Climate Change*, 4(2), 111–116.

Cai, W., Santoso, A., Wang, G., Wu, L., Unsal, S., Lin, X., ... & McPhaden, M. J. (2021). Changing El Niño–Southern Oscillation in a warming climate. *Nature Reviews Earth & Environment, 2*(9), 628–644. https://doi.org/10.1038/s43017-021-00199-z

Cane, M. A. (1992). Tropical Pacific ENSO models: ENSO physics and phenomenology. In Climate System Modeling (ed. Trenberth, K. E.), Cambridge University Press, pp. 583–614.

Capotondi, A., Wittenberg, A. T., Newman, M., Di Lorenzo, E., Yu, J.-Y., Braconnot, P., ... & Yeh, S.-W. (2015). Understanding ENSO diversity. *Bulletin of the American Meteorological Society, 96*(6), 921–938. https://doi.org/10.1175/BAMS-D-13-00117.1

Counillon, F., Keenlyside, N. S., Toniazzo, T., Koseki, S., Demissie, T., Bethke, I., & Wang, Y. (2021). Relating model bias and prediction skill in the equatorial Atlantic. *Climate Dynamics, 56*(7–8), 2617–2630. https://doi.org/10.1007/s00382-020-05605-8

Carton, J. A., & Huang, B. (1994). Warm events in the Tropical Atlantic. Journal of Physical Oceanography, 24, 888-903.

Chang, P., Ji, L., & Li, H. (1997). A decadal climate variation in the tropical Atlantic Ocean from thermodynamic air–sea interactions. *Nature*, *385*(6616), 516–518. https://doi.org/10.1038/385516a0

Chang, P., Saravanan, R., Ji, L., & Hegerl, G. (2006). The effect of local sea surface temperatures on atmospheric circulation over the tropical Atlantic sector. *Journal of Climate, 19*(12), 176–191. https://doi.org/10.1175/JCLI3689.1.

Chen, B., Zhang, L., & Wang, C. (2024). Distinct impacts of the central and eastern Atlantic Niño on the European climate. Geophysical Research Letters, 51, e2023GL107012. https://doi.org/10.1029/ 2023GL107012.

Chiang, J. C. H., Kushnir, Y., & Giannini, A. (2001). Deconstructing Atlantic intertropical convergence zone variability: Influence of the local cross-equatorial SST gradient and remote forcing from the eastern equatorial Pacific. *Journal of Geophysical Research: Atmospheres, 107*(D1), 4004. https://doi.org/10.1029/2000JD000307

Clement, A. C., Seager, R., & Cane, M. A. (2010). Mechanisms of SST variability in the tropical Atlantic. *Journal of Climate*, *23*(14), 3586–3601. https://doi.org/10.1175/2010JCLI3306.1

Counillon, F., Keenlyside, N. S., Bethke, I., Wang, Y., Bentsen, M., & Gao, Y. (2021). Seasonal-to-decadal prediction with the Norwegian Climate Prediction Model. *Climate Dynamics, 57*(9–10), 2577–2604. https://doi.org/10.1007/s00382-021-05683-8

Davey, M. K., Huddleston, M. R., Sperber, K. R., Braconnot, P., Bryan, F., Chen, D., Colman, R., Cooper, C., Cubasch, U., Delecluse, P., DeWitt, D., Fairhead, L., Flato, G., Gordon, C., Hogan, T., Ji, M., Kimoto, M., Kitoh, A., Knutson, T., Latif, M., … Zebiak, S. E. (2002).

STOIC: A study of coupled model climatology and variability in tropical ocean regions. *Climate Dynamics*, *18*(5), 403–420. https://doi.org/10.1007/s00382-001-0188-6.

Ding, H., N. S. Keenlyside, and M. Latif. (2010). Equatorial Atlantic interannual variability: the role of heat content, J. Geophys. Res., 115, C09020. https://doi.org/10.1029/2010JC006304

Dippe, T., Greatbatch, R. J., & Ding, H. (2018). On the relationship between Atlantic Niño variability and Atlantic equatorial mode. *Journal of Climate, 31*(2), 561–578. https://doi.org/10.1175/JCLI-D-17-0380.1

Dippe, T., Greatbatch, R. J., & Ding, H. (2019). On the limited predictability of Atlantic Niño. *Climate Dynamics, 52*(7–8), 4975–4991. https://doi.org/10.1007/s00382-018-4413-4

Doi, T., Richter, I., & Masumoto, Y. (2019). Estimating the role of SST in atmospheric surface wind variability over the tropical Atlantic and Pacific. *Climate Dynamics*, 53, 1–2, 261–274. https://doi.org/10.1007/s00382-018-4582-8.

Exarchou, E., Ortega, P., Rodríguez-Fonseca, B., Losada, T., Polo, I., & Prodhomme, C. (2021). Impact of equatorial Atlantic variability on ENSO predictive skill. Nature Communications, 12(1), 2–9. https://doi.org/10.1038/s41467-021-21857-2.

Folland, C. K., Palmer, T. N., & Parker, D. E. (1986). Sahel rainfall and worldwide sea temperatures, 1901–85. *Nature*, *320*(6063), 602–607.

Foltz, G. R., & McPhaden, M. J. (2010). Abrupt equatorial wave-induced cooling of the Atlantic cold tongue in 2009. Geophysical Research Letters, 37, doi:10.1029/2010GL0455.

Foltz, G. R., & McPhaden, M. J. (2010). The 2005 and 2006 Atlantic Niño events. *Ocean Science*, *6*(1), 81-92.

Fu, R., Dickinson, R. E., Chen, M., & Wang, H. (2001). How Do Tropical Sea Surface Temperatures Influence the Seasonal Distribution of Precipitation in the Equatorial Amazon?. Journal

of Climate, 14(20), 4003-4026. https://doi.org/10.1175/1520-0442(2001)014<4003:HDTSST>2.0.CO;2.

Giannini, A., Saravanan, R., & Chang, P. (2003). Oceanic forcing of Sahel rainfall on interannual to interdecadal timescales. *Science*, *302*(5647), 1027–1030.

Giese, B. S., & Carton, J. A. (1994). The Seasonal Cycle in Coupled Ocean-Atmosphere Model. Journal of Climate, 7(8), 1208-1217. https://doi.org/10.1175/1520-0442(1994)007<1208:TSCICO>2.0.CO;2.

Goldenberg, S. B., Landsea, C. W., Mestas-Nuñez, A. M., & Gray, W. M. (2001). The recent increase in Atlantic hurricane activity: Causes and implications. *Science*, *293*(5529), 474–479. https://doi.org/10.1126/science.1060040.

Gray, W. M., Landsea, C. W., Mielke , P. W., Jr., & Berry, K. J. (1992). Predicting Atlantic Seasonal Hurricane Activity 6–11 Months in Advance. Weather and Forecasting, 7(3), 440-455. https://doi.org/10.1175/1520-0434(1992)007<0440:PASHAM>2.0.CO;2.

Grodsky, S. A., and Carton, J. A. (2001). Coupled land/atmosphere interactions in the West African Monsoon. Geophysical Research Letters, vol. 28, no. 8, Pages 1503-1506.

Grodsky, S. A., and Carton, J. A. (2003). The Intertropical Convergence Zone in the South Atlantic and the Equatorial Cold Tongue. Journal of Climate, Volume 16.

Hartmann, D. L., Hendon, H. H., & Houze, R. A. (1984). Some implications of the mesoscale circulations in tropical cloud clusters for large-scale dynamics and climate. *Journal of the Atmospheric Sciences, 41*(1), 68–80.

Hastenrath, S., & Heller, L. (1977). Dynamics of climatic hazards in Northeast Brazil. *Quarterly Journal of the Royal Meteorological Society*, *103*(435), 77–92. https://doi.org/10.1002/qj.49710343505

Houghton, R.W. (1983). Seasonal variation of the subsurface thermal structure in the Gulf of Guinea, J. Phys. Oceanogr., 13, 2070–2081.

Hu, Z.-Z., & Huang, B. (2007). The predictive skill and the most predictable pattern in the tropical Atlantic: The effect of ENSO. Monthly Weather Review, 135(5), 1786–1806. https://doi.org/10.1175/MWR3393.1.

Houze, R. A. (1982). Cloud clusters and large-scale vertical motions in the tropics. *Journal of the Meteorological Society of Japan. Ser. II, 60*(1), 396–410. https://doi.org/10.2151/jmsj1965.60.1_396

Illig, S., Bachèlery, M.-L., & Lübbecke, J. F. (2020). Why do Benguela Niños lead Atlantic Niños? Journal of Geophysical Research: Oceans, 125, e2019JC016003. https://doi.org/10.1029/2019JC016003.

Ingo Richter, Shang-Ping Xie, Yushi Morioka, Takeshi Doi, Bunmei Taguchi & Swadhin Behera.(2017). Phase locking of equatorial Atlantic variability through the seasonal migration of the ITCZ. *Clim Dyn***48**, 3615–3629. https://doi.org/10.1007/s00382-016-3289-y.

Janicot, S., and Sultan, B. (2001). Intra-seasonal modulation of convection in the West African monsoon. Geophysical Research Letters, vol. 28, no. 3, Pages 523-526.

Jansen, M. F., Dommenget, D., & Keenlyside, N. (2009). Tropical Atmosphere–Ocean Interactions in a Conceptual Framework. Journal of Climate, 22(3), 550-567. https://doi.org/10.1175/2008JCLI2243.1.

Jiang, X., McPhaden, M. J., Richter, I., & Behera, S. K. (2025). Multi-season lead prediction of Atlantic Niño facilitated by Pacific Ocean precursors. *Geophysical Research Letters, 52*(6), e2024GL111494. https://doi.org/10.1029/2024GL111494

Jouanno, J., Hernandez, O., & Sanchez-Gomez, E. (2017). Equatorial Atlantic interannual variability and its relation to dynamic and thermodynamic processes, Earth System Dynamics, 8, 1061-1069, doi:10.5194/esd-8-1061-2017.

Kalnay et al., (1996) The NCEP/NCAR 40-year reanalysis project, Bull. Amer. Meteor. Soc., 77, 437-470.

Keenlyside, N. S., & Latif, M. (2007). Understanding equatorial Atlantic interannual variability. Journal of Climate, 20, 131–142, doi:10.1175/JCLI3992.1.

Keenlyside, N. S., Ding, H., & Latif, M. (2013). Potential of equatorial Atlantic variability to enhance El Niño prediction. Geophysical Research Letters, 40(10), 2278–2283. https://doi.org/10.1002/grl.50362.

Kim, D., Lee, S.-K., Lopez, H., Foltz, G. R., Wen, C., West, R., & Dunion, J. (2023). Increase in Cape Verde hurricanes during Atlantic Niño. *Nature Communications*, *14*, 3704. https://doi.org/10.1038/s41467-023-39467-5.

Kirtman, B. P., Min, D., Infanti, J. M., Kinter III, J. L., Paolino, D. A., Zhang, Q., ... & LaRow, T. E. (2009). Current status of ENSO prediction skill in coupled ocean–atmosphere models. *Climate Dynamics*, 32(7-8), 647–664. https://doi.org/10.1007/s00382-008-0397-3.

Kim, W., Webster, P. J., Curry, J. A., & Chang, H.-Y. (2023). Atlantic Niño's modulation of tropical cyclone activity. *Nature Geoscience*, *16*, 214–221.

Knight, J. R., Allan, R. J., Folland, C. K., Vellinga, M., & Mann, M. E. (2006). A signature of persistent natural thermohaline circulation cycles in observed climate. *Geophysical Research Letters*, *32*(20). https://doi.org/10.1029/2005GL024233

Kushnir, Y., Robinson, W. A., Chang, P., & Robertson, A. W. (2006). The physical basis for predicting atlantic sector seasonal-to-interannual climate variability*. Journal of Climate, 19(23), 5949-5970. https://doi.org/10.1175/jcli3943.1.

Lamb, P. J. (1978). Large-scale tropical Atlantic surface circulation patterns associated with sub-Saharan weather anomalies. *Tellus*, *30*(3), 240–251.

Latif, M. and Grotzner. A. (2000). The equatorial Atlantic oscillation and its response to ENSO. Climate Dyn.,16,213–218.

Li, T., & Philander, S. G. H. (1997). On the Seasonal Cycle of the Equatorial Atlantic Ocean. Journal of Climate, 10(4), 813-817. https://doi.org/10.1175/1520-0442(1997)010<0813:OTSCOT>2.0.CO;2.

Li, T., & Zhou, W. (2020). Preconditioning of the Atlantic Niño by cross-equatorial SST gradients. *Geophysical Research Letters*, 47(8), e2020GL087000.

Liu, T., Duan, W., Yang, D., & Ren, H. (2021). Basin-wide response of the tropical oceans to ENSO: A review. *Advances in Atmospheric Sciences*, 38(3), 571–582.

Li, X., Tan, W., Hu, Z.-Z., & Johnson, N. C. (2023). Evolution and prediction of two extremely strong Atlantic Niños in 2019–2021: Impact of Benguela warming. Geophysical Research Letters, 50(12), e2023GL104215. https://doi.org/10.1029/2023GL104215.

Lübbecke, J. F., & McPhaden, M. J. (2012). On the inconsistent relationship between Pacific and Atlantic Niños. *Journal of Climate, 25*, 4294–4303. https://doi.org/10.1175/JCLI-D-11-00553.1

Lübbecke, J. F., & McPhaden, M. J. (2013). A comparative stability analysis of Atlantic and Pacific Niño modes. Journal of Climate, 26, 5965–5980, doi:10.1175/JCLI-D-12-00758.1.

Lübbecke, J. F., Rodríguez-Fonseca, B., Richter, I., Martín-Rey, M., Losada, T., Polo, I., & Keenlyside, N. S. (2018). Equatorial Atlantic variability—Modes, mechanisms, and

global teleconnections. *Wiley Interdisciplinary Reviews: Climate Change*, *9*(4), e527. https://doi.org/10.1002/wcc.527.

Lübbecke, J. F., & McPhaden, M. J. (2017). On the link between mean state biases and prediction skill in the tropics: an atmospheric perspective. *Climate Dynamics, 50*(9-10), 3355–3374. https://doi.org/10.1007/s00382-017-3809-4.

Lübbecke, J. Tropical Atlantic warm events. Nature Geosci6, 22–23 (2013). https://doi.org/10.1038/ngeo1685.

Luo, J.-J., S. Masson, S. Behera, and T. Yamagata. (2008). Extended ENSO predictions using a fully coupled ocean-atmosphere model. J. Climate, 21, 84-93.

Martín-Rey, M., Polo, I., Rodríguez-Fonseca, B., & Lazar, A. (2019). Interannual variability of the Atlantic Niño: The role of ocean dynamics. *Climate Dynamics*, *52*(3–4), 2053–2071.

McPhaden, M. J., Zebiak, S. E., & Glantz, M. H. (2006). ENSO as an integrating concept in Earth science. *Science*, 314(5806), 1740–1745. https://doi.org/10.1126/science.1132588.

Mitchell, T.P.; Wallace, J.M. (1992). The annual cycle in equatorial convection and sea surface temperature. J. Clim. 5, 1140–1156.

Mohino, E., Janicot, S., & Bader, J. (2011). Sahel rainfall and decadal to multi-decadal sea surface temperature variability. *Climate Dynamics, 37*(3–4), 419–440. https://doi.org/10.1007/s00382-010-0867-2.

Murakami, H., Levin, E. J., Delworth, T. L., Gudgel, R. G., & Hsu, P. C. (2018). Dominant role of subtropical Pacific warming in extreme Eastern Pacific Hurricane seasons: 2015 and the future. *Journal of Climate, 31*(2), 552–571.

Murtugudde, R., Seager, R., & Busalacchi, A. J. (2001). Oceanic processes associated with anomalous events in the tropical Atlantic. *Journal of Climate*, *14*(2), 206–223.

Neelin, J. D., Battisti, D. S., Hirst, A. C., Jin, F. F., Wakata, Y., Yamagata, T., & Zebiak, S. E. (1998). ENSO theory. *Journal of Geophysical Research: Oceans, 103*(C7), 14261–14290.

Nnamchi, H.C., Latif, M. Predictable equatorial Atlantic variability from atmospheric convection-ocean coupling. npj Clim Atmos Sci 8, 149 (2025). https://doi.org/10.1038/s41612-025-01041-9.

Nnamchi, H. C., Latif, M., Keenlyside, N. S., Kjellsson, J., & Richter, I. (2021). Diabatic heating governs the seasonality of the Atlantic Niño. *Nature Communications*, *12*(1), 1-10. https://doi.org/10.1038/s41467-020-20452-1.

Nnamchi, H. C., Li, J., Kucharski, F., Kang, I.-S., Keenlyside, N. S., Chang, P., & Farneti, R. (2015). Thermodynamic controls of the Atlantic Niño. Nature Communications, 6, 8895, doi:10.1038/ncomms9895. http://www.nature.com/doifinder/10.1038/ncomms9895.

Nnamchi, H. C., Li, J., Kucharski, F., Kang, I.-S., Keenlyside, N. S., Chang, P., & Farneti, R. (2016). An equatorial-extratropical dipole structure of the Atlantic Niño. Journal of Climate, 29, 7295–7311, doi:10.1175/JCLI-D-15-0894.1.

Nobre, P., & Shukla, J. (1996). Variations of sea surface temperature, wind stress, and rainfall over the tropical Atlantic and South America. *Journal of Climate*, *9*(10), 2464–2479.

Okumura, Y., & Xie, S.-P. (2006). Some overlooked features of tropical Atlantic climate leading to a new Niño-like phenomenon. Journal of Climate, 19(22), 5859–5874. https://doi.org/10.1175/jcli3928.1.

Park, JH., Yang, YM., Ham, YG. et al. Significant winter Atlantic Niño effect on ENSO and its future projection. npj Clim Atmos Sci 7, 238 (2024). https://doi.org/10.1038/s41612-024-00790-3.

Philander, S. G. H., & Pacanowski, R. C. (1981). Response of equatorial oceans to periodic forcing. *Journal of Geophysical Research: Oceans*, *86*(C3), 1903-1916. https://doi.org/10.1029/JC086iC03p01903.

Philander, S. G. H., & Pacanowski, R. C. (1986). A model of the seasonal cycle in the tropical Atlantic Ocean. *Journal of Geophysical Research: Oceans*, *91*(C12), 14192–14206. https://doi.org/10.1029/JC091iC12p14192.

Planton, Y., J. Vialard, E. Guilyardi, M. Lengaigne, and T. Izumo, 2018: Western Pacific oceanic heat content: A better predictor of La Niña than of El Niño. Geophys. Res. Lett., 45, 9824–9833, https://doi.org/10.1029/2018GL079341.

Polo, I., Rodríguez-Fonseca, B., Losada, T., & García-Serrano, J. (2008). Tropical Atlantic variability modes (1979–2002). *Part I: Time-evolving SST modes related to West African rainfall*. *Journal of Climate*, *21*(24), 6457–6475.

Prigent, A., Lübbecke, J.F., Bayr, T. et al. Weakened SST variability in the tropical Atlantic Ocean since 2000. Clim Dyn 54, 2731–2744 (2020). https://doi.org/10.1007/s00382-020-05138-0.

Prodhomme, C., Voldoire, A., Exarchou, E., Deppenmeier, A.-L., García-Serrano, J., & Guemas, V. (2019). How Does the Seasonal Cycle Control Equatorial Atlantic Interannual Variability? *Geophysical Research Letters*, *46*(2), 916–925. https://doi.org/10.1029/2018GL080837

Rayner N.A., Parker D.E., Horton E.B., Folland C.K., Alexander L.V., Rowell D.P., Kent E.C., Kaplan A. (2003) Global analyses of sea surface temperature, sea ice, and night marine air temperature since the late nineteenth century. J. Geophys. Res., 108: 4407. https://doi.org/10.1029/2002jd002670.

Rebert, J. P., Donguy, J. R., Eldin, G., & Wyrtki, K. (1985). Relations between sea level, thermocline depth, and dynamic height in the tropical Pacific Ocean. *Journal of Geophysical Research: Oceans, 90*(C6), 11719–11725. https://doi.org/10.1029/JC090iC06p11719

Richter I. , Xie S. , Behera S. , Doi T. , & Masumoto Y. (2012). Equatorial atlantic variability and its relation to mean state biases in cmip5. Climate Dynamics. 42(1-2):171-188. https://doi.org/10.1007/s00382-012-1624-5.

Richter, I., & Tokinaga, H. (2020). On the forcing mechanisms of the Atlantic Niño. *Climate Dynamics*, *55*(1), 359–372.

Richter, I., & Xie, S.-P. (2008). On the origin of equatorial Atlantic biases in coupled general circulation models. Climate Dynamics, 31, 587-598.

Richter, I., Behera, S. K., Masumoto, Y., Taguchi, B., Sasaki, H. , & Yamagata, T. (2013). Multiple causes of interannual sea surface temperature variability in the equatorial Atlantic Ocean. Nature Geoscience, 6, 43–47, doi:10.1038/ngeo1660.

Richter, I., Keenlyside, N. S., & Xie, S.-P. (2014). Surface temperature biases and their relation to SST variability in CMIP5 models. *Climate Dynamics*, *42*(1–2), 161–176. https://doi.org/10.1007/s00382-012-1620-5.

Richter, I., Xie, S.-P., Morioka, Y., Doi, T., Taguchi, B., & Behera, S. (2017). Phase locking of equatorial Atlantic variability through the seasonal migration of the ITCZ. Climate Dynamics, 48, 3615–3629, doi:10.1007/s00382-016-3289-y.

Richter, I., Doi, T., Behera, S. K., Keenlyside, N., & Cravatte, S. (2018). On the link between mean state biases and prediction skill in the tropics: An atmospheric perspective. *Climate Dynamics, 50*(9–10), 3355–3374. https://doi.org/10.1007/s00382-017-3809-4

Rodrigues, R. R., Taschetto, A. S., Gupta, A. S., & Foltz, G. R. (2020). Common cause for severe droughts in South America and marine heatwaves in the South Atlantic. *Journal of Climate*, *33*(1), 405–420.

Rodrigues, R. R., Haarsma, R. J., Campos, E. J. D., & Ambrizzi, T. (2011). The Impacts of Inter–El Niño Variability on the Tropical Atlantic and Northeast Brazil Climate. *Journal of Climate*, *24*(13), 3402-3422. https://doi.org/10.1175/2011JCLI3983.1

Ruiz-Barradas, A., Nigam, S., & Carton, J. (2000). Atlantic air–sea interaction and seasonal predictability. *Journal of Climate*, *13*(22), 3282–3297.

Servain, J., Wainer, I., Ayina, H. L., & Roquet, H. (2000). The relationship between the simulated climatic variability modes of the tropical Atlantic. International Journal of Climatology, 20, 939–953, doi:10.1002/1097-0088(200007)20:9<939::AID-JOC511>3.0.CO;2- V

Silva P, Wainer I, Khodri M. (2021). Changes in the equatorial mode of the Tropical Atlantic in terms of the Bjerknes Feedback Index. Clim Dyn 56(9):3005–3024. https://doi.org/10.1007/s00382-021-05627-w.

Tang, Y., Zhang, R.-H., Liu, T., Duan, W., Yang, D., Zheng, F., Ren, H., Lian, T., Gao, C., Chen, D., et al. (2018). Progress in ENSO prediction and predictability study. Natl. Sci. Rev., 5, 826–839.

Thorncroft, and Coauthors, 2003: The JET2000 project: Aircraft observations of the African easterly jet and African easterly waves. Bull. Amer. Meteor. Soc., 84, 337–351.

Timmermann, A., An, S.-I., Kug, J.-S., Jin, F.-F., Cai, W., Capotondi, A., Cobb, K. M., Lengaigne, M., McPhaden, M. J., Stuecker, M. F., Stein, K., Wittenberg, A. T., Yun, K.-S., Bayr, T., Chen, H.-C., Chikamoto, Y., Dewitte, B., Dommenget, D., Grothe, P., Guilyardi, E., … Zhang, X. (2018). El Niño–Southern Oscillation complexity. *Nature*, *559*(7715), 535–545. https://doi.org/10.1038/s41586-018-0252-6.

Tokinaga, H., & Xie, S.-P., (2011). Weakening of the equatorial Atlantic cold tongue over the past six decades. Nature Geoscience, 4, 222–226, doi:10.1038/ngeo1078.

Trenberth, K. E., Branstator, G. W., Karoly, D., Kumar, A., Lau, N. C., & Ropelewski, C. (1998). Progress during TOGA in understanding and modeling global teleconnections associated with tropical sea surface temperatures. *Journal of Geophysical Research: Oceans*, 103(C7), 14291–14324. https://doi.org/10.1029/97JC01444.

Vallès-Casanova, I., Arsouze, T., & Lazar, A. (2020). On the spatiotemporal diversity of atlantic niño and associated rainfall variability over west africa and south america", Geophysical Research Letters, vol. 47, no. 8. https://doi.org/10.1029/2020gl087108.

Wang, C. (2019). Atlantic Niño dynamics and predictability: A review. *Advances in Atmospheric Sciences*, *36*(5), 469-484.

Wang, C., & Picaut, J. (2004). Understanding ENSO physics—A review. In F. F. Jin, S. E. Zebiak, M. Latif, & J. Park (Eds.), *Earth's Climate: The Ocean-Atmosphere Interaction* (Vol. 147, pp. 21–48). American Geophysical Union. https://doi.org/10.1029/147GM02.

Wang, C., Xue, Y., & He, S. (2021). Regional climate responses to Atlantic Niño: An updated view. *Journal of Climate*, 34(12), 4321–4338.

Worou, K., Goosse, H., Fichefet, T., & Kucharski, F. (2022). Weakened impact of the Atlantic Niño on the future equatorial Atlantic and Guinea Coast rainfall. *Earth System Dynamics, 13*(2), 231–249. https://doi.org/10.5194/esd-13-231-2022.

Wu, L., & Tang, Y. (2019). Indian Ocean Dipole leads to Atlantic Niño. *Nature Communications*, 10, 1235.

Xie, S.-P., & Philander, S. G. H. (1994). A coupled ocean–atmosphere model of relevance to the ITCZ in the eastern Pacific. *Tellus A: Dynamic Meteorology and Oceanography*, *46*(4), 340–350. https://doi.org/10.3402/tellusa.v46i4.15484

Xie, S.-P., Kosaka, Y., Du, Y., Hu, K., Chowdary, J. S., & Huang, G. (2013). Indo-western Pacific ocean capacitor and coherent climate anomalies in post-ENSO summer: A review. *Advances in Atmospheric Sciences*, *30*(4), 734–744. https://doi.org/10.1007/s00376-012-2140-1.

Xie, S. P., & Carton, J. A. (2004). Tropical Atlantic variability: Patterns, mechanisms, and impacts. In S. Wang (Ed.), *Earth's Climate: The Ocean-Atmosphere Interaction* (Vol. 147, pp. 121–142). American Geophysical Union. https://doi.org/10.1029/147GM07.

Xu, Z., Patricola, C. M., & Chang, P. (2014). Oceanic origin of southeast tropical Atlantic biases in coupled models. *Climate Dynamics,* *43*(11), 2915–2930. https://doi.org/10.1007/s00382-013-2026-3.

Yang, Y., Wu, L., Cai, W. et al. (2022). Suppressed Atlantic Niño/Niña variability under greenhouse warming. Nat. Clim. Chang. 12, 814–821. https://doi.org/10.1038/s41558-022-01444-z.

Zebiak S. E., & Cane, M. A. (1987). A Model El Niño-Southern Oscillation. Monthly Weather Review, 97(3), 163-172.

Zebiak, S. E. (1993). Air–sea interaction in the equatorial Atlantic region. *J. Climate*, **6,**1567–1586.

Zhang, L., and Han, W. (2021). Indian Ocean Dipole leads to Atlantic Niño. Nat Commun 12, 5952. https://doi.org/10.1038/s41467-021-26223-w.

Zhao, Y., Zheng, F., Lian, T., & Chen, D. (2020). Impact of Indian Ocean conditions on Atlantic Niño: A modelling study. *Climate Dynamics*, 54(5–6), 3211–3225.

Zuo H, Balmaseda MA, Tietsche S, Mogensen K, Mayer M. (2019). The ECMWF operational ensemble reanalysis–analysis system for ocean and sea ice: a description of the system and assessment. Ocean Sci.15:779–808. doi:10.5194/os-15-779-2019.